



Norwegian University of
Science and Technology

Hydrodynamic optimization of bulk and tank ship hulls

Haakon Utby

Marine Technology

Submission date: June 2016

Supervisor: Sverre Steen, IMT

Norwegian University of Science and Technology
Department of Marine Technology



MASTER THESIS IN MARINE TECHNOLOGY

SPRING 2016

FOR

Haakon Utby

Hydrodynamic optimization of bulk and tank vessels

Slow ships, like large bulkers and tankers, usually have high block coefficients with blunt bows. The dimensions, including the high block, are mainly chosen to maximize cargo carrying capacity. Earlier studies, such as that reported in the PhD thesis of Lindstad, indicate that significant power savings might be obtained by lifting some of the restrictions on main dimensions, allowing for construction of more slender hull shapes.

The objectives of the thesis are to:

Determine what is typically the optimum block coefficient of a bulk or tank ship

How much power might be saved going from current design to what is found as the optimum design.

To fulfill the objectives it is foreseen that the candidate will have to perform some kind of optimization of the hull form. It is expected that the optimization shall mainly be limited to main dimensions, and it is also expected that the number of variables to vary will be quite limited.

The thesis must clearly argue choices of dimensions to vary, range of variation and chosen computational tools.

In the thesis the candidate shall present his personal contribution to the resolution of problem within the scope of the thesis work.

Theories and conclusions shall be based on mathematical derivations and/or logic reasoning identifying the various steps in the deduction.

The thesis work shall be based on the current state of knowledge in the field of study. The current state of knowledge shall be established through a thorough literature study, the results of this study shall be written into the thesis. The candidate should utilize the existing possibilities for obtaining relevant literature.

The thesis should be organized in a rational manner to give a clear exposition of results, assessments, and conclusions. The text should be brief and to the point, with a clear language. Telegraphic language should be avoided.

The thesis shall contain the following elements: A text defining the scope, preface, list of contents, summary, main body of thesis, conclusions with recommendations for further work, list of symbols and acronyms, reference and (optional) appendices. All figures, tables and equations shall be numerated.



NTNU Trondheim
Norwegian University of Science and Technology
Department of Marine Technology

The supervisor may require that the candidate, in an early stage of the work, present a written plan for the completion of the work. The plan should include a budget for the use of computer and laboratory resources that will be charged to the department. Overruns shall be reported to the supervisor.

The original contribution of the candidate and material taken from other sources shall be clearly defined. Work from other sources shall be properly referenced using an acknowledged referencing system.

The thesis shall be submitted electronically (pdf) in DAIM:

- Signed by the candidate
- The text defining the scope (signed by the supervisor) included
- Computer code, input files, videos and other electronic appendages can be uploaded in a zip-file in DAIM. Any electronic appendages shall be listed in the main thesis.

The candidate will receive a printed copy of the thesis.

Supervisor : Professor Sverre Steen
Start : 18.01.2016
Deadline : 10.06.2016

Trondheim, 24.02.2016

Sverre Steen
Supervisor

Preface


This master thesis is a part of a Master of Science within naval architecture at the Norwegian University of Science and Technology (NTNU). It is written during the spring semester of 2016 and delivered to the Department of Marine Technology. Professor Sverre Steen has been the supervisor of this master thesis.

The work presented in this thesis is the product of an effort evenly distributed throughout entire spring semester 2016. This has prevented an unnecessary high workload towards the deadline, resulting in a thesis I myself find having a satisfying quality.

The results from my project thesis delivered December 2016 proved inexpedient to investigate any further in a master thesis. Therefore, the subject treated in this thesis was new to me with little self-produced material to start with. The work on this thesis has introduced me to a new subject within naval architecture which I have enjoyed working with and given me new perspectives and knowledge within the field.

During the work with the thesis I have encountered new software such as ShipX and DELFTship. A lot of work in this thesis has been put into understanding and mastering these programs. The results of the hours spent on understanding and mastering the programs is not necessary reflected in results presented in this report. The knowledge is nonetheless valuable knowledge which may prove useful in a later career as a naval architect.

A special thank is given to my supervisor Professor Sverre Steen at the Department of Marine Technology, for weekly meetings and guidance throughout the semester. This has been valuable for solving the challenges faced during the work with this thesis and structuring the progress of the work. Haakon Lindstad at MARINTEK also deserves a thanks for giving valuable insight within the field of shipping.



Haakon Utby, Trondheim June 10th 2016

Abstract

International shipping transports more than 80 percent of global trade. Traditionally bulk carriers have been built to minimize construction cost and maximize cargo-carrying capacity, neglecting hydrodynamic characteristics. By 2025, all new ships will be required to be 30% more energy efficient than those built in 2014.

When designing bulk ships, a number of restrictions have already been applied even before the naval architect has stated designing the ship, e.g. port restrictions, canals and legislative limitations. This thesis investigate how speed performance and power requirements may be improved by lifting some of the restriction on main dimensions when designing ship hulls. Lindstad et al. (2013) introduce the idea that increasing the breadth of bulk carriers while keeping the length, draft and displacement constant, and thereby reducing the block coefficient, will be an efficient way of reducing the resistance and fuel consumption of a ship.

Lindstad et al. (2013) uses an empirical model based on Holtrop and Mennen (1984) and conclude that the brake power is reduced with reduced block coefficient. However, when evaluating hull dimensions outside the range the empirical data is based on, the result obtained has high uncertainty. Numerical methods using CFD has been applied in combination with CAD program to optimize hull lines. Using CFD to calculate added resistance in waves is however very computational demanding and time consuming and can hardly be applied in an optimization process. By using a simplified numerical method on a wide range of hull designs, this thesis attempts to bridge the gap between the idea of Lindstad et al. (2013) and the numerical approach used in simulation based design.

Based on an adaption of a commercial bulk carrier (CBC) and MOERI KVLCC2 there has been designed two series of ships with a deadweight of 80 000 tons. The block coefficient varies from 0,59 to 0,8 for the MOERI KVLCC2 series and 0,64 to 0,87 for the CBC series. When designing the hull and ship lines the focus has been on optimizing the bow, the transition between the bow and parallel midship area (forward shoulder), the parallel midship body and the stern area.

Initially, the two numerical calculations programs ShipX and Michlet was tested. ShipX calculates the wave resistance of conventional monohull ships using potential theory. To make ShipX more robust it satisfies the boundary condition of the surface some distance away from the hull surface. The satisfying of the boundary condition makes it less prone to catch details in different hulls. Using Geritsma & Beukelman method combined with strip-theory approximation the added resistance in waves is calculated. Michlet is an open source research code utilizing thin ship theory to calculate wave resistance. The essential assumption is that the hull is thin, that is, the breadth is small compared to all other characteristic lengths of the problem. A benchmarking with the MOERI KVLCC2 show that results from ShipX are correlating best with experimental results. ShipX is therefore used to calculate the calm water resistance and added resistance in waves for the two design series.

When comparing the brake power as a function of block coefficient calculated using empirical and numerical methods there is a clear disagreement in the results. For both of the design series the empirical calculations show a decreasing brake power with decreasing block coefficient, giving no clear optimum. For the CBC series the numerical calculations show an optimal block coefficient of 0,73. For the MOERI KVLCC2 series the numerical calculations show an optimal block coefficient of 0,78. In additions, results indicate that for a given block coefficient moving the longitudinal center of buoyancy (LCB) backward reduce the wave resistance.

From the results it is concluded that the optimal block coefficient for ships in the New Panamax and Capesize segment ($60\,000 < \text{dwt} < 200\,000$) is in the range of 0,73-0,78 with a slight increase as the displacement increases. Today the average block coefficient for ships of this size is above 0,84. The percentage reduction in brake power from $C_b=0,84$ to the optimal $C_b=0,73$ is a total of 22,81%. Reducing the block coefficient from the current average of 0,84 to the optimal range can reduce the brake power, and thus total fuel consumption and emissions to air with 22,81%, saving a total of 17,05 million tons of CO₂ emissions and up to US\$ 1 326,4 million in fuel savings on a yearly basis.

A recommendation for further work is to further develop the hull series where a combination of length and breadth is varied. The effect of a variation of the length in combination with breadth can then be investigated. Using more comprehensive numerical methods (e.g. computational fluid dynamics) to calculate the calm water resistance of each hull may give a more precise answer with a higher credibility. For new technology and design principles to be implemented in shipping it also has to be proven economically sustainable. A total assessment of the profit and cost of the recommended changes have to be investigated.

Sammendrag

Internasjonal skipsfart transporterer mer enn 80 % av verdens globale handel. Tradisjonelt har bulkskip vært bygd for å minimere byggekostnader og maksimere lastekapasitet og dermed forsømt hydrodynamiske egenskaper. Innen 2025 må alle nye skip være 30% mer energieffektive enn skip bygd i 2014.

Når man designer et bulkskip har en rekke restriksjoner blitt påført allerede før skipsarkitekten begynner sitt arbeid, f.eks. haverestriksjoner, kanaler og lovgitte restriksjoner. Denne masteroppgaven undersøker hvordan ytelsene og effektbehovet kan bli redusert ved å løfte på noen av restriksjonene på hoveddimensjonene når man designer bulkskip. Lindstad et al. (2013) introduserer ideen at å øke bredden på bulkskip samtidig som man holder lengde, dypgang og deplasement konstant, og dermed reduserer blokkoeffisienten, vil være en effektiv måte å redusere motstanden og brenselforbruket.

Lindstad et al. (2013) bruker en empirisk modell basert på Holtrop and Mennen (1984) og konkluderer med at effektbehovet reduseres med redusert blokkoeffisient. Det er derimot slik at når man evaluerer skrogdimensjoner utenfor området den empiriske dataen er basert på, vil resultat være preget av høy usikkerhet. Numeriske metoder som anvender CFD har blitt anvendt i kombinasjon med CAD program for å optimere skroglinjer. Bruk av CFD til å beregne tilleggsmotstand i bølger er derimot veldig beregningstungt og tidkrevende og kan derfor ikke brukes i en optimaliseringsprosess. Ved å anvende en forenklet numerisk modell på en rekke skrog, forsøker denne masteroppgaven å tette gapen mellom Lindstad et al. (2013) sin ide og de numeriske metodene brukt i simuleringsbasert design.

Basert på en tilpasning av et kommersielt bulk skip (CBS) og MOERI KVLCC2 har det blitt designet to serier av skip med en dødvekt på 80 000 tonn. Blokkoeffisienten varierer fra 0,59 til 0,8 for MOERI KVLCC2 serien og fra 0,64 til 0,87 for CBS serien. Når seriene ble designet var fokuset på å optimalisere baugen, overgangen mellom baug og midtskipet, det parallelle midtskipet og akterskipet.

Innledningsvis ble de to numeriske beregningsprogrammene ShipX og Michlet utprøvd. ShipX beregner bølgemotstanden til konvensjonelle enkeltskrog ved bruk av potensial teori. For å gjøre ShipX mer robust tilfredstiller det grensebetingelsene til overflaten et stykke fra skroget. Tilfredstillingen av grensebetingelsene gjør det mindre tilbøyelig til å fange opp detaljer i skroget. Tilleggs motstand i bølger blir beregnet ved å bruke Geritsma & Beukelman med stripeteori tilnærming. Michlet er en åpen kildekode som anvender tynnskipeteori for å beregne bølgemotstanden. Den grunnleggende forutsetningen er at skroget er tynt, dvs. at bredden på skroget er liten sammenlignet med lengden. En benchmark av de to programmene ved bruk av MOERI KVLCC2 viser at ShipX korrelerer best med eksperimentelle resultater. ShipX er derfor brukt for å beregne bølgemotstand og tilleggsmotstand i bølger for de to designseriene.

Når man sammenligner effekten som en funksjon av blokkoeffisient, ved bruk av empiriske og numeriske metoder, er det en klar uoverensstemmelse i resultatene. For begge designseriene viser de empiriske beregningene et minkende effektbehov ved redusert blokkoeffisient, uten noe klar optimalpunkt.

For CBC serien viser de numeriske beregningene en optimal blokkoeffisient på 0,73. For MOERI KVLCC2 serien viser de numeriske beregningene en optimal blokkoeffisient på 0,78. I tillegg viser resultatene at for en gitt blokkoeffisient vil det redusere bølgeomotstanden å flytte oppdriftsenteret akterut.

Ut fra resultatene kan man konkludere med at for skip i New Panamax og Capesize segmentet ($60\,000 < \text{dwt} < 200\,000$) er den optimale blokkoeffisienten i området fra 0,73-0,78, med et svakt økende optimalpunkt for økende deplasement. I dag er den gjennomsnittlige blokkoeffisienten for skip av dette deplasementet 0,84. Den prosentvise reduksjonen i effektbehov fra en blokkoeffisient på 0,84 til den optimale 0,73 er 22,81%. Denne reduksjonen tilsvarer en utslippsreduksjon på 17,05 millioner tonn CO₂ og US\$ 1 326,4 millioner i sparte drivstoffutgifter årlig.

En anbefaling for videre arbeid er å videreutvikle designseriene hvor en kombinasjon av lengde og bredde er variert. Effekten av en variasjon i lengde i kombinasjon med bredde kan da bli undersøkt. Ved å anvende mer omfattende numeriske metoder (f.eks. CFD) for å beregne stille vannsmotstanden for hvert skrog kan man få mer nøyaktige og pålitelige svar. For at nye teknologi og designfilosofier skal bli implementert i skipsfart må det vise seg økonomisk bærekraftig. En totalvurdering av besparelser og utgifter bør derfor gjennomføres.

Contents

Scope of work.....	II
Preface.....	IV
Abstract	V
Sammendrag	VII
List of figures	XI
List of tables	XII
List of symbols.....	XIII
List of acronyms and abbreviations	XVI
1 Introduction	1
1.1 Background and motivation	1
1.2 World bulk carrier fleet	3
1.3 Design restrictions for bulk carriers	4
1.4 Previous work	7
1.5 Structure of thesis	11
2 Bulk carrier designs.....	12
2.1 KVLCC2 series.....	19
2.2 CBC series	20
3 Methods for resistance calculations.....	25
3.1 ShipX.....	25
3.1.1 Calm water resistance	25
3.1.2 Added resistance in waves	27
3.1.3 Gerritsma & Beukelman	29
3.1.4 Speed loss vs power increase.....	30
3.1.5 Importing designs to ShipX from DELFTship	31
3.2 Michlet.....	32
3.3 Benchmarking of numerical calculations.....	34
3.4 Empirical methods.....	36
4 Results.....	39
4.1 Comparison of calculation of added resistance in waves	39
4.2 Brake power as function of block coefficient.....	41
4.3 Effect of LCB on added resistance	43
4.4 Effect of LCB on brake power	44

4.5	Influence of bow design on calm water resistance	46
4.6	Influence of stern design on calm water resistance.....	47
4.7	Admiralty coefficient for Colombo Express and KVLCC2.....	48
5	Discussion.....	51
6	Conclusion.....	57
7	Recommendation for further work	58
8	References	59
	Appendix.....	62
	Appendix A Hull grids for the MOERI KVLCC2 series	62
	Appendix B Hull grids for the CBC series	63
	Appendix C Calm water resistance prognosis for the CBC series.....	64
	Appendix D Results from numerical and empirical calculations	65

List of figures

Figure 1 Block coefficient of Capesize and New Panamax bulk carriers as a function of deadweight (Kristensen, 2012)	4
Figure 2 Panamax (B>30.48m) transits through the Panama Canal (Canal de Panamá, 2013). 6	
Figure 3 Modification of aft lines of KVLCC1 by particle swarm optimization (Kim et al., 2016)	9
Figure 4 Design spiral for ship design (Taggart, 1980)	12
Figure 5 Optimal LCB for high-block ships	13
Figure 6 Optimum prismatic coefficient as a function of Froude number (Larsson & Raven, 2010).....	14
Figure 7 Significance of blunt and sharp bow with regards to wetted surface	15
Figure 8 Wave system created by pronounced shoulders (Steen, 2011)	16
Figure 9 Angle of run (Holden et al., 1980)	18
Figure 10 The hull grid for the widest and narrowest design in the MOERI KVLCC2 design series	19
Figure 11 Sectional area curve for the MOERI KVLCC2 design series	20
Figure 12 The hull grid for the widest and narrowest design in the CBC series	21
Figure 13 Sectional area curve for the CBC design series	22
Figure 14 Hull grid for original and modified bow of the CBC $C_b=0,8$	24
Figure 15 Added resistance in waves as the difference between still water resistance and total resistance (Arribas, 2007)	28
Figure 16 Typical wavelength dependence of added resistance R_{aw} of a ship at moderate Froude numbers in regular head sea waves (Faltinsen, 1990)	28
Figure 17 Comparison of Grigson friction line and ITTC57	33
Figure 18 Comparison of experimental results from Osaka University and MOERI with numerical results from Michlet and ShipX	34
Figure 19 Effective power for CBC series at 13 knots calculated by ShipX and Michlet.....	35
Figure 20 Effective calm water power for MOERI KVLCC2 at 13 knots	35
Figure 21 Added power in waves calculations for the CBC series at 13 knots	39
Figure 22 Added power in waves calculations for the MOERI KVLCC2 series at 13 knots	40
Figure 23 Comparison of brake power in waves as function of block coefficient at 13 knots for the CBC series	41
Figure 24 Comparison of brake power in waves as function of block coefficient at 13 knots for the MOERI KVLCC2 series	42
Figure 25 Effect of LCB on the added power required to maintain 13 knots in waves	44
Figure 26 Effect of LCB on the brake power required to maintain 13 knots in waves	45
Figure 27 Comparison of wave resistance coefficient of the original and modified bow of the CBC $C_b=0,8$ design.....	46
Figure 28 Sectional area curve for the original and modified bow of the CBC $C_b=0,8$ design	46
Figure 29 Calm water resistance for two different stern designs of the CBC $C_b=0,78$ design.	47
Figure 30 Admiralty coefficient for design variations of Colombo Express and MOERI KVLCC2	49
Figure 31 Sectional areas of the Colombo Express scaled design and the MOERI KVLCC2 $C_b=0,8$ design.....	50

List of tables

Table 1 Variation of the MOERI KVLCC2 design series..... 19
Table 2 Variation of the CBC design series..... 21
Table 3 Variation of LCB for the CBC $C_b=0,73$ design 23
Table 4 Variation of LCB for the CBC $C_b=0,68$ design 23

List of symbols

Symbol	SI unit	Explanation
R_{aw}	[N]	Mean added resistance in an irregular seaway
h_0	[-]	Standard deviation of the relative vertical motion amplitude between the ship and the free surface at the propeller position
H_s	[m]	Significant wave height
C_s	[-]	Still water coefficient
A_{33}	[kg]	Two dimensional added mass
AC	$[\frac{s^{\frac{8}{3}}}{N^{\frac{1}{3}}m^{\frac{2}{3}}}]$	Admiralty coefficient
A_M	[m ²]	Cross-sectional Area
B	[m]	Breadth
b	[-]	Constant in Katsoulis formula
B_{33}	[Nm/s]	Two dimensional damping coefficient
B_{WL}	[m]	Breadth waterline
c	[-]	Constant in Katsoulis formula
C_P	[-]	Prismatic Coefficient
C_V	[-]	Visocus resistance coefficient
C_w	[-]	Wave resistance coefficient
d	[-]	Constant in Katsoulis formula
f	[-]	Constant in Katsoulis formula
F_N	[-]	Froude number
k	[-]	Constant in Katsoulis formula
k	[-]	Form factor
L	[m]	Lenght
L_{WL}	[m]	Lenght waterline
P_D	[W]	Delivered power
P_E	[W]	Effective power
Q	[Nm]	Hull torque
Q_0	[Nm]	Open water torque

R_W	[N]	Wave resistance
S	[m ²]	Wetted surface
T	[m]	Draft
T	[N]	Propeller thrust
V	[m/s]	Ship speed
V_{za}	[m/s]	Amplitude of the relative vertical motion between the ship and waves
V_A	[m/s]	Speed of advance
β	[rad]	Wave propagation direction
ω	[1/s]	Wave frequency
C_b	[-]	Block coefficient
∇	[m ³]	Volume displacement
w	[-]	Wake fraction
η_0	[-]	Open water efficiency
η_H	[-]	Hull efficiency
η_R	[-]	Relative rotative efficiency
C_{lw}	[tons/m ³]	Lightweight coefficient
Δ	[kg]	Weight displacement
C_R	[-]	Residual resistance coefficient
C_F^{ITTC}	[-]	ITTC frictional resistance coefficient
C_{TS}	[-]	Calm water resistance coefficient
ΔC_F	[-]	Hull roughness coefficient
C_{AAS}	[-]	Air resistance coefficient
C_{BDS}	[-]	Resistance coefficient for transom stern
R_{TS}	[N]	Calm water resistance
ρ	[kg/m ³]	Water density
λ	[m]	Wave length
$S(\omega)$	[m ² s]	Wave spectrum
h_0	[m]	Propeller shaft immersion in calm water

R_n	[-]	Reynolds number
R_{APP}	[N]	Appendage resistance
R_A	[N]	Model ship correlation resistance
R_{TR}	[N]	Additional pressure resistance due to transom immersion
R_B	[N]	Additional pressure resistance of bulbous bow near the water surface
C_w	[-]	Wave drag coefficient
C_A	[-]	Aerodynamic drag coefficient
ρ_a	[kg/m ³]	Air density
U_a	[m/s]	Wind speed relative to ship speed

List of acronyms and abbreviations

Acronym	Explanation
CAD	Computer Aided Design
CFD	Computational Fluid Dynamics
CO ₂ e	CO ₂ equivalents
dwt	Deadweight tons
GHG	Greenhouse gas
GT	Gross tonnage
IMO	International Maritime Organization
LCB	Longitudinal center of buoyancy
LCG	Longitudinal Center of Gravity
LOA	Length Over All
L _{pp}	Length Between Perpendiculars
MCR	Maximum Continuous Rating
NURBS	Non-Uniform Rational Basis Spline
PSO	Particle Swarm Optimization
RANS	Reynolds averaged Navier-Stokes
RAO	Response Amplitude Operator
SBD	Simulation Based Design
SQP	Sequential quadratic programming
TEU	Twenty-foot equivalent unit
ULC	Ultra Large Containership
ULCC	Ultra Large Crude Carriers
VLBC	Very Large Bulk Carriers
VLCC	Very Large Crude Carriers

1 Introduction

1.1 Background and motivation

International shipping transports more than 80 per cent of global trade. Shipping is the most energy efficient and cost-effective method of international transportation for most goods; it provides a dependable, low-cost means of transporting goods globally, facilitating commerce and helping to create prosperity among nations and peoples (IMO, 2016a).

According to IMO (2015) in the year 2012, total shipping emissions were approximately 938 million tons CO₂ or 961 million tons CO₂e for GHGs (greenhouse gasses) combining CO₂, CH₄ and N₂O. For the period 2007–2012 shipping accounted for, on average, approximately 3,1% of annual global CO₂ and approximately 2.8% of annual GHGs on a CO₂e. If the global temperature increase is to be limited to 2C° within 2100, the shipping industry have to reduce it emissions by 60 percent, the same as other industries.

Based on existing ships the International Maritime Organization (IMO) has set a baseline for emissions. Ships built in the future will have to beat that baseline by a set amount, which will get progressively tougher over time. By 2025, all new ships will be required to be 30% more energy efficient than those built in 2014 (IMO, 2016b).

The world fleet has the potential to reduce emissions by 2030 by 500 MT or 30% below baseline in a cost efficient way, and by close to 60% if all measures are included (DNV, 2010). There is no single measure to obtain that reduction but the aggregated effect of several measures are identified by DNV to obtain a reduction. The measures include voyage execution, steam plant operational improvements, engine monitoring, hull condition and weather routing. The focus on how optimizing hull dimensions can contribute to emission reduction has been to a much less extent been researched.

Traditionally bulk carriers have been built to minimize construction cost and maximize cargo-carrying capacity. This has been economically sustainable due to low fuel prices for international shipping. The low fuel prices do not act as an incentive for designing energy efficient ships with good hydrodynamic characteristics. As fuel prices have been rising the last decade energy inefficient hulls are being punished with rising ship operating costs and show their vulnerability for the fluctuation in fuel prices. Recent fuel price falls in 2016 have to some extent weakened the focus and removed the economic benefits of reducing fuel consumptions of ships. However, the future IMO requirements will be an incentive for designing energy efficient ships independent of rise or fall in the fuel prices.

Combined there are several factors pushing towards increased energy efficient ships in general, and in light of the previous design philosophies for bulk ships it is expected that bulk carriers have a significant potential for improvement. Today, naval architects face a number of restrictions on main dimensions before the design of a hull even has begun. There are restrictions given by the owner of the ship, port restrictions, restrictions by canals and rivers and legislative limitations. The restrictions faced may lead to suboptimal designs and solutions, giving ships with unnecessary high fuel consumption and emissions.

It is therefore of great interest to investigate how speed performance and power requirements may be improved by lifting some of the restriction on main dimensions when designing ships hulls. If the cost savings surpass the expenses required to lift some of the restriction, both cost and emissions may be reduced.

Lately we've seen a greater awareness around how the power requirements in waves and actual sea conditions differs from the power requirement in calm water conditions. The two conditions might require different designs to optimize performance, and there has been a shift towards adapting designs to better performance in waves and actual sea conditions.

Lindstad et al. (2013) introduce the idea that increasing the breadth of bulk carriers while keeping the length, draft and displacement constant, and thereby reducing the block coefficient, will be an efficient way of reducing the resistance and fuel consumption of a ship. For a given displacement, a ship design with a reduced block coefficient is postulated to reduce the fuel consumption pr. freight unit. Lindstad et al. (2013) uses an empirical model based on Holtrop and Mennen (1984) to calculate the effect on the brake power of different block coefficients given a constant length, draft and displacement i.e. the breadth is varied to change the block coefficient. The result show that the brake power is reduced with a decreasing block coefficient. Being based on empirical formulas there are weaknesses to the method proposed by Lindstad et al. (2013), since empirical formulas are based on previous designs and not necessarily reflecting the characteristics of unconventional ship designs. When evaluating hull dimensions outside the range the data the empirical data is based on, the result obtained has high uncertainty. This is due to the fact that results then are obtained extrapolating the regression analysis which the empirical method applies. Empirical models only use main characteristics of a design to calculate the power requirement, meaning that there is necessary not an actual ship design being evaluated.

With increasing computational power, the possibility to perform more advanced Computational Fluid Dynamics (CFD) calculations within a shorter time span increases. Combining these calculations with a Computer Aided Design (CAD) program, hull lines can be improved directly based on feedback from CFD calculations. Examples of this approach is further described in the Previous work section. The coupling between CFD resistance calculations and CAD programs opens for very powerful and efficient design processes. The applications of this method is today, in large extent, limited to optimize a given hull design with restricted hull dimension. This is due to the fact that the optimization often happens after the main dimensions of the hull has been fixed, leaving little room for larger changes. Thus, the method combining CFD resistance calculations and CAD programs is applied optimizing a single hull. Compared to Lindstad et al. (2013) this method will fail in producing an optimal design that covers a wide range of hull dimension, thus possibly sub optimizing around a single hull design with restricted dimensions. CFD also have a weakness in calculating the added resistance in waves since the current available calculation models are unstable and very time consuming. If added resistance in waves is included in the optimization process, CFD can hardly be applied.

This master thesis investigates the effect on power requirements of bulk carriers with reduced block coefficient using actual ship designs and numerical tools for the resistance calculations, including added resistance due to waves.

The ship designs disregard current dimensional restrictions to not exclude the possibility of finding optimal hull designs outside the restrictions. Using actual ship designs and numerical tools will reduce the uncertainty of the empirical calculations and give a more credible conclusion about the effect on brake power of reduced block coefficient on bulk carrier designs. By using a simplified numerical method with less computational time it is possible to cover a wide range of hull designs where the dimensions are varied. By doing using a simplified numerical method on a wide range of hull designs, this thesis attempts to bridge the gap between the idea of Lindstad et al. (2013) and the methods used in simulation based design. The results are compared with the results obtained by Lindstad et al. (2013) and Holtrop and Mennen (1984) to see if the trend with reduced brake power for reduced block coefficient also is found using numerical calculations methods. This thesis further investigates how the added resistance in waves varies with the variation in hull design and the longitudinal center of buoyancy.

1.2 World bulk carrier fleet

Bulk carriers are merchant ships that carry dry good in the cargo holds. The goods transported may be coal, grain, cement and ore, or other products that don't need to be packed during transport. The cargo holds of bulk carriers are across the whole breadth to maximize the cargo capacity of the ships. The cargo holds are separated in compartments each covered with hatches. The hatches allow for loading and unloading of goods and at the same time prevent water filling the cargo holds during transit.

Some bulk carriers are fully equipped to load and unload goods unaided. Bulk carriers able to unload unaided are referred to as self-discharges or geared carriers. Bulk carriers without the possibility to unload by itself is referred to as ungeared bulk carriers. To ease the unloading of goods the sides of the cargo holds are sloped.

According to Amdahl and Fuglerud (2003) the average size of the world bulk carrier fleet is 50 000 deadweight tons (dwt). In total numbers bulk carriers in 2014 made up 12,9% of the world merchant fleet (Equasis, 2014). In terms of gross tonnage bulk carriers in 2014 made up 35,1% of the worlds merchant fleet total gross tonnage (Equasis, 2014). 77,8% of the worlds bulk carriers are defined as large or very large with a gross tonnage larger than 25 000. When it comes to emissions Psaraftis and Kontovas (2009) estimates that dry bulk vessels emit 18% of the total CO₂ emission of the world commercial fleet above 400 GT excluded passenger ships.

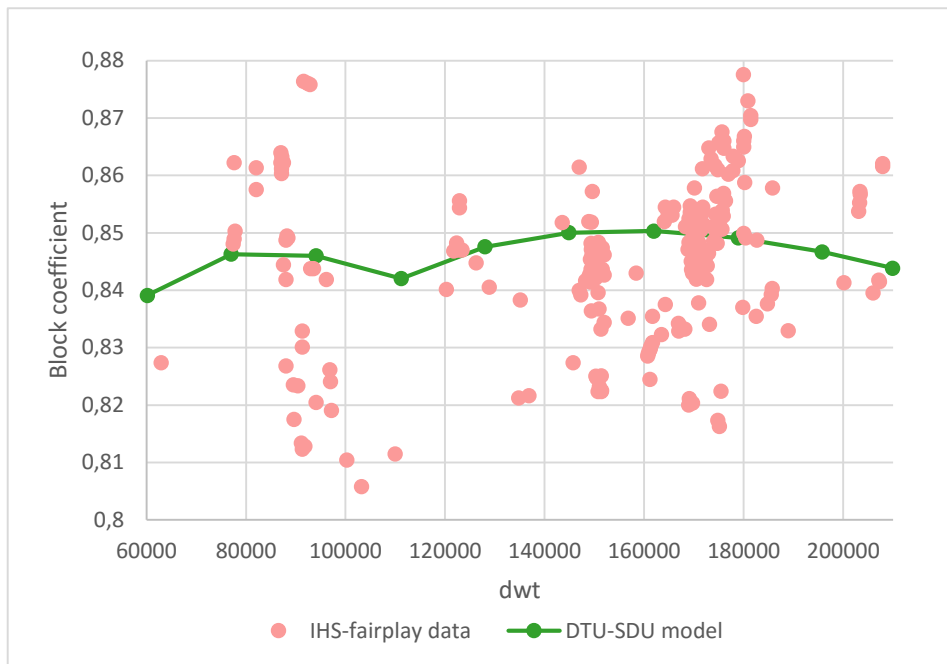


Figure 1 Block coefficient of Capesize and New Panamax bulk carriers as a function of deadweight (Kristensen, 2012)

In Figure 1 the block coefficient of Capesize and New Panamax bulk carriers (60 000<dwt<200 000) can be seen as a function of deadweight. The graph is based on data extracted from the IHS-Fairplay database. There is a spread in the data but the lowest block coefficients all exceed 0,78. The fullest bulk carriers have a block coefficient of 0,88. The DTU-SDU model is the average block coefficient based on a regression analysis of all the Capesize bulk carriers in the IHS-Fairplay database. As seen from the regression analysis there is not, for any deadweight, a block coefficient below 0,84 in the existing capsizes fleet. Kristensen and Lützen (2012) conclude with that for the last 30-40 years a large part of the world bulk carrier and tank fleet the block coefficient has increased, the length displacement ratio has decreased and the Froude number has either been constant or increased.

1.3 Design restrictions for bulk carriers

When designing bulk ships, a number of restrictions have already been applied even before the naval architect has stated designing the ship. Many ships are designed for a designated route with a specified cargo size. A specified route will have several restrictions. The first restriction a ship is facing are port restrictions. Port restrictions include both draft, height, breadth and length. If the port has a maximum allowable draft less than a ships draft the port is either not accessible, or the ship has to reduce the deadweight to obtain the allowable draft. When reducing the deadweight, the transportation unit cost will increase due to costs connected to running a larger ship with reduced deadweight utilization. The height may be restricted by obstacles such as bridges when arriving a port. The breadth is restricted both by berthage and crane sizes. The length is also restricted by berthage and may also cause problems when navigating to and from a port.

Chinamax are bulk carriers with dimensions less than a length of 360 m, breadth of 65 m and draft of 24 m. Due to the large dimensions Chinamax ships serve a limited numbers of ports worldwide. They are especially serving ports in Brazil transporting iron ore to China, India, Europe and the Middle East.

Q-Max is the limiting size of LNG carriers wanting to dock at the LNG terminals in Qatar. The maximum dimensions are a length of 345 m, breadth of 53,8 m, height of 34,7 m and draft of 12 m.

Handysize and Supramax ship dominate the bulk segment. According to Maritime Connector (2015) they make up 71% of all bulk carriers above 10 000 dwt. Handysize are bulk carriers up to 35 000 dwt and Supramax are up to 59 000 dwt with a length of 150-200 m. Their popularity comes from being able to access a wide range of port all around the world.

As ship size has increased, especially within container shipping, ports have expanded their capacity to accommodate larger ships and remain competitive. In addition to the physical dimensions of the arriving ships, a port also has to adapt with strengthened mooring, increased tug capacity and increased crane and offloading capabilities. Increased crane and offloading capabilities often result in cranes having to be higher and have a larger outreach. International Transport Forum (2015) estimate that the required investments to accommodate for the latest size increase of ships, especially within container shipping, adds up to US\$ 0,4 billion.

In between ports, a ships size dictate where it can sail and which route it can take. Many ships have dimensions which are adapted to various canals, rivers and straits. Malaccamax is the maximum size of vessels passing through the Malacca strait. Malaccamax has a maximum length of 400 m, breadth of 59m and draft of 14,5 m. Suezmax is the limiting dimensions of ships passing through the Suez Canal connecting the Mediterranean Sea with the Red Sea. The Suez Canal have no locks limiting the passing ships and they are only limited by the canals outer dimensions. The maximum ship dimensions are a breadth of 77,5 m, height of 68m and draft of 20,1 m. The length of ships passing the Suez Canal is unlimited. The Suez Canal recently underwent a US\$ 8,2 billion upgrade. The upgrade did not increase the limiting dimensions but increased the number of daily sail throughs from 49 to 97 (BBC, 2015).

The largest bulk carriers are referred to Capesize or Very Large Bulk Carriers (VLBC) with over 100 000 dwt. Their size dictates that they have to travel around Cape of Good Hope or Cape Horn on trans-continental sailing and can only access a limited number of ports. According to Maritime Connector (2015) Capesize and VLBCs make up 10% of the world bulk fleet. However, their large size compared to other bulk carrier segments make them represent 62% of the world bulk carrier deadweight. The world largest bulk carrier is the ore carrier MS Vale Brazil. Completed in 2011 she has a length over all of 362 m, breadth of 65 m, draft of 30,4 m and 402 347 dwt. She operates on routes from Brazil carrying iron ore to ports in Asia and Europe.

Panamax is the limiting dimensions of ships passing the Panama Canal, connecting the Atlantic Ocean and the Pacific Ocean. Today Panamax vessels have dimensions up to length of 294,13 m, breadth of 32,31 m and a draft of 12,04 m. The precise value of the dimensions is due to the fact that they were defined in feet. Panamax ships are characteristics since they often have a very high L/B ratio, typically 6,75 to 7,1, due to breadth restrictions. The high L/B ratio causes problems for both stability and longitudinal hull strength.

When the expansion of the Panama Canal is completed in June 2016 the limiting dimensions, referred to as New Panamax, will be a maximum length of 366 m, breadth of 49 m and draft of 15,2 m. The size of the New Panamax segment will be between the Panamax and Capesize segment, reducing the numbers of ships in the lower part of the Capesize segment. New Panamax bulk carriers are sometimes referred to as “Mini-Cape”.

As seen in Figure 2, the number of Panamax (B>30,48m) transits through the Panama Canal have increased by almost 60% since the mid-1990s. In 2013 Panamax transits made up 58.4% of all transits (Canal de Panamá, 2013). The increase in Panamax transit illustrate the world wide increase in ship size both in the container and bulk ship segment. There are clear signs from the shipping market that advantage will be pursued in the dry bulk sector through increasing ship size (Stott & Wright, 2011). According to Stott and Wright (2011) there has been a growth in “mini-cape” size vessels, more than quadrupling the ships in this size since 2004. “Mini-cape” ships are typically around 160 000 dwt and satisfying the New Panama dimensions. These ships are examples of “early adopters” in the new post-expansion Panamax dry bulk sector.

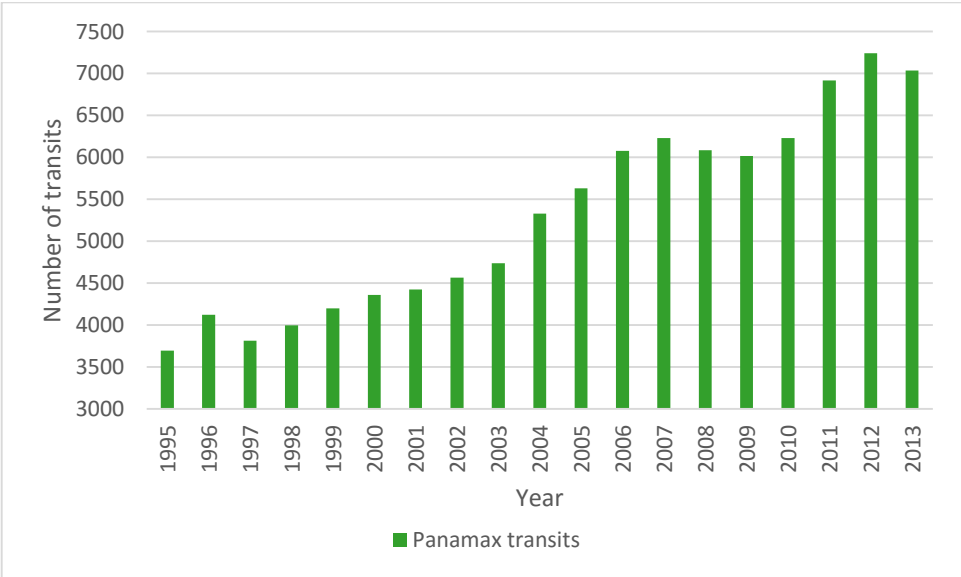


Figure 2 Panamax (B>30.48m) transits through the Panama Canal (Canal de Panamá, 2013)

1.4 Previous work

Lindstad et al. (2013) focus on how the expansion of the Panama Canal allows for new bulk carrier designs by lifting some restrictions on dimensions and the effect of this on brake power. In 2016 the project of expanding the Panama Canal will be completed. The project will create a new lane of traffic along the canal through the construction of a new set of locks, doubling the waterway's capacity (Canal de Panamá, 2016). The expanding of the canal will create a new segment of ships named New Panamax. The New Panamax dimensions will be a length of 366 m, a width of 49 m and draft of 15,2 m. The expansion will allow for increased traffic through the canal but both Ultra Large Crude Carriers (ULCC) and Very Large Crude Carriers (VLCC) tankers and the Maersk E and Trippel E class will still not be able to sail through.

Lindstad et al. (2013) states that earlier the focus has been on maximizing cargo-carrying capacity at the lowest possible building cost and not on minimizing the energy consumption. The paper establishes a new notation for still water resistance based on regression analysis of the existing fleet of bulk, container, tank and deep sea RoRo ships in combination with towing tank test data from MARINTEK. The new notation is presented as an option to using the model presented by Holtrop and Mennen (1984) for slender bulk designs. For added resistance in waves the model applies the STAWAVE-1 method presented by Van der Boom (2010). The STAWAVE-1 method uses breadth, bow length and significant wave height (H_s) as input. It is assumed short waves compared to ship length and small ship motions. North Atlantic conditions are modeled with 4 m waves as a proxy for the significant wave height 2-5,5 m, assuming that the accumulated annual effect of the waves resulting from head-waves, side-waves and following-waves will be 50% of 4 m significant head waves.

In the paper length, draft and displacement are kept constant while the breadth is varied to change the slenderness of the hull. This is done for two series of ships with a length over all of 224 and 246 m. The results show that when the block coefficient is reduced and the hull become slenderer and hence more energy-efficient, the emission per transported unit drops. The results are also combined with three different fuel price scenarios to evaluate the economic benefits of the hull designs. With increased fuel prices the economic benefits of slender bulk designs increase.

The notation used for calculating the still water resistance is used further in a paper by Lindstad et al. (2014). This paper also conclude that slender designs reduce emissions and increases the profit compared to the traditional full bodied designs. The reduction in emissions is in the paper connected to the introduction of the Energy Efficiency Design Index (EEDI) by the International Maritime Organization (IMO).

Bilgili and Celebi (2015) focuses on establishing an emission estimation approach for bulk carriers related to block coefficients. The paper uses regression analysis and real-time fuel consumption to establish the estimation. The real-time data are collected from three bulk carriers ranging from 35 364 DWT to 66 533 DWT. It should be noted that when calculating the block coefficient of the three ships Katsoulis formula is applied. Katsoulis formula was intended to use for block coefficient estimation in early stage design of ships.

Katsoulis formula is given as

$$C_b = k \cdot f \cdot \left[\frac{V}{\sqrt{D}} \right]^d \cdot \left[\frac{L}{B} \right]^{-b-c} \cdot \left[\frac{B}{T} \right]^{-c} \cdot L^{a+b+c+\frac{d}{2}} \quad (1)$$

In Katsoulis formula k, f, d, c, b and a are constants. Katsoulis deduced the values of constants from regression analysis, but unfortunately his values did not appear to give satisfactory agreement with the block coefficients of a wide variety of ship types for which good data was available (Watson, 1998). When Bilgili and Celebi (2015) use the predictive Katsoulis formula to calculate block coefficient of ships with given dimensions they obtain inaccurate coefficients. Even though the regression analysis is based on inaccurate block coefficients, it illustrates a concept of a bottom up approach using ships fuel data to establish a connection between block coefficient and fuel consumption.

Bilgili and Celebi (2015), Lindstad et al. (2014) and Lindstad et al. (2013) all presents empirical methods to optimize the block coefficients of ships with regard to resistance and emissions. The weakness of the methods is that they are empirical and do not present a method to evaluate detailed ship lines. Two ships with the same principal dimensions and block coefficient can have a substantial variation in design. The methods presented are also empirical using data from existing ships. Using these methods for estimating the resistance of ships will therefore not necessarily give accurate results for novel designs differentiating itself from existing designs. The methods are however useful when estimating principal dimensions and block coefficient of a ship in early stage design.

When having deciding upon the principal dimensions and block coefficient of a ship there are several options for how to design the ship lines. The principal dimensions are often decided by the owner or dimension restrictions before the naval architect starts to draw ship lines. Traditionally ship lines and dimensions often have relied on the naval architect's own experience and empirical calculations, to come up with a good and power efficient design. Experimental verification of designs has been available but the cost of running test in towing test limits the number of designs to be tested to a minimum. The lack of experimental or numerical verification of empirical calculations have reduced the process of optimizing hull designs. This may have caused a paradigm with suboptimal dimensional ratios. With increased computational power the opportunity to perform computer aided design has emerged and become more applicable.

Kim et al. (2016) apply parametric modification functions and particle swarm optimization (PSO) to perform hull optimization. A normal way of describing the hull surface is to use non-uniform rational basis spline (NURBS) manipulated with CAD systems. Kim et al. (2016) superimpose a parametric function on the original hull to obtain a modified hull. The superimposed parametric functions are defined as polynomials in the X, Y and Z directions. The advantage using parametric functions is that a limited number of parameters are changed and the effect of the changes can immediately be evaluated. This makes parametric functions more suitable for optimization than NURBS.

PSO is a gradient-free and global optimization algorithm. The PSO simulates the social behavior of a group of individuals by sharing their information during the exploring of design space. Each particle of the swarm has its own (individual) memory to remember the places visited during the exploration, and the swarm has its own collective memory to memorize the best location ever visited by anyone of the particles. Each particle is a potential solution of the optimization problem (Kim et al., 2016).

Sequential quadratic programming (SQP) is an efficient, gradient-based, local optimization algorithm. The method, based on the iterative formulation and solution of quadratic programming subproblems, obtains subproblems using a quadratic approximation of the Lagrangian and by linearizing the constraints (Kim et al., 2016).

As a flow solver Kim et al. (2016) uses a RANS solver utilizing the finite volume method to solve the Reynolds-Average Navier Stokes equations. To model the turbulence close to the hull the $\kappa-\epsilon$ model is applied.

When solving the single-objective function of minimizing the wave resistance coefficient C_w at a fixed ship speed. Kim et al. (2016) conclude that SQP is more efficient and converging faster than PSO. When solving the multi-objective function of minimizing C_w for two ship speeds PSO converges faster and deduces the Pareto optimal set. In addition, the use of parametric functions to describe the hull reduces the number of variables and the computation time. With design variables limited by box constraint and a fixed keel line the PSO reduce the wave resistance coefficient of the KVLCC1 hull with 10,5%. How the aft lines of the KVLCC1 are changed during the optimization process is seen in Figure 3.

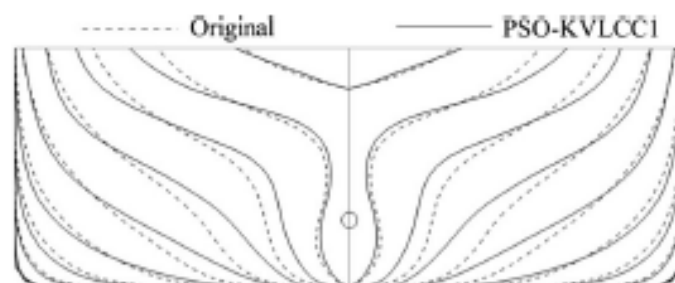


Figure 3 Modification of aft lines of KVLCC1 by particle swarm optimization (Kim et al., 2016)

Simulation based design (SBD) using particle swarm optimization and parametric functions are an efficient way of streamlining the process of optimizing a hull. There are however challenges to the method which still have to be solved to make simulation based design a viable alternative option for ship design. When performing particle swarm optimization there still have to be applied dimensional constraint to limit the computation. If these constraints are poorly chosen, the solution space may not cover the optimal solution and become sub-optimal. The parametrization of the hull has low autonomy to make modifications to the hull since the modification only is dependent of the parametrization. This may be overcome by using more complex parametrization, but this again increases computation time. When applying SBD a suitable flow solver also has to be chosen to obtain a credible result. The challenge with validation and verification of flow solvers are however not any more problematic in SBD than for normal numerical calculations.

The advantage of using CFD to calculate added resistance in waves is that non-linearities and actual free surface and geometry can be included. However, using CFD to calculate the added resistance in waves is very computational demanding and time consuming.

Several publications and studies attempt to estimate the possible savings on hull optimization. Jarabo and McMillan (2013) estimate up to 10% fuel savings compared to “standardized” designs benefiting new technology to optimize hull dimensions. Proposed measures are more extensive use of CFD for full scale flow simulations to verify potential fuel savings, and in greater extent considering intended usage and operating profile of a ship when designing the hull. Moreover, it is estimated a potential 10% fuel savings by retrofitting bulbous bows on ships constructed without, and up to 8% for ships with an existing bulbous bow designed for different operating speeds and loading conditions.

A guidance by ABS (2013) determine that by increasing the length/breadth ratio and/or increasing the length and reducing the block coefficient can provide reductions in propulsion fuel consumption up to 3-5%. This is explained with that over typical ranges of length-breadth ratios and breadth-draft ratios the reduction in wavemaking resistance from increased length and reduced C_b offsets the increases in wetted surface and therefore the frictional resistance. In addition, a further 5-8% propulsion fuel reductions are anticipated through optimization of hull form (lines) and propellers.

In 2013 a joint cooperation between DNV-GL, APL and HHI launched an Ultra Large Containership (ULC) design. The design of the hull is more adapted to “off-design” conditions with slow steaming and reduced deadweight utilization. The design is claimed to be 20% more energy efficient per TEU compared to existing designs and reduce the installed propulsive power with 16% (Maritime Professional, 2012).

DNV-GL has also been involved in a project with Wartsila and SDARI where the aim was to reduce fuel consumption and emissions for a handysize bulk carrier concept design, named Green Dolphin 38. Conservative estimates from the first pilot project carried out on the Green Dolphin 38 design, show that a saving of 2% can be achieved, which equates to 80 tons of fuel/year and a saving of USD 50 000/year. Corresponding figures for a typical Capesize bulk carrier are 200 tons of fuel/year and a saving of US\$ 120 000/year (DNV-GL, 2014).

1.5 Structure of thesis

In this thesis the idea of decreasing the block coefficient of bulk ships with a constant length, draft and displacement is investigated.

The first chapter, Bulk carriers design, describes the current design procedures and philosophies of bulk carriers in general. Two sections then describe how the two design series in this thesis were designed and their characteristics.

The following chapter, Methods for resistance calculations, outlines the theoretical background of the numerical methods used for the calculations of the resistance of the designs. The numerical methods are then benchmarked to decide which method to use in the calculations. Additionally, the empirical methods used are described.

Based on the calculation methods outlined the results from the calculations are presented and described in the Results chapter. In this chapter there is also a short discussion of each individual result. The Discussion chapter addresses the result combined and their implication for future bulk carrier designs. The potential emission and fuel savings are estimated given some rudimentary assumptions. The last part of the chapter discusses the applied method, with its strength and weaknesses.

In the Conclusion chapter a conclusion is drawn based on the results and the discussion. The effect of reducing the block coefficient with constant length, draft and displacement is outlined. The thesis is concluded by the Further work chapter which summarized the aspects that should be investigated to further develop the concept in this thesis.

2 Bulk carrier designs

The process of ship designing is an iterative one. The design of the ship has to balance a number of different elements until a satisfying result is obtained. The main dimensions are governing for the performance of a ship and as previously mentioned there are several design restrictions which can limit the main dimensions of a bulk carrier. A full design process of a ship is an iterative process where the design goes through various steps which are repeated and updated based on previous iterations. The iterative design process usually consists of a concept design feasibility study, a preliminary design, a contract design and is completed with a detailed design. This iterative design spiral with the different processes in each repetition is seen in Figure 4.

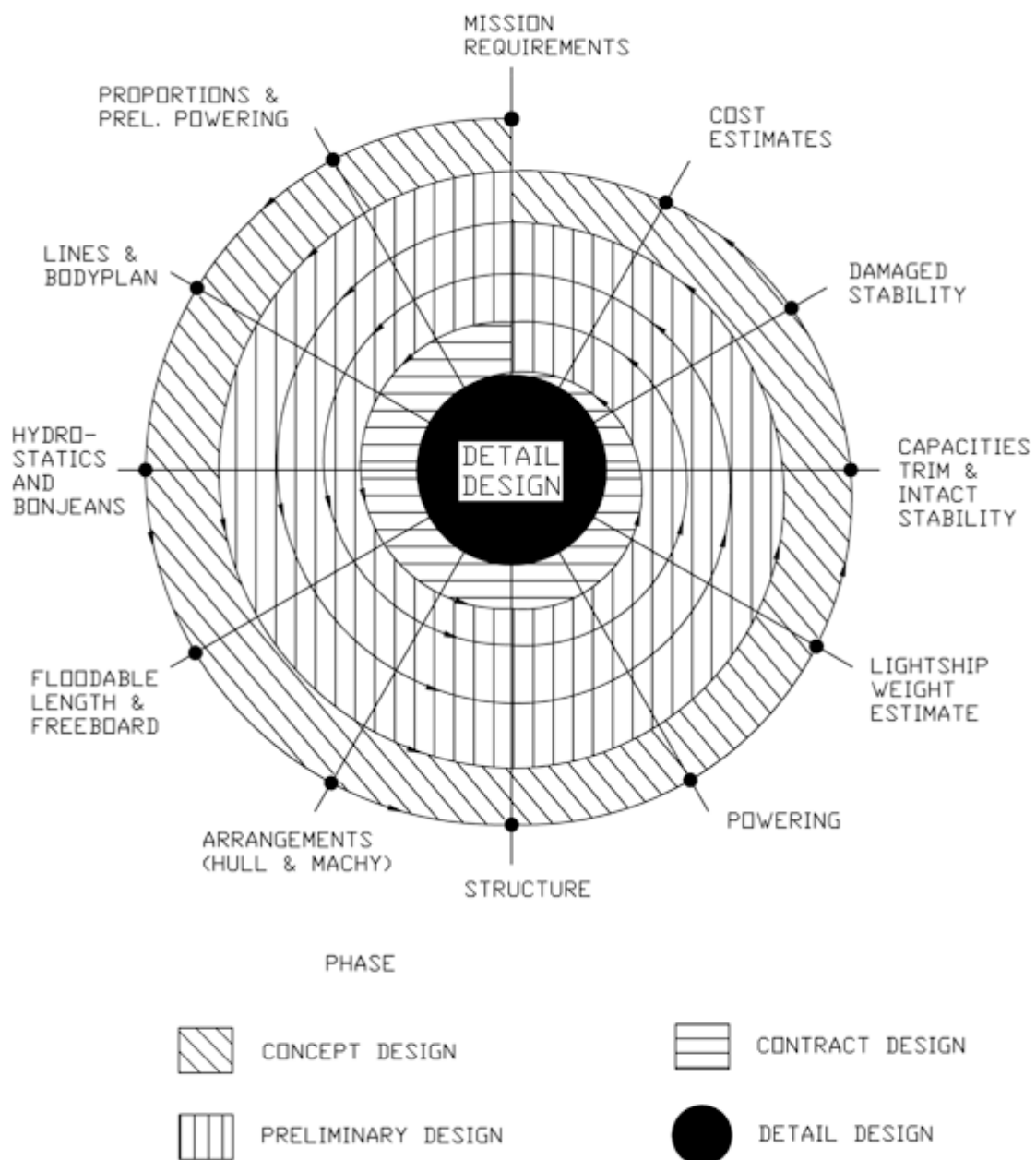


Figure 4 Design spiral for ship design (Taggart, 1980)

The aim of this thesis is not to produce a complete design of a bulk carrier. The process of deciding machinery arrangements, setting up the general arrangement, calculating structural integrity, full stability and damage stability calculations and cost estimations, as illustrated in Figure 4, would be very time consuming and outside the scope of this thesis. The scope of this thesis is to optimize the hydrodynamic properties of bulk carriers. The design spiral is therefore shortened in this thesis with focus only on the design of the hull, ship lines and estimation of powering. The shortened design spiral implies that on a later stage, not assessed in this thesis, the full design of the ships will have to be adapted to the hull design.

When designing the hull and ship lines the focus has been on optimizing the bow, the transition between the bow and parallel midship area (forward shoulder), the parallel midship body and the stern area. Moreover, there has been a focus on the position of the longitudinal center of buoyancy. When deciding the main dimensions, these are decided without considering the dimensional restrictions described in Design restrictions for bulk carriers.

The longitudinal center of gravity (LCB) is the volumetric center of the ship and through this point the buoyancy is acting. The position of the LCB is an indication on how the fullness of the ship is distributed longitudinally. When positioning the LCB the longitudinal center of gravity (LCG) must be considered. If the distance between LCB and the LCG is too big then an unfavorable trim might occur. An aft trim is more favorable since it leads to increased submergence of the propulsion and steering. As seen in Figure 5, Jensen (1994) recommends a LCB behind midship with decreasing block coefficient under approximately 0,7. The LCB is moved backwards if volume is removed from the bow and the towards the stern.

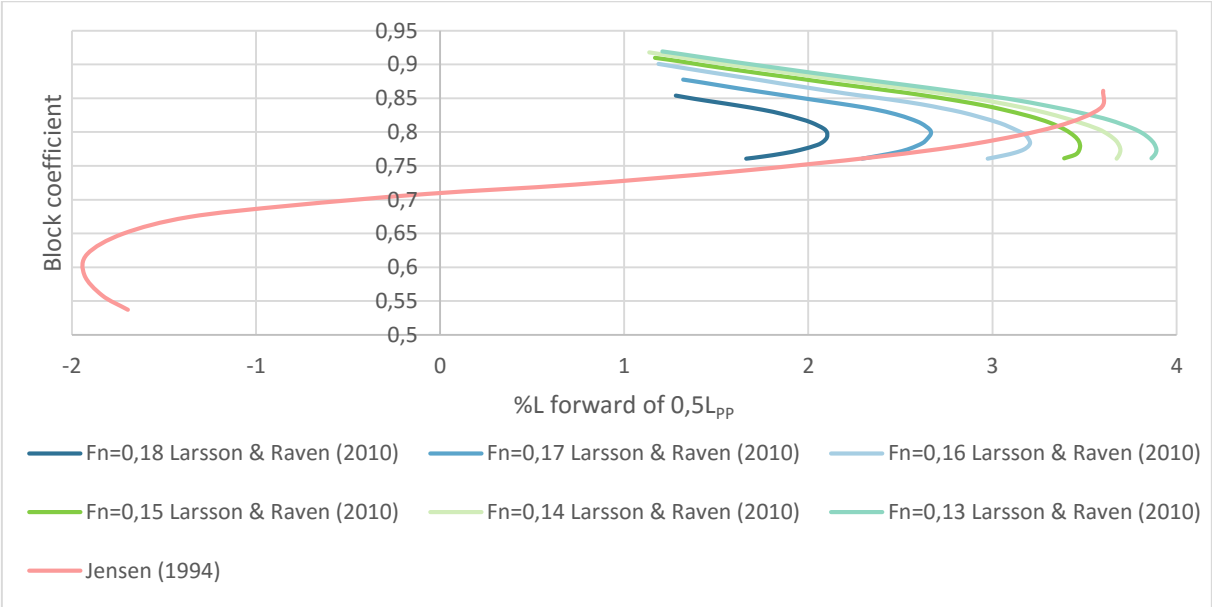


Figure 5 Optimal LCB for high-block ships

For all Froude numbers Larsson and Raven (2010) indicate that when the block coefficient approaches 1 the optimal position of LCB approaches midship. This is a natural consequence of the geometry of a high block ship since a hull with block coefficient of 1 necessarily have to positioned its LCB at the longitudinal center.

From the sectional curve the main ship parameters prismatic coefficient C_P and LCB (LCB). The prismatic coefficient is defined as

$$C_P = \frac{\nabla}{L_{PP} \cdot A_M} \quad (2)$$

In equation (2) ∇ is the displaced volume of the ship, L_{PP} is the length between the perpendiculars and A_M is the cross-sectional area. The block coefficient C_b may be found from C_P by using the midship coefficient C_M given as

$$C_b = C_M \cdot C_P = \frac{A_M}{TB} \cdot \frac{\nabla}{L_{PP} A_M} = \frac{\nabla}{L_{PP} TB} \quad (3)$$

Several publications link the optimal prismatic coefficient to the Froude number. As seen in Figure 6, lower Froude number vessels can have a higher C_P .

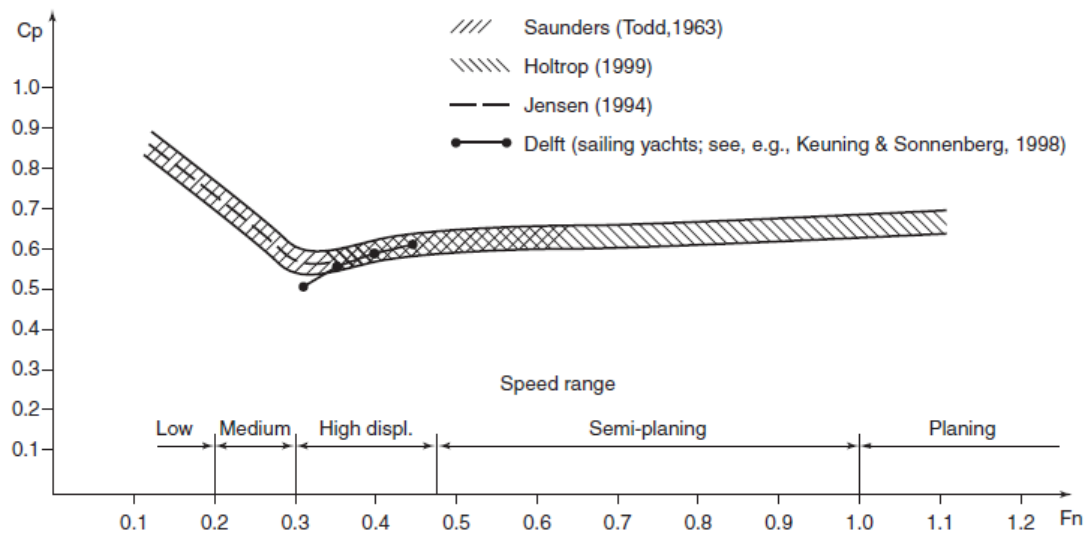


Figure 6 Optimum prismatic coefficient as a function of Froude number (Larsson & Raven, 2010)

Designing the bow of a ship with low Froude number is a balance between the bluntness of the bow to reduce skin friction and the sharpness of the bow to reduce wave resistance. For hulls with $F_n \leq 0,2$ the viscous resistance will be dominating. Minimizing the wetted surface for low Froude number hulls may therefore be effective for decreasing the total resistance. Minimizing the wetted surface with constant displacement can be done by making the bow bluff with a large entrance angle. An example of how a bluff bow minimizes the wetted surface is seen in Figure 7.

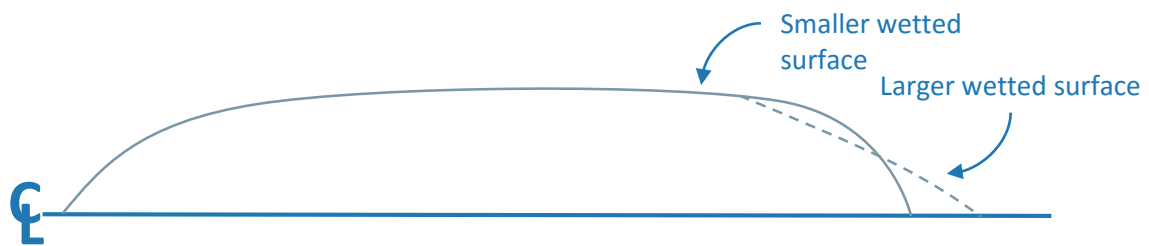


Figure 7 Significance of blunt and sharp bow with regards to wetted surface

For a ship with a medium displacement Froude number ($0,2 \leq F_n \leq 0,3$) the wave resistance is more dominant, favoring a sharper bow. The sharpening of the bow reduces the peak pressure that a bluff bow will cause and may thereby reducing the wave resistance. According to Larsson and Raven (2010), the LCB for a ship with a medium Froude number should be moved backward compared to the low Froude number ship. Moving the LCB aft will move displacement backwards sharpening the bow and creating a finer water entrance.

Resistance reductions in the region 5-20% has been obtained with bulbous bows between $F_N = 0,17 - 0,70$ (Steen & Minsaas, 2014). For a conventional bow there will be a downward pointing flow in the region above the inflexion point in the potential flow streamlines. Below the inflexion point, the innermost flow moves upwards. The combination of the downward and upward flow will create a vortex type separation that increases the resistance. By fitting a bulb at the bow, the downward flow will be more horizontal reducing the vortex separation. For F_N higher than 0,25 the main task of the bulb is to create a wave which is out of phase with the bow wave, and thereby (partly) canceling this wave. At small F_N the effect of a bulbous bow is moving volume forward and thereby removing displacement from the forward shoulder, making the water entrance finer.

To avoid a blunt bow and increased wave resistance from the bow wave, the bow may be sharpened and displacement moved aft. Moving displacement aft may create a more pronounced forward shoulder. A pronounced forward shoulder will increase the normal curvature of the hull. A too large normal curvature of the hull in the flow direction will cause unnecessarily deep wave troughs. Such curvatures may be avoided with a suitable shape of the sectional area (Larsson & Raven, 2010). A suitable shape will in this context imply a smooth transition between the bow area and parallel midship, with one continuous curvature in sectional area curve and waterlines.

If a ship has a very low L/B ratio the breadth of the ship can create very pronounced shoulders. Pronounced shoulders are rarely seen on existing ship designs since they often lead to the creation of several different distinct wave patterns at once, as seen in Figure 8. The wave patterns are hard to adjust in such a way that they are cancelling each other, creating several wave crests and troughs. The creation of the wave systems increases the wave resistance of the ship. The forward shoulder can be reduced, by moving volume backward to the aft shoulder. According to Larsson and Raven (2010), experiments indicate that this may reduce the resistance by 12% to 15% for a relatively high Froude number.

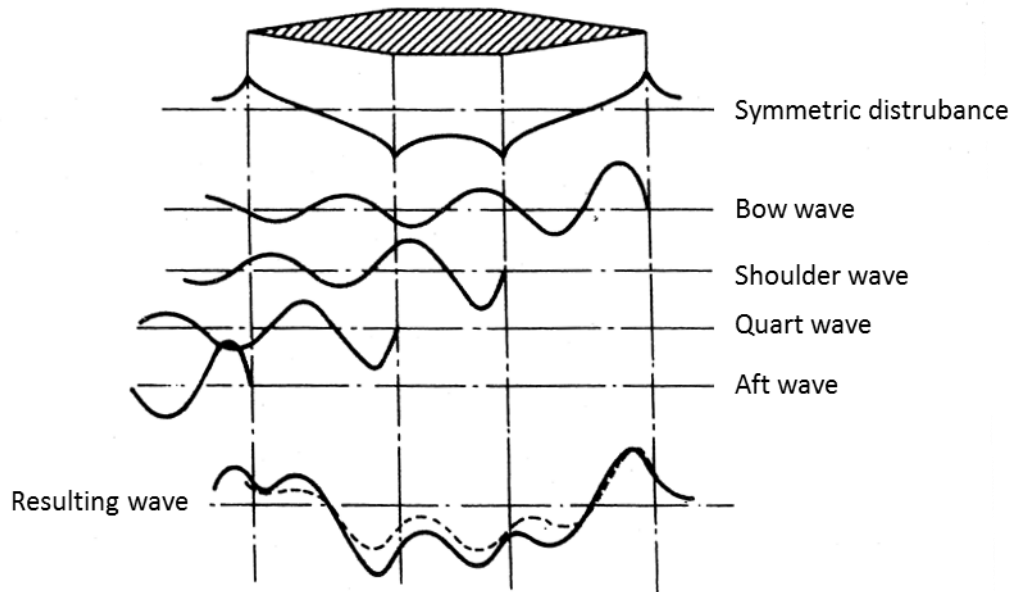


Figure 8 Wave system created by pronounced shoulders (Steen, 2011)

The midship section coefficients C_m is given as

$$C_m = \frac{A_m}{B_m \cdot T_m} \quad (4)$$

In equation (4) the subscript m denotes the midship section. Increasing the midship section coefficient with constant block coefficient may increase the run length and thereby decreasing the separation resistance, increase the entrance length and thereby decreasing the wave resistance and increase the frictional resistance due to increased wetted surface. When designing the midship section there is very often a horizontal flat bottom without any rise of floor for hulls with a $C_m > 0,9$. When designing some ship types, the midship section coefficients is to a certain degree dictated by the cargo transported e.g. containers. For bulk carriers the cargo does not affect the external midship design to large extent.

When designing the stern the wake fraction w is important. The wake fraction is defined as

$$w = 1 - \frac{V_A}{V} \quad (5)$$

In the equation for the wake fraction V_A is the local axial fraction. The most traditional stern is the V-shape, which has the lowest resistance (Larsson & Raven, 2010). However, the wake distribution for a V-shaped stern is very undesirable. A V-shaped high wake area is concentrated around the propeller center. This causes low propeller efficiency and large probability for vibrations and cavitation. When designing a V-shaped stern the floor lines should begin to lift immediately after the parallel body ends, to give a V-shape which will allow the hull to enter the water smoothly when the ship is pitching (Larsson & Raven, 2010).

A U-shaped and bulb shaped stern reduces variations in the propeller loading. The reduced variation in the propeller loading gives increased propeller efficiency, less cavitation and less vibration. The U-shaped and bulb shaped stern has a bilge vortex originating from the inflexion points at the stern. The vortex bilge increases the viscous resistance. The increased viscous resistance of the hull counteracts the increased propeller efficiency and therefore the main advantage of the U-shaped and bulb stern is the reduced vibration and cavitation.

For any ship the delivered power is desired to be minimized, not just the bare hull resistance isolated. To reduce the delivered power, the interaction between the hull and propeller must be considered. The power required to overcome the ship resistance at a given speed is denoted as effective power P_E . The propeller of a ship needs to deliver a higher power than the effective power since the propeller efficiency is below 1.0. In calm water the power delivered to the propeller, P_D , is given as

$$P_D = \frac{P_E}{\eta_D}, \quad \eta_D = \eta_0 \eta_H \eta_R \quad (6)$$

Where η_0 is the open water efficiency, η_H is the hull efficiency and η_R is the relative rotative efficiency. The hull efficiency is the ratio between the effective power P_E and the power delivered by the propeller and is proportional to the thrust T and speed of advance V_A . The hull efficiency can be written as

$$\eta_H = \frac{P_E}{P_T} = \frac{R_T V}{T V_A} \quad (7)$$

The relative rotative efficiency is the ratio between the torque delivered behind the hull and in open water. The difference in torque found behind the hull and in open water is due to two main reasons – because of the heterogeneous wake behind the model, the flow conditions over a given blade section as it rotates differ greatly from those in open water, so that the efficiency of any particular blade element will not necessarily be the same, and the relative amounts of laminar and turbulent flow on the propeller blades may be different in the two cases, the turbulence in the water behind the hull being greater than that in open water (Lewis, 1988).

The relative rotative efficiency is given as

$$\eta_R = \frac{\eta_B}{\eta_0} = \frac{Q_0}{Q} \quad (8)$$

Where Q_0 is the torque measured in open water when the propeller is delivering thrust and Q is the torque measured behind the hull.

Both η_H and η_R are influenced by the stern hull design. By systematical varying hull form parameters Holden et al. (1980) give guidelines for stern designs that optimize propeller performance. One of the guidelines is that waterlines should be finished with no abrupt corners or large waterline angles, blunt waterline angles must be avoided and the maximum angle of run should be kept below 30 deg. The angle of run as defined by Holden et al. (1980) is seen in Figure 9. Separation, particularly of the bubble type, should be as thin as possible to minimize momentum losses (Larsson & Raven, 2010). To obtain a good wake field and sufficient flow conditions at the propeller the stern needs to be slender.

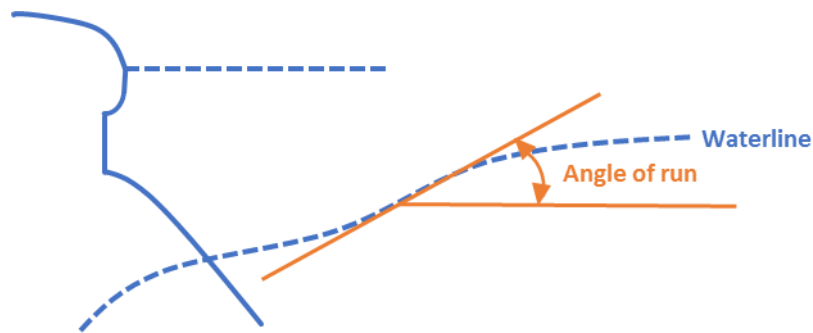


Figure 9 Angle of run (Holden et al., 1980)

Optimizing the total performance of the hull propeller and not only focusing on resistance makes it necessary to compromise some parts of the design. Designs with a LCB placed far back, may prove beneficial for added resistance in waves but indicates a full bodied stern where vortex separation and propeller inflow may cause problems. Therefore, designs with a LCB far aft is often disregarded due to poor propeller inflow conditions as a result of steep angles of run.

To design the hulls in this thesis the CAD program DELFTship was applied. DELFTship uses NURBS as a mathematical model to generate and represent surfaces and curves. Using NURBS is an efficient and intuitive way to create surfaces and curves.

To have a basis for the variation of the hull dimensions, two hull design series were created in DELFTship. Using a design series based on a parent hull as a basis for variation ensure that the geometrical features of each hull is comparable with other hulls within the same design series. The parent hulls in DELFTship consist of several stations describing the geometry of the hull. When creating the different hull design in a design series the ship station was kept as constant as possible. The stations were only moved in the transverse or longitudinal direction to obtain the correct dimensions, LCB and displacement. All the hulls designed in DELFTship can be found as .FBM files in the electronic appendix.

2.1 KVLCC2 series

The first hull design series is based on the MOERI KVLCC2 hull. The MOERI KVLCC2 hull is an academic hull designed to work as a benchmark model for both numerical and experimental results. It is widely recognized as a hydrodynamic well designed hull. The full scale dimensions of the MOERI KVLCC2 is a length of water line of 325,5 m, breadth of waterline of 58,0 m and draft of 20,8 m. To meet the dimensions of the longest series described in Lindstad et al. (2013) the hull was scaled to a length over all of 246 m and a draft of 14,5 m.

The displacement of all the design variations of the scaled MOERI KVLCC2 model was sought towards 93 500 m³, equivalent to 95 873 tons. This assumes a deadweight of 80 000 tons, equal to the deadweight in Lindstad et al. (2013), and a light ship weight of 15 873 tons. The lightweight coefficient is given as

$$C_{lw} = \frac{\text{Lightweight}[\text{tons}]}{L_{PP} \cdot B \cdot T} \quad (9)$$

Using the regression analysis of Kristensen (2012) the lightweight coefficient of a ship with given displacement is $C_{lw} = 0,0817 - 0,0000000486 \cdot DWT$. Comparing this with the assumed lightweight of the two design series, it is apparent that the assumed lightweight of the design series is proportionally oversized. In retrospect, this indicates that the actual deadweight of the MOERI KVLCC2 design series is somewhat higher than 80 000 tons.

The variations of the scaled version of the MOERI KVLCC2 parent hull is seen in Table 1. The hull grid for the widest and narrowest design in the MOERI KVLCC2 series is seen in Figure 10. The remaining hull grid is seen in Appendix A Hull grids for the MOERI KVLCC2 series. For all the designs there is assumed no trim.

Table 1 Variation of the MOERI KVLCC2 design series

L_{WL} [m]	239,764	239,763	239,763	239,763	239,763	239,763
B_{WL} [m]	45,008	41,908	38,53	35,458	33,472	32,652
∇ [m³]	95140,7	94243,5	93683,2	93560,4	93595,2	93543,5
Δ [tons]	97909,3	96986	96409,3	96283	96318,8	96265,6
C_b [-]	0,593	0,6308	0,682	0,7402	0,7844	0,8036
Wetted surface[m²]	12923,15	12883,17	12865,78	12926,12	12864,96	12956,44

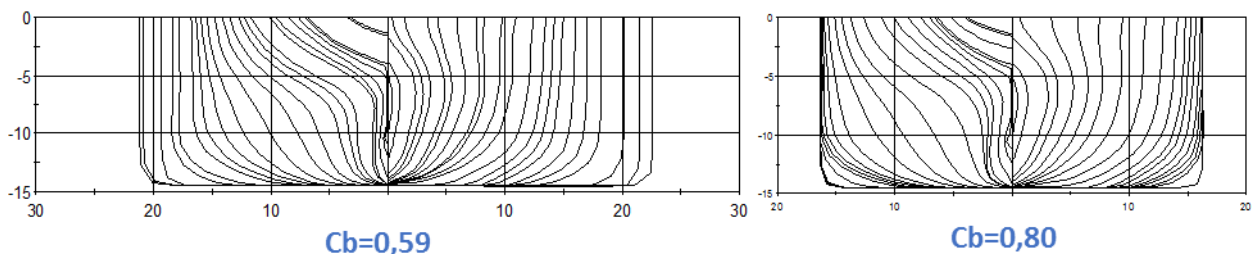


Figure 10 The hull grid for the widest and narrowest design in the MOERI KVLCC2 design series

The sectional area curves of the MOERI KVLCC2 design series is seen in Figure 11. The sectional area curve illustrates the how the sectional area is distributed longitudinally and the distribution of volume. As seen from Figure 11 the widest designs have very sharp transitions at the midship area. This is a necessary design feature to satisfy both the required breadth, length and displacement. A further development of the designs might have eliminated the sharp transition but the basic shape will remain.

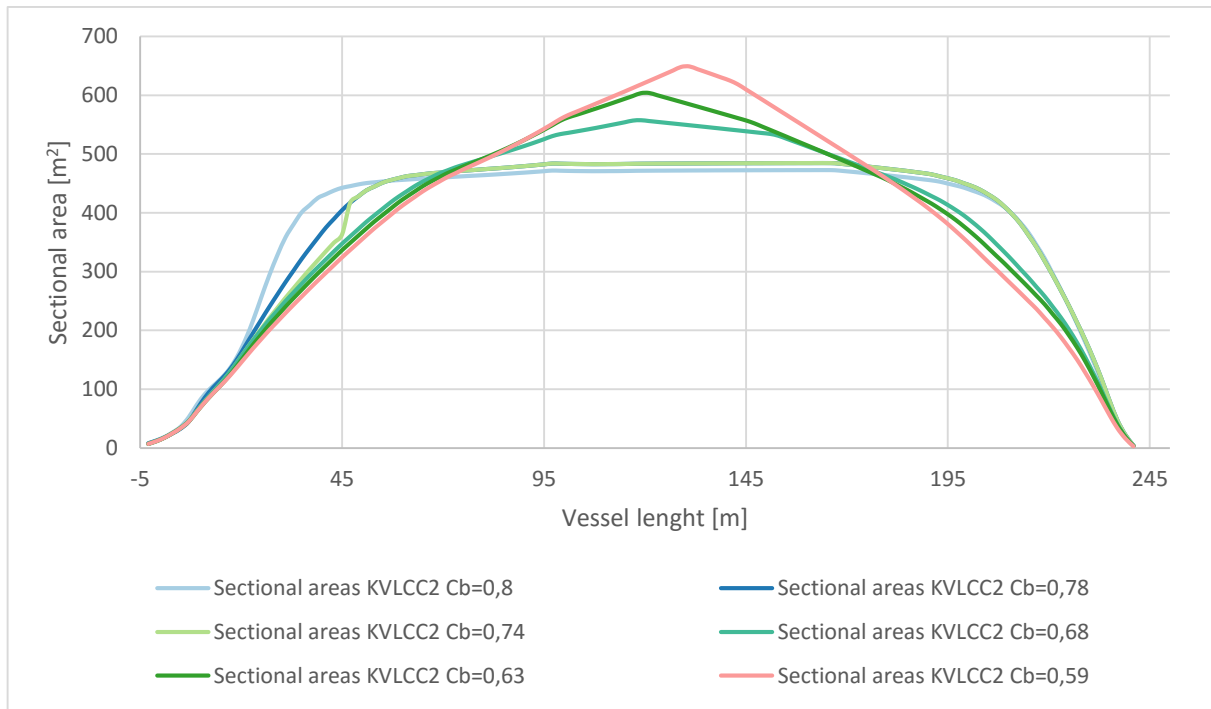


Figure 11 Sectional area curve for the MOERI KVLCC2 design series

The MOERI KVLCC2 hull is based on modern tanker designs. The bow of the hull is quite slender bow with a low entrance angle. There is a O-type faired-in bulb at the bow of the KVLCC2 series.

The breadth of the designs is evenly distributed until full breadth of each design. Compared to the CBC series the KVLCC2 series have a sharper stern shape. The sharper stern V-shape of the KVLCC2 series is more traditional and has according to Larsson and Raven (2010) the lowest resistance of the possible stern shapes.

2.2 CBC series

The second design series is an adaption of the hull design of a commercial bulk carrier. The commercial bulk carrier (CBC) is based on a self discharge dry bulk ship built in 1996. The dimensions of the CBC is a length over all of 199,7 m, breadth of 32,2 m and molded depth of 9,1 m. The dimensions of the CBC are smaller than the dimensions of the ships described in Lindstad et al. (2013). To meet the dimensions of the shortest series described in Lindstad et al. (2013) the hull was scaled to a length over all of 224 m and a draft of 14,5 m. The scaling implies that there are some deviations in the dimensional ratios of the scaled design compared to the original CBC hull, making it longer and shallower.

To have designs comparable with the main dimensions of a ship with LOA of 224 m and deadweight 80 000 tons, as presented in Lindstad et al. (2013), the CBC parent hull was designed with the variations seen in Table 2. The breadth of each design is increased with 10%, 20%, 30% and 40% compared to the Panamax breadth of 32,2 m. The total displacement assumes a light ship weight up to 15% of the deadweight. For all the designs there is assumed no trim.

Table 2 Variation of the CBC design series

L_{WL} [m]	216,809	216,809	216,809	216,809	215,518
B_{WL} [m]	32,2	35,42	38,598	41,895	45,076
∇ [m³]	88677	90075,6	89348,8	90381,2	91616,9
Δ [tons]	91257,5	92696,8	91948,8	93011,3	94283,0
C_b [-]	0,8581	0,7924	0,7212	0,6722	0,6333
Wetted surface [m²]	11979,4	11963,88	11898,49	11891,16	12066,16

The hull grid for the widest and narrowest design in the CBC series is seen in Figure 12. The remaining hull grids are seen in Appendix B Hull grids for the CBC series.

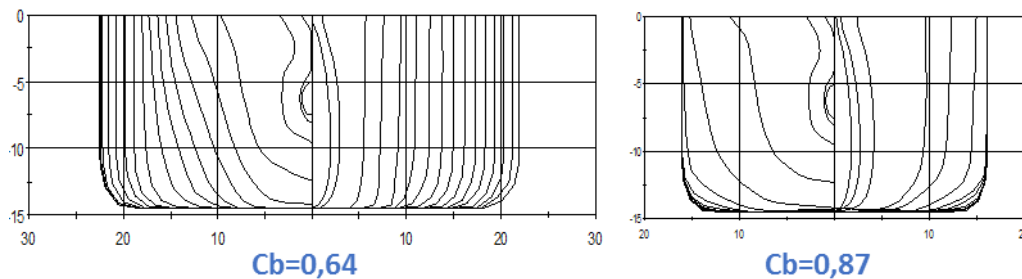


Figure 12 The hull grid for the widest and narrowest design in the CBC series

The CBC series have a Δ -type faired-in bulb, where the bulb is dropped shaped with the center of gravity is positioned in the lower part of the bulb. The bow is elongated vertically due to the scaling of the original CBC design.

The scaling has changed the breadth-draft ratio making to bow slender compared to conventional bulb designs. There has been no specific optimization of the bulb shape to reduce the wave resistance of each individual design in the series. The optimization of the bow to reduce wave resistance would be time consuming and outside the scope of this thesis.

From the bow and aft the transition from the bow is designed with smooth waterlines without any pronounced shoulders. For the designs with the lowest block coefficient and largest breadth the length-breadth ratio implies that there inevitably will be a pronounced shoulder around midships. The midship section of the CBC series have a midship section coefficient of 0,99. For the lowest block coefficient designs the length of the parallel midship section is however very short to provide smooth waterlines towards the bow and stern.

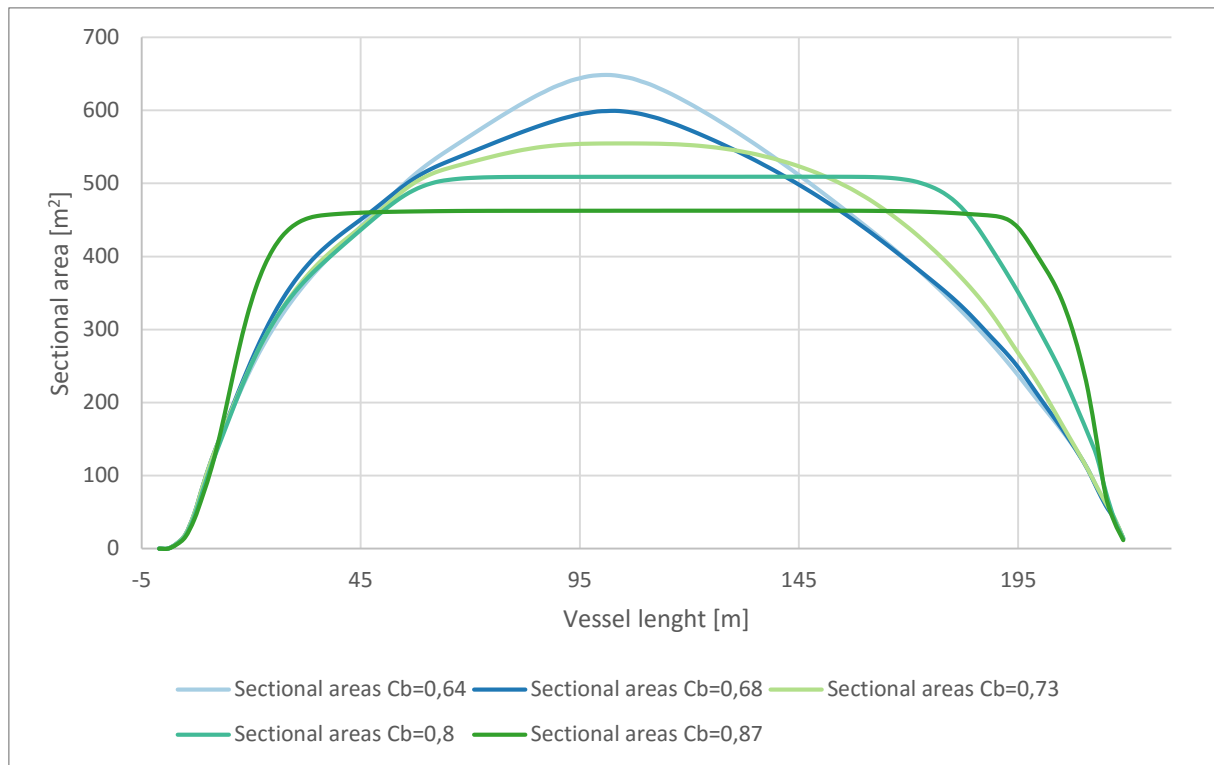


Figure 13 Sectional area curve for the CBC design series

In Figure 13 the sectional area curve for the CBC series is seen. Compared to the MOERI KVLCC2 series the CBC series have a smoother longitudinal distribution of the sectional area. It illustrates how the designs with reduced block coefficient move displacement from the bow section aft to the midship section. According to the prevailing design principles this will contribute to the reduction of the wave resistance.

A U-shaped stern is desirable from a hull efficiency and vibration point of view (Larsson & Raven, 2010). The stern of the CBC series has a U-shaped stern with a pronounced propeller hub. A pronounced hub is also known as a bulb stern. By going from the V-shape, via the U-shape to the bulb shape, the (propeller) vortex becomes stronger and stronger because the bilge radius gets smaller and smaller in the region in front of the propeller. This is a well-known and safe way to optimize the stern from a hull efficiency and vibration point of view (Larsson & Raven, 2010). The pronounced propeller hub of the CBC series results in waterlines with run angles above 30 degrees at the stern. Waterlines with angles of run above 30 degrees have risks of vortex separation increasing the total resistance. To investigate the effect of the unfavorable CBC series stern design an optional design for the $C_b=0,73$ design was created. The optional designed has lower angles of run to reduce the probability of separation. The optional design is compared with the original stern design to find any possible effects on the total resistance.

To investigate the effect of the position of the LCB the center has been moved systematically to six different positions for the $C_b=0,73$ and $C_b=0,63$ designs of the CBC series. This is done to investigate in what degree the position of the LCB effect the calm water resistance and added resistance in waves.

The variation of the $C_b=0,73$ design is seen in Table 3 and the variation of the $C_b=0,63$ design is seen in

Table 4. The position of the LCB is chosen to cover a range indicated by Jensen (1994) to be optimal, as seen in Figure 5. It should be noted that the position of the LCB as a percentage away from $L_{PP}/2$ is different in DELFTship and ShipX. This is due to different ways of defining the L_{PP} . The absolute position of the LCB measured as a function of total ship length is approximately equal in DELFTship and ShipX. Any deviation in the position of the LCB will be due to the importing of the hull geometry to ShipX from DELFTship.

Table 3 Variation of LCB for the CBC $C_b=0,73$ design

Displacement [tons]	C_b in ShipX	LCB from $L_{PP}/2$ DELFTship	LCB from $L_{PP}/2$ ShipX
91888,3	0,7207	-0,5 %	-1,836 %
91961,7	0,7213	0,0 %	-1,345 %
91576,1	0,7183	0,5 %	-0,868 %
91614,8	0,7186	1,0 %	-0,397 %
91958,4	0,7227	1,5 %	0,125 %
91908,1	0,722	2,0 %	0,615 %

Table 4 Variation of LCB for the CBC $C_b=0,68$ design

Displacement [tons]	C_b in ShipX	LCB from $L_{PP}/2$ DELFTship	LCB from $L_{PP}/2$ ShipX
92516,7	0,668	-0,5 %	-1,863
92891,2	0,6724	0,0 %	-1,42
93011,3	0,6722	0,5 %	-0,856
92707,7	0,6714	1,0 %	-0,376
92736,6	0,6728	1,5 %	0,107
92786,6	0,6731	2,0 %	0,624

CBC has a different bow design compared to the MOERI KVLCC2. The bow of the CBC has a sharper transition from the bow area to the full breadth and has a sharper increase in the sectional area curve. The bow of the MOERI KVLCC2 is fuller and at the same time more distributed in the longitudinal direction. This means that the bow section of the MOERI KVLCC2 is longer and reaches full breadth further aft compared to the CBC. The longitudinal distribution of fullness implies that the bow of the MOERI KVLCC2 will have a reduced wave resistance compared to the original bow of the CBC. To investigate this the CBC $C_b=0,8$ design is modified with a bow with the same design as the MOERI KVLCC2 $C_b=0,8$ design.

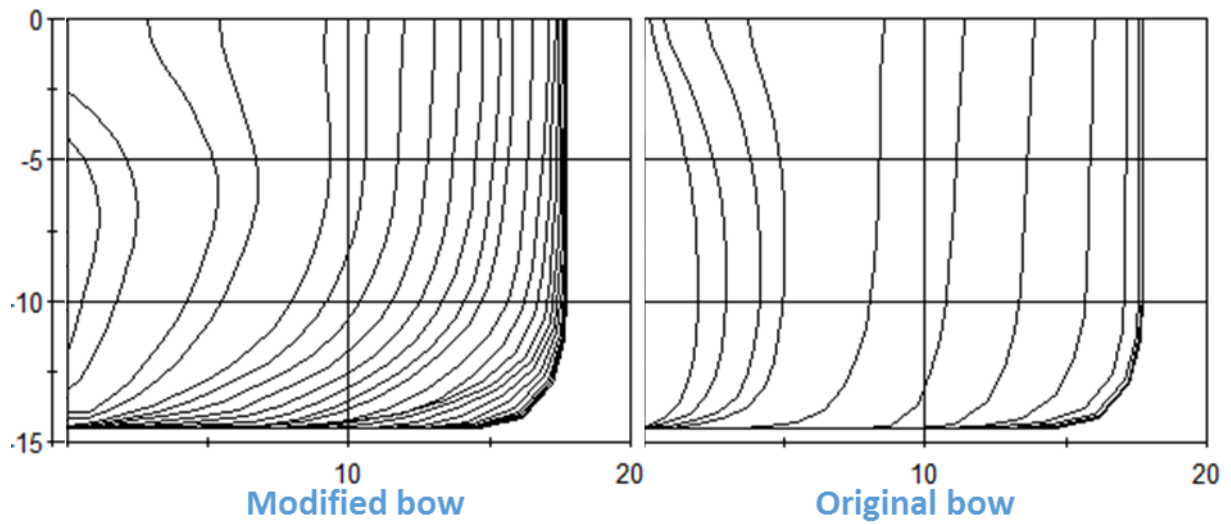


Figure 14 Hull grid for original and modified bow of the CBC $C_b=0,8$

In Figure 14 the hull grid for the two different bow designs are seen. Note that the distance between and number of stations are different in the two hull grids.

3 Methods for resistance calculations

This section introduces the numerical and empirical resistance calculation methods considered to calculate the calm water resistance and added resistance in waves. The initial choice of ShipX and Michlet as numerical calculation programs is based on an evaluation of a range of programs available based on the entry level and user threshold, computational time and the assumed accuracy of the program. The 3 first sections in this chapter explains the theoretical background for the numerical programs ShipX and Michlet and benchmarks the two numerical methods to conclude with which is most reliable to use in further calculations. The last section in this chapter presents the empirical methods of Holtrop and Mennen (1984) and Lindstad et al. (2013).

3.1 ShipX

3.1.1 Calm water resistance

Waveres is a ShipX plugin for calculating wave resistance. Waveres calculates the wave resistance of conventional monohull ships using potential theory (Steen & Fathi, 2000). Waveres can therefore be used as a fast and computational efficient way to calculate wave resistance for ships.

According to J.N. Newman (1976) the non-linear dynamic free-surface condition on the exact free surface can be written as

$$U \frac{\partial \phi}{\partial x} + \frac{1}{2} \left[\left(\frac{\partial \phi}{\partial x} \right)^2 + \left(\frac{\partial \phi}{\partial y} \right)^2 + \left(\frac{\partial \phi}{\partial z} \right)^2 \right] + g\zeta = 0 \text{ on } z = \zeta(x, y) \quad (10)$$

Further the kinematic free-surface condition is

$$U \frac{\partial \zeta}{\partial x} - \frac{\partial \phi}{\partial z} + \frac{\partial \phi}{\partial y} \frac{\partial \zeta}{\partial y} + \frac{\partial \phi}{\partial x} \frac{\partial \zeta}{\partial x} = 0 \text{ on } z = \zeta(x, y) \quad (11)$$

In equation (10) and equation (11) $\zeta(x, y)$ is the free surface condition. The body boundary condition on the exact body surface S_B can be written as

$$\frac{\partial \phi}{\partial n} = -U \cdot n_1 \text{ on } S_B \quad (12)$$

The normal vector on the body surface is $\vec{n} = (n_1, n_2, n_3)$ where the positive direction is into the fluid domain.

According to Steen and Fathi (2000) the problem in equation (12) is solved in two levels in Waveres. The first level use linear classical free-surface condition on the mean water surface. To correct for non-linearities at the bow 2½D methods are used in the second level.

When solving the linear approximation, the ship is assumed fairly slender. The non-linearities in the non-linear dynamic free-surface condition are neglected and the velocity potential ϕ is solved. The pressure is found from the velocity potential and the wave resistance R_w can be written as

$$R_w = \int_{S_b} P n_1 dS \quad (13)$$

The 2½D methods used to correct for non-linearities, are based in two-dimensional Laplace equation and three dimensional nonlinear free-surface conditions. For practical applications one assumes that the additional nonlinear effect is only important in the bow region and the 2½D methods are used from the bow to the section with local Froude number larger than Fn_{loc}^{min} , but not for the section after the midship (Steen & Fathi, 2000). In Waveres $Fn_{loc}^{min} = 0.6$, due to typical design Froude number for ships with low block coefficient.

Waveres is applicable to monohulls with a Froude number range of 0.15-0.45 and achieve best results in this range. Waveres is based for use on hulls with a block-coefficient C_b lower than 0,6 to 0,7. To make Waveres more robust it satisfies the boundary condition of the surface some distance away from the hull surface. The satisfying of the boundary condition makes it less prone to catch details in different hulls. Validation by comparing model tests and results from Waveres show that the numerical results agree well with the experimental.

Potential theory calculations do not include any viscous effects. When not including viscous effects resistance due to vortex shedding will not be included. For full hull forms, the effect of the aft body shape will not be reflected in the results.

When Waveres performs the calculation the output is the wave resistance coefficient C_W , a modified viscous resistance coefficient C_V and a correction factor F_{ds} . The residual resistance coefficient is defined as

$$C_R = C_W + C_V^{Waveres} - C_F^{ITTC} \cdot (1 + k) = C_W + C_F^{ITTC} \cdot (1 + k) \cdot F_{ds} \quad (14)$$

In equation (14) k is the form factor. In Waveres the form factor is calculated by using Holtrop's form factor for $C_b < 0.6$ and MARINTEKs form factor if $C_b > 0.7$. In the intermediate region $0.6 < C_b < 0.7$ linear interpolation is used. There is also an option to enter the form factor manually if other calculation methods are preferred. MARINTEK's formula is given as

$$k = 0.6\varphi + 145\varphi^{3,5} \text{ where } \varphi = \frac{C_B}{L_{WL}} \sqrt{((T_{AP} + T_{FP}) \cdot B)} \quad (15)$$

The form factor according to Holtrop is calculated as

$$k = -0.07 + 0.487118C_{14} \cdot \left(\frac{B}{L}\right)^{1,06806} \left(\frac{T}{L}\right)^{0,46106} \left(\frac{L}{L_R}\right)^{0,46106} \left(\frac{L^3}{L_R^3}\right)^{0,121563} (1 - C_p)^{-0.604247} \quad (16)$$

Where

$$C_{14} = 1 + 0.011 \cdot C_{stern} \text{ and } L_R = L \cdot (1 - C_p + 0.06 \cdot C_p \cdot \frac{LCB}{4C_p - 1}) \quad (17)$$

The residual resistance coefficient in equation (14) is combined with other resistance coefficients to find the calm water resistance coefficient. The calm water resistance coefficient of a ship is, according to Steen (2014) written as

$$C_{TS} = C_R + (1 + k) \cdot (C_{FS} + \Delta C_F) + C_{AAS} + C_{BDS} \quad (18)$$

The coefficients in equation (18) are defined as

$$C_{FS} = \frac{0.075}{(\log R_{nS} - 2)^2} \text{ Frictional resistance coefficient} \quad (19)$$

$$\Delta C_F = [110 \cdot (H \cdot V)^{0.21} - 403] \cdot C_F^2 \text{ Hull roughness coefficient} \quad (20)$$

$$C_{AAS} = \frac{\rho_a C_{DS} A_{TS}}{\rho_S S_S} \text{ Air resistance coefficient} \quad (21)$$

$$C_{BDS} = \frac{0.029 \cdot \left(\frac{S_{BS}}{S_S}\right)^{\frac{3}{2}}}{C_{FS}^{\frac{1}{2}}} \text{ Resistance coefficient for transom stern} \quad (22)$$

The total calm water resistance of a ship is

$$R_{ts} = \frac{1}{2} \rho \cdot V^2 \cdot S \cdot C_{TS} \quad (23)$$

When calculating the total calm water resistance, the air resistance is calculated based on the hull area above the waterline and a superstructure with an assumed area of 320 m². In the current version of Waveres the effects of trim, sinkage and transom stern is not included. The transom stern is included by the resistance coefficient for transom stern.

3.1.2 Added resistance in waves

A ship moving in waves will have an additional resistance from the calm water resistance. This resistance is referred to as added resistance in waves (R_{AW}). Model experiments in a model basin are normally carried out in regular or irregular head waves with the ship model towed at constant speed, and added resistance is measured as the difference between the mean added resistance in waves and the still water resistance measured at the same speed (Arribas, 2007). The difference between the still water resistance and mean added resistance in waves is illustrated in Figure 15.

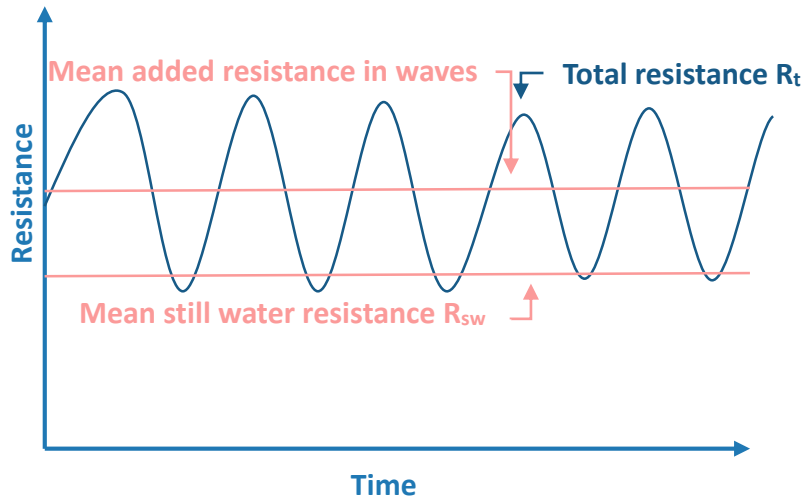


Figure 15 Added resistance in waves as the difference between still water resistance and total resistance (Arribas, 2007)

According to Arribas (2007) the added resistance is a non-viscous phenomenon dependent on radiated waves created by ship hull motions and incident waves reflected of the ship hull. Faltinsen (1990) states that the resistance from the bow wave reflection is dominant at small wavelengths compared to ship length while the added resistance due to ship motions is dominant at large wavelengths. As seen in Figure 16 the forces are at its maximum for $\lambda/L \approx 1$. Based on Figure 16 short waves are defined as $\frac{L_{WL}}{\lambda} \geq 0.5$ and long waves are defined as $\frac{L_{WL}}{\lambda} < 0.5$.

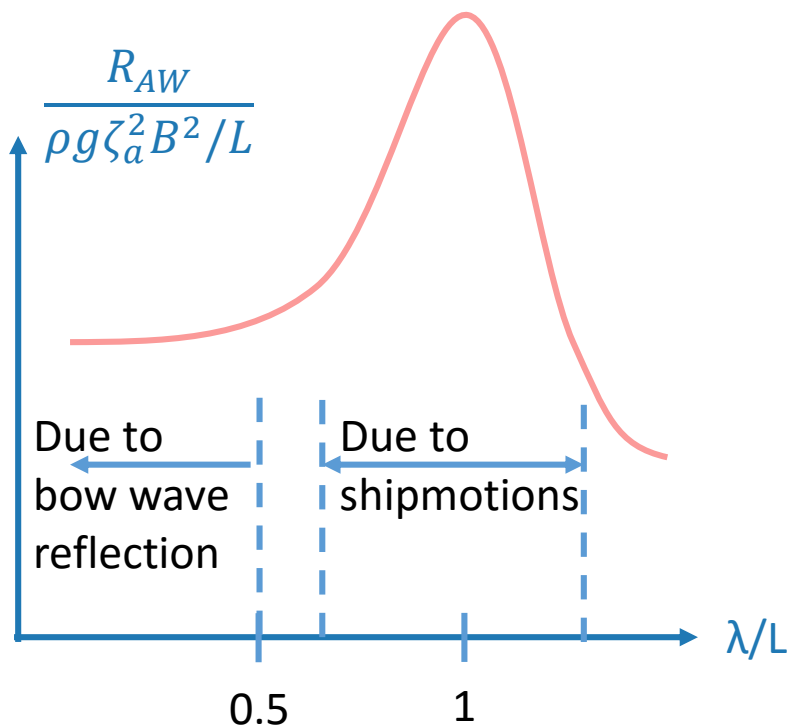


Figure 16 Typical wavelength dependence of added resistance R_{aw} of a ship at moderate Froude numbers in regular head sea waves (Faltinsen, 1990)

3.1.3 Gerritsma & Beukelman

The MARINTEK software Veres calculates the added resistance in waves using two different approaches. These two methods are referred to as Gerritsma & Beukelman and Pressure integration respectively

The Gerritsma & Beukelman method for calculating the added resistance in waves is based on a strip-theory approximation. Using strip theory implies that the variation of the flow in the cross-sectional plane is much larger than the variation of the flow in longitudinal direction (Faltinsen, 1990). This means that Gerritsma & Beukelman methods should be used with care for vessel with an unconventional hull geometry.

The method is based on calculating the added resistance in waves from determining the radiated energy of the damping waves. Gerritsma and Beukelman (1971) states that for the considered ships the added resistance in waves varies linearly as the squared wave height at constant wave length and constant forward speed. The equation for the added resistance in waves is given as

$$R_{AW} = \frac{k}{2\omega} \int_L \left(B_{33}^{2D} + U \frac{d}{dx} A_{33}^{2D} \right) V_{za}^2(x) dx \quad (24)$$

L is here denoted as the length of the ship and B_{33}^{2D} and A_{33}^{2D} are the two dimensional damping and added mass, respectively. V_{za}^2 is the amplitude of the relative vertical motion between the ship and waves. From the fact that V_{za} appears as a quadratic form in the integrand in equation (24), it follows that the resistance increase in waves is not merely the sum of the resistance increase of a ship oscillating in calm water and the resistance increase of a motionless ship in waves (Gerritsma & Beukelman, 1971).

The method presented by Gerritsma & Beukelman in 1971 is only valid for longitudinal waves i.e. head sea waves. Loukakis and Sclavounos (1977) extended the method to be valid for oblique waves. The derivation of the extension requires a thorough mathematical and physical reasoning, which is not presented in this thesis.

The Gerritsma and Beukelman method is known to give conservative estimates of the added resistance (Fathi & Hoff, 2015). According to Faltinsen (1990) the quality of the predictions of the added resistance in waves is sensitive to the accuracy of the calculations of the relative vertical velocity. In addition, being based on strip theory the method will neglect the effect of reflection of waves from the bow of the ship. Neglecting the effect of reflection will affect the accuracy for short waves at moderate Froude numbers.

When calculating the added resistance in waves Gerritsma & Beukelman is used. According to Guo (2011) Gerritsma & Beukelman will satisfactory predict the added resistance in long waves well but not for short waves. For low Froude numbers the method slightly underestimates the added resistance but very well for higher Froude numbers and zero speed. It is therefore recommended by Guo (2011) to combine Gerritsma & Beukelman with Faltinsen's asymptotic formula using the R -function described in Fujii and Takahashi (1975).

When calculating the added resistance in waves two approaches are used in this thesis. The first approach uses a regular wave with significant wave height of 4nm and a peak period of 10 s. The second approach uses a weighted scatter diagram representing the route from Mongstad to New York. A weighted scatter diagram consists of the long term statistics from several scatter diagram. Each scatter diagram represents a specific area and are weighted in the final scatter diagram according to the ratio the ship route has in each area. The weighted scatter diagram applied in this thesis is obtained from Nordås and Steen (2012). For both the regular waves and the weighted scatter diagram in ShipX the Pierson-Moskowitz wave spectrum is used. The Pierson-Moskowitz spectrum describes a fully developed sea obtained from measurements in the North Sea and is therefore a sufficient representation of conditions in the North Atlantic.

3.1.4 Speed loss vs power increase

When steaming in waves the master has several option for how to tackle this situation. The added resistance in waves will increase the total resistance if the speed is kept constant. If the propulsion system has additional power, the speed can be kept constant by increasing the output equivalent to the added power required to overcome the added wave resistance. Due to increased rpm to maintain constant speed the propulsion efficiency η_D will be reduced.

If the ship propulsion system operates at constant torque or at maximum continuous engine rating the rpm is reduced until equilibrium in torque is obtained. The reduction of rpm and power result in an involuntary speed loss in waves. Speed loss may also be voluntary to avoid slamming, green water on deck severe ship motions or propeller ventilation which reduces propulsion efficiency. Which of the two strategies the master will chose depends on many different factors such as weather, fuel price, available propulsion power, ship sea characteristics and time constraints for delivering the goods. A combination where the speed is reduced, but the power increased not to lose too much time, may also be applied.

In the ShipX Ship and Speed Powering plugin, both the required power to maintain speed in waves and the speed loss in waves is available. This gives two options when comparing the performance of different hulls: Compare the obtained speed at constant power for all ships or compare the required power to obtain a benchmark speed in waves. Comparing the obtainable speed for a constant power will mimic a more realistic shipping situation. However, in this thesis the ship designs are compared at a constant benchmark speed. Comparing the ship designs at a constant benchmark speed makes the results comparable to the empirical results obtained by Holtrop and Mennen (1984) and Lindstad et al. (2013)

In ShipX the speed loss is composed of the added resistance in waves, the thrust reduction in waves based on propulsion positioning, torque increase in waves based on engine limitations and wind resistance.

The mean added resistance in an irregular seaway can, according to Ringen et al. (2012), be calculated by combining the added resistance with a selected wave spectrum

$$\overline{R_{aw}} = 2 \int_0^{\infty} S(\omega) \left(\frac{\overline{F_1}(\omega; \beta)}{\xi a^2} \right) d\omega \quad (25)$$

Where $S(\omega)$ is the wave spectrum, $\overline{R_{aw}}$ is the mean added resistance in an irregular seaway and $\frac{\overline{F_1}(\omega; \beta)}{\xi a^2}$ is the added resistance operator function for a regular wave as a function of wave frequency ω and wave propagation direction β . The added resistance is calculated using Gerritsma & Beukelman.

When the ship moves in waves, the change in relative submergence of the propeller may lead to ventilation and cavitation and for extreme conditions with large vessel motions, the in-and-out of water effect will result in a sudden drop of thrust and torque following a hysteresis pattern.

In irregular waves, the loss effects are calculated as mean values over a wave period with the instantaneous value of the immersion h/R expressed as

$$\frac{h}{R} = \frac{h_0}{R} + \frac{S_a \sin(\omega t)}{R}$$

Where h_0 is the propeller shaft immersion in calm water and S_a is the standard deviation of the relative vertical motion amplitude between the ship and the free surface at the propeller position. The relative motion of the propeller is found in the ship RAOs.

To simplify and limit the amount of input data, the input for the engine is engine output [kW] at maximum continuous rating (MCR), engine rate of revolutions, gear ratio engine:propeller, mechanical efficiency, specific fuel consumption at 25, 50, 80 and 100% MCR [g/kWh], maximum percentage torque overload [%] and power settings to be used in calculations. Except for engine output, all these inputs are kept constant for all the calculations performed.

The propeller characteristics are developed using the Optimum Propeller Wizard function in SHipX. Based on the given number of propellers, number of blades, rate of revolution, maximum propeller diameter and submergence of shaft the optimal propeller diameter, optimal pitch ratio and blade area ratio is calculated. The blade area ratio is calculated using Burrills formula. Based in these inputs the open water efficiency η_0 is calculated.

3.1.5 Importing designs to ShipX from DELFTship

To perform calculations in ShipX the hull designs have to be imported from DELFTship. When importing the hull designs from DELFTship to ShipX they were imported as DXF 3D curves. DXF is a CAD file format for data interoperability between CAD programs. When importing DXF 3D curves to ShipX the curves will be translated into 3D lines, contour lines and stations distributed along the longitudinal length of the ship. The stations are created by defining several points with Y and Z value at the stations constant X value. The surface of the hull is defined by straight lines between the defined points. This is opposed to NURBS which creates a number of splines representing the surface.

The different methods of generating the geometry of the hull in ShipX and DELFTship lead to some discrepancies between the hydrostatic values of the same hull in the two programs.

The more coarse geometry of ShipX defined by straight lines, and not splines as in DELFTship, results in details of the hull in DELFTship are simplified and flattened out. The consequence of the hull line flattening is especially seen in the areas of the bulb and stern where hull lines are most detailed.

Another consequence of the geometry generation in ShipX is that sections of the stations lines appear jagged. The points defining the station lines are not evenly distributed horizontally. The jagged sections of the stations appear where the defining points are spaced up to 2 m apart in full scale. ShipX has the possibility to alter the geometry of a hull in the program. This is done manually point by point or through the hull transformation function where the main characteristics, prismatic coefficient, LCB and section lengths can be changed. The hull transformation function has limited applicability and only provide reasonable results and designs for small changes. This leaves altering the hull point by point the only option. With 40 stations and up to 40 points per station any manual alterations would be very time consuming. The most practical way is therefore to import the changed geometry from an external program (DELFTship) and keep the imported hull geometry unchanged, despite jagged station lines.

3.2 Michlet

Michlet is an open source research code utilizing thin ship theory to calculate wave resistance. The essential assumption is that the hull is thin, that is, the breadth is small compared to all other characteristic lengths of the problem. The resulting solution can be expressed in terms of a distribution of sources in the centerplane of the hull, with the local source strength proportional to the longitudinal slope of the hull (J. N. Newman, 1977).

Michlet only calculates the far-field waves. Near-field effects are most prominent close to the hull, especially near the bow, and die away quickly as the distance from the bow increases. Far-field waves are the waves far behind the ship where near-field effects are negligible. Wave resistance is the energy that is needed to sustain the far-field wave pattern (Cyberiad, 2015).

In Michlet skin friction is calculated either using ITTC 1957 or the Grigson friction line. The Grigson friction line is alternative to the ITTC presented by Grigson (1993) and created by plotting experimental data on frictional coefficients. Grigson found that the ITTC' 57 line did not provide an accurate representation of this data. To improve the accuracy required a change from the simple formula used for ITTC'57 and the use of two separate formulas for respectively the Reynold's number ranges of tank test models and ships (Watson, 1998).

According to Grigson (1993) the frictional coefficient in the model range $1.5 \cdot 10^6 < R_n < 2 \cdot 10^7$ is written as

$$C_f = \frac{[0.03 + 0.1377(\log R_n - 6.3)^2 - 0.06334(\log R_n - 6.3)^4]}{0.075} \cdot \frac{0.075}{(\log R_n - 2)^2} \quad (26)$$

The Reynold number is defined as $Re = \frac{vL}{\nu}$ where v is the ship speed, L is the characteristic length and ν is the kinematic viscosity. The frictional coefficient in the model range $10^8 < R_n < 4 \cdot 10^9$ is written as

$$C_f = \frac{[1.032 + 0.0286(\log R_n - 8)^2 - 0.006273(\log R_n - 8)^4]}{0.075} \cdot \frac{0.075}{(\log R_n - 2)^2} \quad (27)$$

The ITTC 1957 friction line is by ITTC (2002) defined as

$$C_f = \frac{0.075}{(\log R_n - 2)^2} \quad (28)$$

A comparison of the two different friction lines is seen in Figure 17.

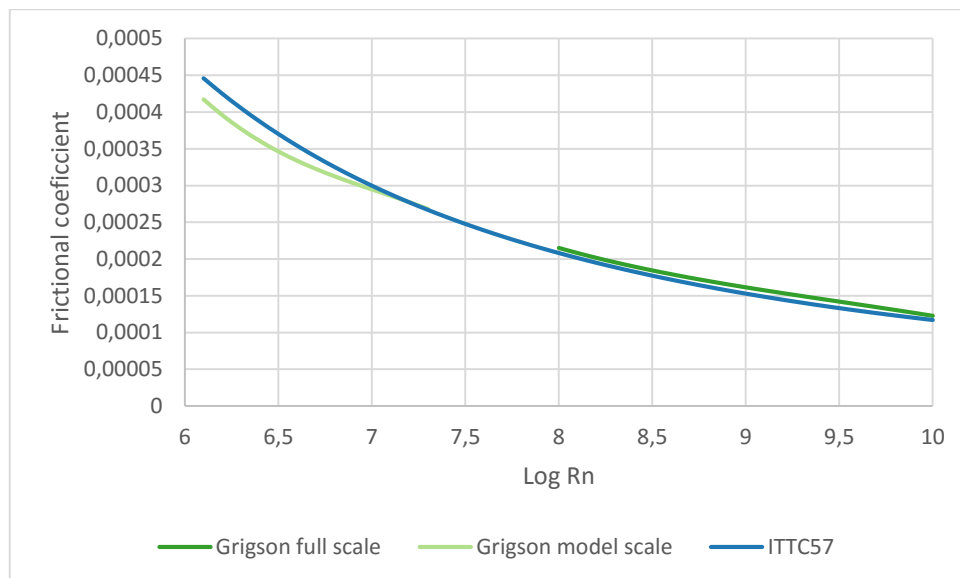


Figure 17 Comparison of Grigson friction line and ITTC57

At higher Froude numbers the agreement is reasonable, particularly in the context of experimental variations resulting from different turbulence stimulators and model lengths. At lower speed, however, the theory (Grigson friction line) seems to exaggerate the effects of interference by comparison with the experiments (J. N. Newman, 1977). Based on this the ITTC57 friction line is used to calculate the frictional resistance in Michlet.

DELFTship has a dedicated export function for exporting designs from DELFTship to Michlet. The dedicated function for exporting designs makes the exporting seamless and consistent for all designs. Michlet only allows importing of symmetric hulls, but this is not a limitation in this thesis.

3.3 Benchmarking of numerical calculations

ShipX and Michlet have to different approaches for calculating the calm water resistance. As earlier described, Michlet applies thin ship theory and ShipX applies potential theory. Being an academic standard hull there exist several publications investigating the resistance of the MOERI KVLCC2. By comparing result published in Larsson et al. (2013) the numerical calculations in ShipX and Michlet can be benchmark against experimental results for the MOERI KVLCC2. Larsson et al. (2013) presents experimental model test performed by MOERI and University of Osaka (OU) in connection with the Gothenburg 2010 CFD workshop.

The model tests performed by MOERI and OU was conducted in different model scales. The model scale resistance is therefore not directly comparable, but the residual resistance coefficient is independent of scale and comparable. There were performed several runs for the same speed by OU. The residual resistance applied in the benchmarking is the average of the results from OU and MOERI. The results are then scaled to full scale using the methods described in ITTC (1999).

In Figure 18 the calm water resistance for the full scale hull of MOERI KVLCC2 is calculated using the numerical results from ShipX and Michlet and the experimental results from MOERI and OU.

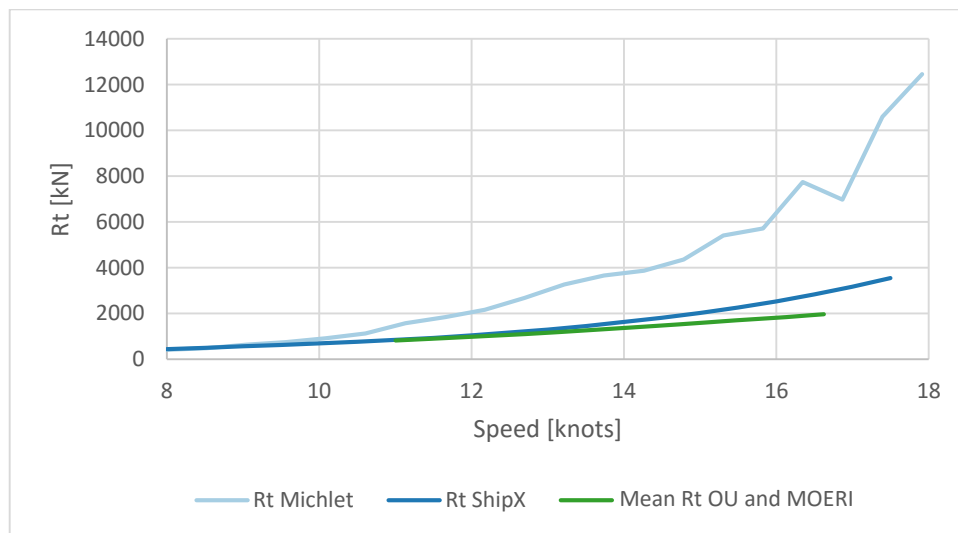


Figure 18 Comparison of experimental results from Osaka University and MOERI with numerical results from Michlet and ShipX

From the results it is evident that for the velocities investigated by OU and MOERI that the results from ShipX are closest to the experimental results. As the speed increases the resistance calculated by Michlet increases substantially, unlike the two other results. A similar comparison for the CBC series, with the same trend of increasing calm water resistance with increasing speed for the Michlet results, is found in Appendix C Calm water resistance prognosis for the CBC series.

For both the CBC hull series and the MOERI KVLCC2 hull series the calm water resistance is calculated using ShipX and Michlet. The calculations are done for the same velocities and otherwise same external conditions.

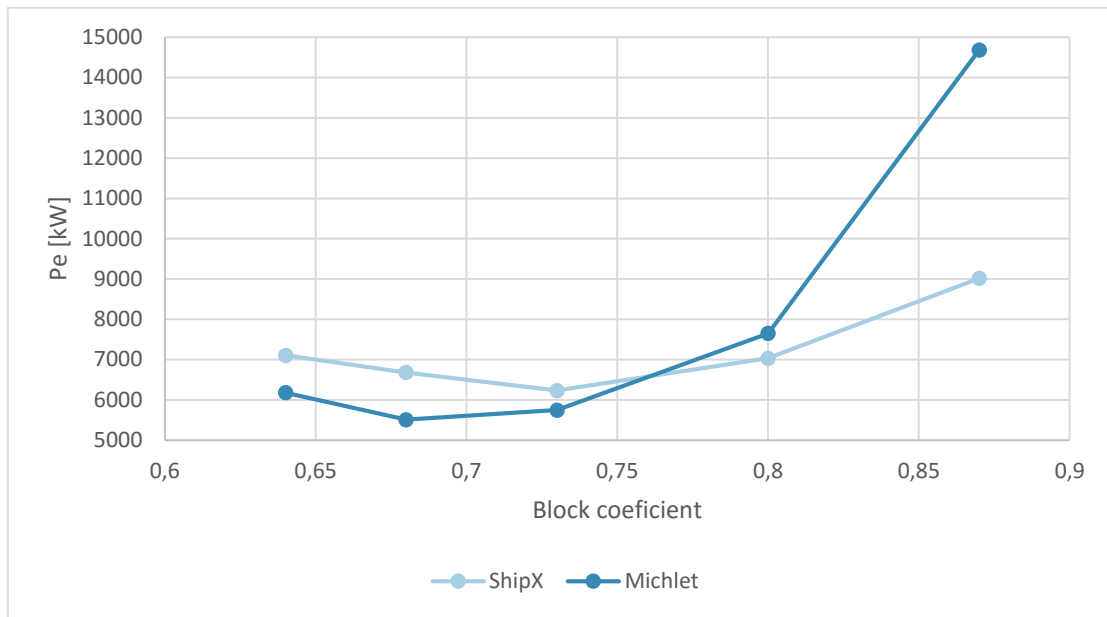


Figure 19 Effective power for CBC series at 13 knots calculated by ShipX and Michlet

As seen in Figure 19 the effective power calculated at 13 knots calculated by ShipX and Michlet follow the same trend for a block coefficient up to 0,8. After a block coefficient of 0,8 Michlet calculates a significantly higher effective power then ShipX.

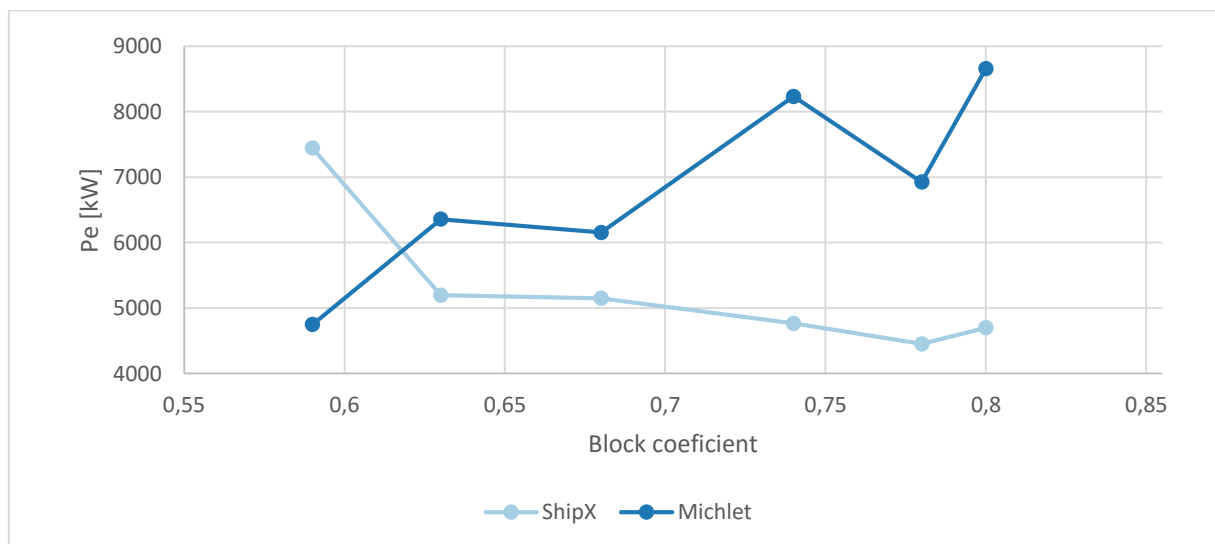


Figure 20 Effective calm water power for MOERI KVLCC2 at 13 knots

In Figure 20 the effective calm water power for the MOERI KVLCC2 series at 13 knots calculated by ShipX and Michlet are shown. As seen the required power calculated by ShipX has a steadily decreasing trend as the block coefficient increases. For a block coefficient of 0,59 the ShipX results have, what appears to be, an outlier deviating from the remaining results.

The effective power calculated by Michlet show an increasing trend with increasing block coefficient. For a block coefficient of 0,78 there is a clear drop in the effective power deviating from the effective power trend otherwise calculated by Michlet.

When benchmarking the resistance calculation of KVLCC2 by ShipX and Michlet, it is evident that the ShipX calculations are closest to the experimental results from OU and MOERI. The resistance calculated by ShipX are both closer to the OU and MOERI result and also follow the trend better, as seen in Figure 18. The resistance calculation by Michlet have a rapidly increasing trend with irregularities as the speed increases. The benchmarking is only performed for the full scale design of the KVLCC2, since it is the only design with experimental results available. This means that the benchmarking is only performed for one specific design in a speed range from 8 to 17,9 knots with no variation in block coefficient. The remaining designs within the MOERI KVLCC2 series and the entire CBC series has only been subject to benchmarking against each other (as seen in Figure 19 and Figure 20) and not any experimental results.

Based on the benchmarking of KVLCC2 and the comparison of the resistance calculations performed with Michlet and ShipX for both of the design series, ShipX proves to be the most reliable tool for calculating the calm water resistance. When considering the theory which is the basis for the calculations, it is also clear that ShipX is better suited in these calculations. Based on thin ship theory, Michlet gives good results for ships with a high L/B ratio. When the L/B ratio become low the sink and sources placed on the ship center plane will not be able to represent the ship hull sufficiently. Some of the designs considered in this thesis have a L/B ratio as low as 4,78. For these ratios Michlet will not be expected to give good results. Due to these limitations in Michlet, the results from Michlet are not use to draw any conclusion or identify any trends in this thesis.

3.4 Empirical methods

Based on 334 model tests Holtrop and Mennen (1984) presents a regression model for full-scale power predictions. It differs from earlier statistical methods, e.g. Doust and O'Brien (1959), with the fact that it does not only use statistical data but also considers the physics behind ship resistance. The analysis use the same sub-division of the total resistance into components as Holtrop and Mennen (1982). The sub-division of the resistance into components are seen in equation (29)

$$R_{Total} = R_F(1 + k_1) + R_{APP} + R_W + R_B + R_{TR} + R_A \quad (29)$$

The components in equation (29) are given as

R_F	Frictional resistance according to the ITTC-1957 formula
$(1 + k_1)$	Form factor of the hull
R_{APP}	Appendage resistance
R_W	Wave resistance
R_B	Additional pressure resistance of bulbous bow near the water surface
R_{TR}	Additional pressure resistance due to transom immersion
R_A	Model-ship correlation resistance

The wave resistance R_W is based on a theoretical expression given by Havelock (1914). The model-ship correlation resistance R_A is based on 168 data point from full-scale trials on new built ships. The form factor $1 + k_1$ is based on a regression analysis and given in equation (30)

$$1 + k_1 = 0,93 + 0,487118c_{14} \left(\frac{B}{L}\right)^{1,06806} \left(\frac{T}{L}\right)^{0,46106} \left(\frac{L}{L_R}\right)^{0,121563} \left(\frac{L^3}{\nabla}\right)^{0,36486} (1 - C_p)^{-0,604247} \quad (30)$$

The definition of the remaining resistance components is not given in this thesis and can be found in Holtrop and Mennen (1984). The components are very comprehensive and among others take into account the mid-ship coefficient, type of afterbody, number of propellers, number of blades, expandable propeller disk area and area of transom stern.

The weak point of Holtrop and Mennens method, as in Hollenbach's method (not presented in this thesis), is the representation of the bulb. However, Holtrop and Mennens method is a result of the most extensive statistical analyses of model test results ever made (Steen & Minsaas, 2014).

Lindstad et al. (2013) presents a new notation based on regression analysis of the existing fleet of bulk, container, tank and deep sea RoRo vessels. This is combined with data from the MARINTEK towing tank enables to take into account more modern and slender designs then previously considered.

Lindstad et al. (2013) uses a notation where the total brake power of a ship P is a product of 5 different factors, as seen in equation (31)

$$P = K \cdot (P_S + P_W + P_a) + P_{aux} \quad (31)$$

Here K gives the propeller (propulsion) coefficient efficiency as a function of the vessel speed and sea conditions seen in equation (32)

$$K = \eta \left(v, H_{\frac{1}{3}} \right) = \max \left(\frac{1}{\eta \left(j + k \cdot \sqrt{\frac{v}{V_d}} \right)}, \frac{1}{\eta \left(1 - r \cdot H_{\frac{1}{3}} \right)} \right) \quad (32)$$

η corresponds to the propulsion efficiency at the design speed V_d at calm sea $H_{\frac{1}{3}}$. The still water power is given in equation (33)

$$P_S = \frac{\rho \cdot C_S \cdot S \cdot v^3}{2}, \quad C_S = P_{Sref} \cdot \frac{S \cdot F_n \cdot C_B}{S_{ref} \cdot F_{nref} \cdot C_{Bref}} \quad (33)$$

C_s is the still water coefficient of the ship. It is derived by using reference values for power, wetted surface, Froude number and block coefficient from a reference ship. It is then multiplied with the wetted surface of the design which is being investigated. The additional power required in waves is given by equation

$$P_w = \frac{C_w \cdot \rho \cdot g \cdot \left(\frac{H_1}{2}\right)^2 \cdot B^2}{L} \cdot (v + u), C_w = C_{wref} \cdot \frac{\sqrt{\frac{B}{L_f}}}{\sqrt{\frac{B_{ref}}{L_{fref}}}} \quad (34)$$

Based on known drag coefficient for the reference vessel, C_{wref} , the wave drag coefficient C_w for alternative designs is found. The drag coefficient for the reference vessel may be found using the STAwave-1 method. Van der Boom (2010) presents the STAwave-1 method using simple ship dimension to calculate the added resistance in waves for a ship. The method is given in equation (35)

$$\bar{R}_{aw} = -\frac{1}{16} \rho g H_s^2 B \sqrt{\frac{B}{L_b}} \quad (35)$$

H_s is the significant wave height, B is the ship breadth and L_b is the distance from the bow to 95% of maximum breadth on the waterline. Lindstad et al. (2013) use a significant wave height of 4 m as a proxy for the significant wave height of 2-5,5 m and assume that the accumulated annual effect of the waves resulting from head-waves, side-waves and following-waves will be 50% of 4 m significant head waves. The proxy is meant to represent the conditions and typical seas faced by ships operating in the North Atlantic, based on Bales et al. (1981) showing that ships in the North Atlantic will face waves with a significant wave height of 2-5,5m 55% of the time.

The last factor of the total brake power in Lindstad et al. (2013) is the wind resistance given in equation (36)

$$P_a = \frac{C_a \cdot \rho_a \cdot A \cdot (v + u_a)^3}{2} \quad (36)$$

In equation (36) C_a is the aerodynamic drag coefficient, ρ_a is the air density, A is the surface area projected for the wind and u_a is the wind speed relative to the ship speed.

When compared to Holtrop and Mennen (1984) the results show that for a variation in breadth with a constant length, draft and displacement Lindstad et al. (2013) only predict a marginally different brake power.

4 Results

All the settings and raw results from the calculations in ShipX may be found in the electronic appendix as ShipX Ship Exchange files. The results from the numerical and empirical calculation may be found in Appendix D Results from numerical and empirical calculations.

4.1 Comparison of calculation of added resistance in waves

The added power in waves calculations in ShipX are performed using the Geritsma & Beukelman method for calculating the added resistance in waves based on a strip-theory approximation. The added power in waves is found as the difference between the effective power in calm water and the effective power in waves. Lindstad et al. (2013) uses the STAwave-1 method to calculate the added resistance in waves. In Figure 21 there is a comparison between the results for the CBC series at 13 knots obtained in ShipX and with STAwave-1. In Figure 22 the results for the MOERI KVLCC2 with the same calculation methods are seen. In the two figures STAwave-1 refers to added power in waves calculated with the STAwave-1 method, P_{wave} is the difference between the calm water resistance and the resistance calculated using $H_s=4$ m regular head waves and Mongstad-NY the difference between the calm water resistance and the resistance calculated using a weighted scatter diagram simulating the route from Mongstad to New York.

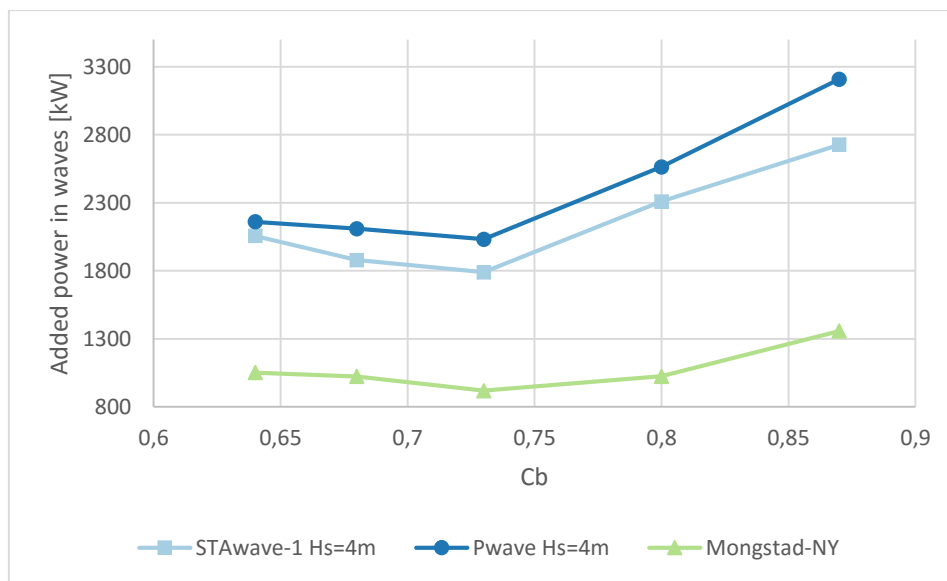


Figure 21 Added power in waves calculations for the CBC series at 13 knots

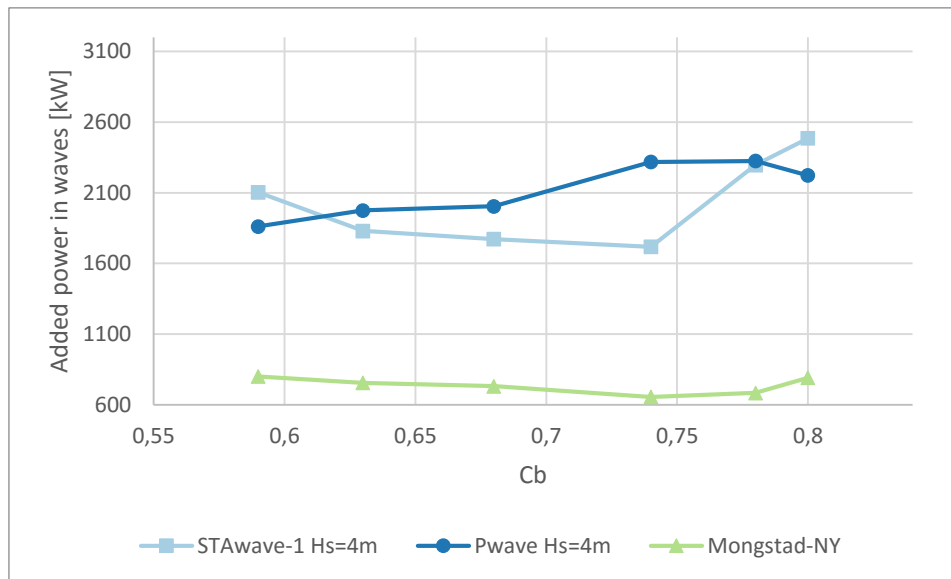


Figure 22 Added power in waves calculations for the MOERI KVLCC2 series at 13 knots

The results in Figure 21 and Figure 22 show that the calculations with regular waves and the STAwave-1 method are of the same order and magnitude. For the CBC series, the trend for the added power in regular waves, the added power calculated with the STAwave-1 method and the Mongstad-New York calculations has a very similar trend with a decrease until a block coefficient of 0,73 and then an increase of the added power in waves. The calculations for the MOERI KVLCC2 series show that the regular waves and STAwave-1 method both show an increasing added power in waves with increasing block coefficient.

It is worth noticing that in average, using the weighted scatter diagram gives 46,7% of the added power in waves for the regular wave calculations for the CBC series and 35,2% for the MOERI KVLCC2 series.

When calculating the added resistance in waves Figure 21 and Figure 22 show that the results from with regular head waves with $H_s=4$ m as a proxy correlate well with the calculations using the STAwave-1 method. The CBC series have a length of 224 m and the MOEI KVLCC2 series have a length of 246m. Assuming a length to height ratio for the waves of 7 gives a λ/L ratio of 0,125 and 0,113 respectively. As seen in Figure 16 a λ/L ratio of 0,125 and 0,113 is well within the λ/L range where the added resistance is dominated by bow wave reflection. Assuming low λ/L ratios it is therefore not surprising that the results from the STAwave-1 method coincide with the added power in waves calculated with Gerritsma & Beukelman. The assumption of Lindstad et al. (2013), that the accumulated annual effect of the waves resulting from head-waves, side-waves and following-waves will be 50% of 4 m significant head waves, proves to be quite accurate for the CBC Series (46,7%) but less accurate for the MOERI KVLCC2 series (35,2%). This is when comparing with the added power in waves calculated from the weighted scatter diagram representing the North Atlantic. The North Atlantic is considered a harsh environment characterized with high waves and strong winds compared to other trading routes.

It is therefore natural that the assumption of Lindstad et al. (2013) will not be as accurate for other and more benign seas. For others seas the significant wave height will have to adjusted to better match the conditions in question.

When calculating the added power in waves, the weighted scatter diagram is assumed omnidirectional, meaning that waves are assumed to be equal from all direction. It is not likely that in a true journey across the North Atlantic that the waves will be equal from all sides. Instead it is likely that over a period of time the waves will be coming from one direction, depending on the wind direction and then later shift to another direction for a longer period. How accounting for this would affect the results is not investigated any further in this thesis.

4.2 Brake power as function of block coefficient

When combining the added power in waves with the calm water power, the total brake power for a ship in waves is found. The power requirements in waves, calculated as the calm water power and 50% of the added power in regular 4 m waves, is compared with the power calculated with the weighted scatter diagram for Mongstad-New York, the brake power calculated by the model presented in Lindstad et al. (2013) and the brake power using Holtrop and Mennen (1984) added a 15% sea margin. The comparison for the CBC series at 13 knots is seen in Figure 23. The comparison for the MOERI KVLCC2 series at 13 knots is seen in Figure 24.

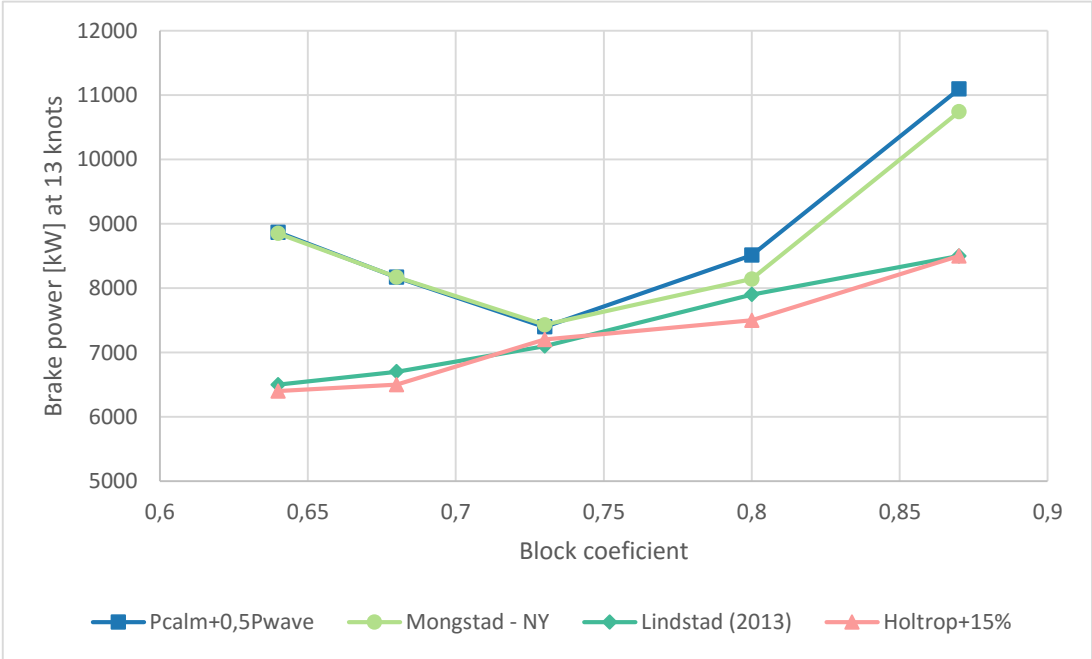


Figure 23 Comparison of brake power in waves as function of block coefficient at 13 knots for the CBC series

In Figure 23 it is clear that the results from Lindstad et al. (2013) and Holtrop and Mennen (1984) have the same trend with an increasing brake power with increasing block coefficient. The calculation with regular waves and the weighted scatter diagram correlate well and have both a minimum for a block coefficient of 0,73. For a block coefficient of 0,73 the brake power of all the four calculation methods are within a 5% range.

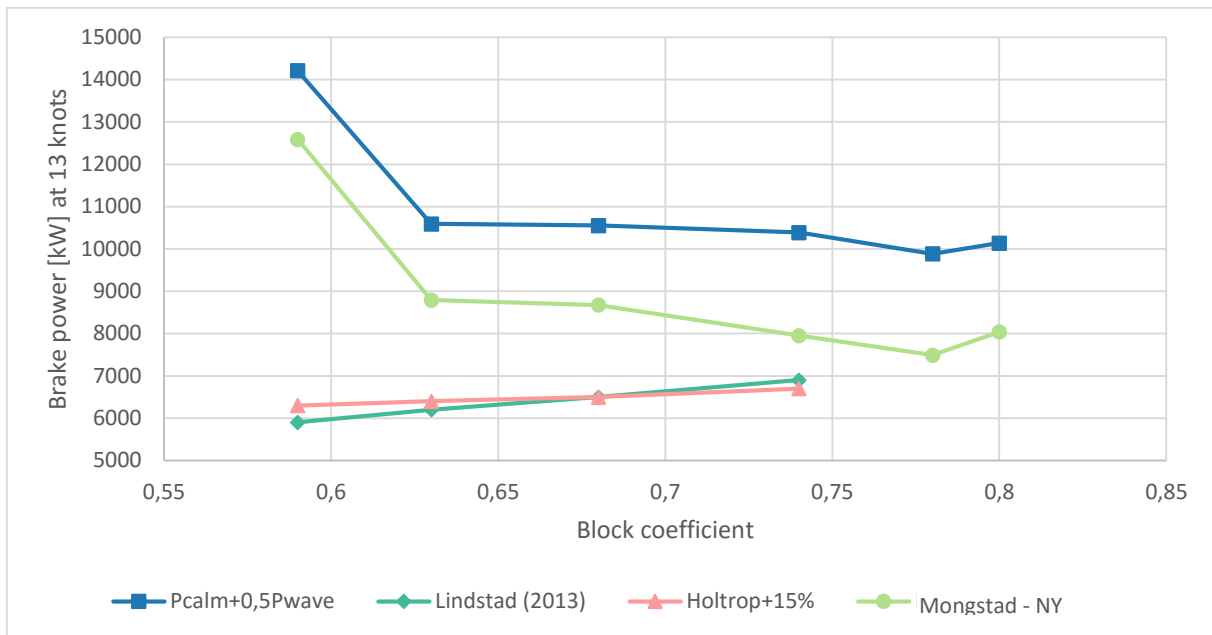


Figure 24 Comparison of brake power in waves as function of block coefficient at 13 knots for the MOERI KVLCC2 series

In Figure 24 it is shown that Lindstad et al. (2013) and Holtrop and Mennen (1984) calculate a lower brake power than the calculation with regular waves and the weighted scatter diagram for all block coefficients. The trend is also different with an increasing brake power for increasing block coefficient for Lindstad and Holtrop and Mennen while the numerical calculations with regular waves and the weighted scatter diagram decrease for increasing block coefficient with a minimum at a block coefficient of 0,78. Both the calculation with regular waves and the weighted scatter diagram have an apparent outlier for a block coefficient of 0,59.

When comparing the brake horse power as a function of block coefficient it is clear that the optimal block coefficient of the CBC series is lower than the optimal block coefficient for the MOERI KVLCC2 series. Figure 23 show that for the CBC series there is a clear optimal block coefficient at 0,73 and Figure 24 show an optimal block coefficient of 0,78 for the MOERI KVLCC2 series. The calculations for the MOERI KVLCC2 series are performed at a smaller block coefficient range compared to the CBC series. It is however apparent that as for the CBC series the MOERI KVLCC2 series have an increasing brake power when the block coefficient approach 0,8. Preferably the MOERI KVLCC2 series would have contained a design with a block coefficient above 0,8 to give more confidence of the optimal block coefficient of 0,78. On the other hand, the MOERI KVLCC2 series is designed to coincide with the block coefficient of the designs with a length of 246 m presented in Lindstad et al. (2013) ranging from 0,59 to 0,74.

Lindstad et al. (2013) and Holtrop and Mennen (1984) both show that for a constant length, draft and displacement reducing the block coefficient will decrease the required brake horse power in a linear relation. Being empirical methods based on previous towing tank results the methods are most accurate within the dimension range of previous tested hulls. For abnormal low or high block coefficients there will be little empirical data and the methods will in large extend be extrapolations based on regression analysis.

To a certain point an increased breadth and lower block coefficient gives a slenderer hull making it possible to move fullness from the bow section to mid-section. Moving fullness from the bow section to mid-section gives a finer water entrance for the hull thus a possibly decrease of the bow wave. It is also possible to remove fullness from the aft getting an equal effect and possibly reducing the aft wave. At some point this effect may be counteracted by shoulder and quart waves created by the pronounced shoulders necessary to fulfil the dimensional requirements of length, draft, breadth and displacement. It is therefore not obvious that the trend suggested by Lindstad et al. (2013) and Holtrop and Mennen (1984) shall persist for bulk carriers with low block coefficients ($C_b < 0,7$).

The results from the CBC series and MOERI KVLCC2 series contradicts the results from Lindstad et al. (2013) and the results calculated using Holtrop and Mennen (1984). In the block coefficient range of 0,7 to 0,8 the results from ShipX correlate well with the empirical results for the CBC series before there is an increase in the required calculated brake power or increasing block coefficient by ShipX.

It is worth noticing that the results from the MOERI KVLCC2 series calculations with regular waves and weighted scatter diagram, seen in Figure 24, are higher than the empirical results. This indicates that the design has a higher brake power than the empirical estimations. The original design of the MOERI KVLCC2 is assumed to be a well design hull with good hydrodynamic properties. The benchmarking show that ShipX in a satisfactory manner manages to calculate the wave resistance of MOERI KVLCC2. The cause of the discrepancy between the numerical and empirical results is not clearly identified but believed to be attributed to the design scaling. The trend with increasing brake power for both decreasing and increasing block coefficient with an optimal in the proximity of 0,78 is believed to be consistent, also for designs with lower overall resistance.

4.3 Effect of LCB on added resistance

By systematically moving the LCB, the effect on the added resistance is investigated. In the CBC series systematic variations of the LCB is performed for the designs with a block coefficient of 0,73 and 0,68. In Figure 25 the added power required to keep a speed of 13 knots is seen for different positions of LCB.

The added power in waves to maintain 13 knots calculated by STAwave-1 and regular waves is slightly increasing for forward LCB for both block coefficients. For the weighted scatter diagram there is not any clear decrease or increase as the LCB moves.

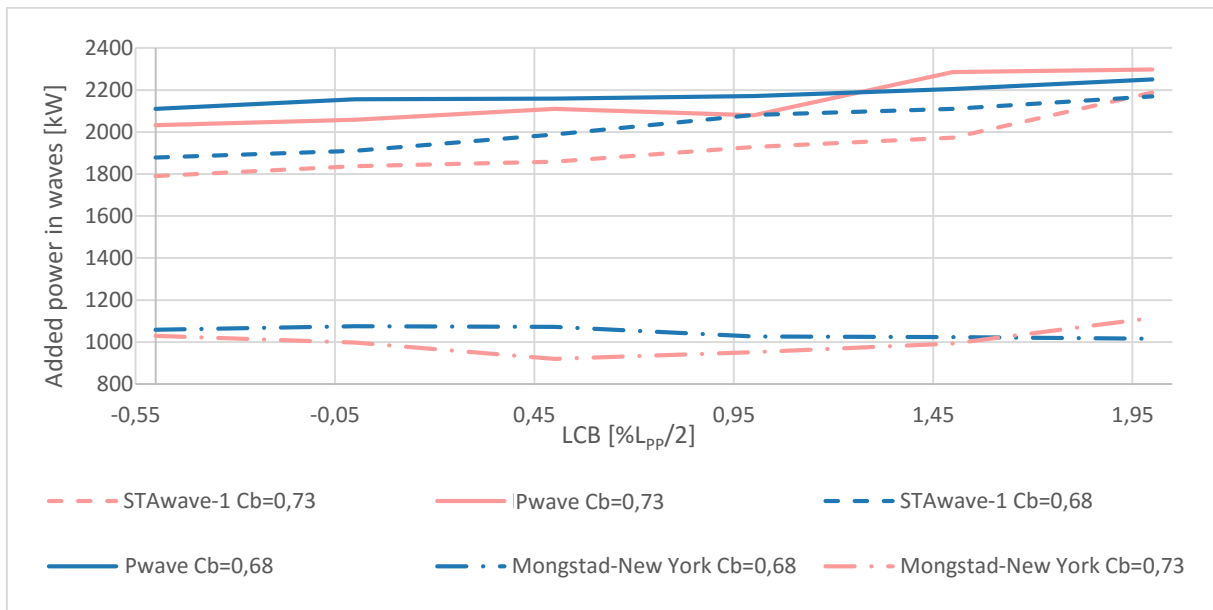


Figure 25 Effect of LCB on the added power required to maintain 13 knots in waves

In Figure 25 there is difference in the trend between the results obtained by STAwave-1 and the regular waves compared to the results obtained with the weighted scatter diagram. When using the weighted scatter diagram, the waves are assumed omnidirectional from 0,45, 90, 135 and 180 degrees' direction. The omnidirectional assumption will reduce the effect of a sharpen bow on the added resistance in waves compared to pure head waves. For an omnidirectional weighted scatter diagram the design of the entire hull, not just the bow, will affect the added resistance in waves. For stern and stern quartering waves the stern design is just as important and may in waves actually give a resistance decrease due to a positive net force from the waves. It is natural that for the regular pure head waves, compared to the omnidirectional weighted scatter diagram, the decreasing effect on the added resistance in waves of moving the LCB aft and sharpening the bow is more prominent.

4.4 Effect of LCB on brake power

The effect of the position of the LCB on the brake power to maintain 13 knots has been investigated for a block coefficient of 0,68 and 0,73 in the CBC series. The results are seen in Figure 26. $P_{\text{calm}} + 0,5P_{\text{wave}}$ the calculation using the significant wave height of 4 m as a proxy for the significant wave height of 2-5,5 m according to the assumption of Lindstad et al. (2013).

Figure 26 show that the power calculations for the regular wave and weighted scatter diagram have different values but follow the same trends. The sea margin, that is the power required to overcome the added power in waves, is for the block coefficient of 0,73 in average 25,9% and for the block coefficient of 0,68 in average 22,5%.

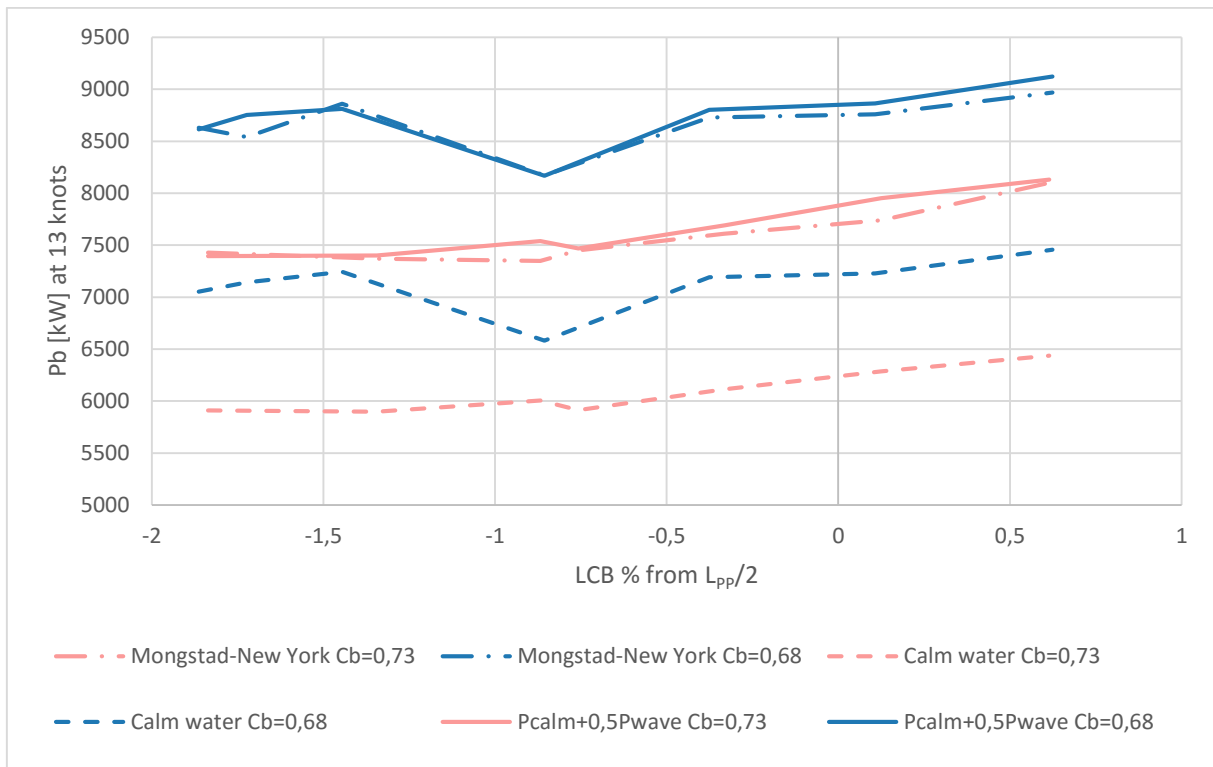


Figure 26 Effect of LCB on the brake power required to maintain 13 knots in waves

When looking at the brake power as a function of LCB position there is a trend showing increasing power for forwards LCB. The dominating component of the total brake power is the calm water component. Combining Figure 25 and Figure 26 it is clear that the effect of the positions of the LCB on the added power in waves is small. This indicates that position of the LCB mainly minimize the calm water resistance at medium Froude numbers, having a small effect on the added power in waves.

4.5 Influence of bow design on calm water resistance

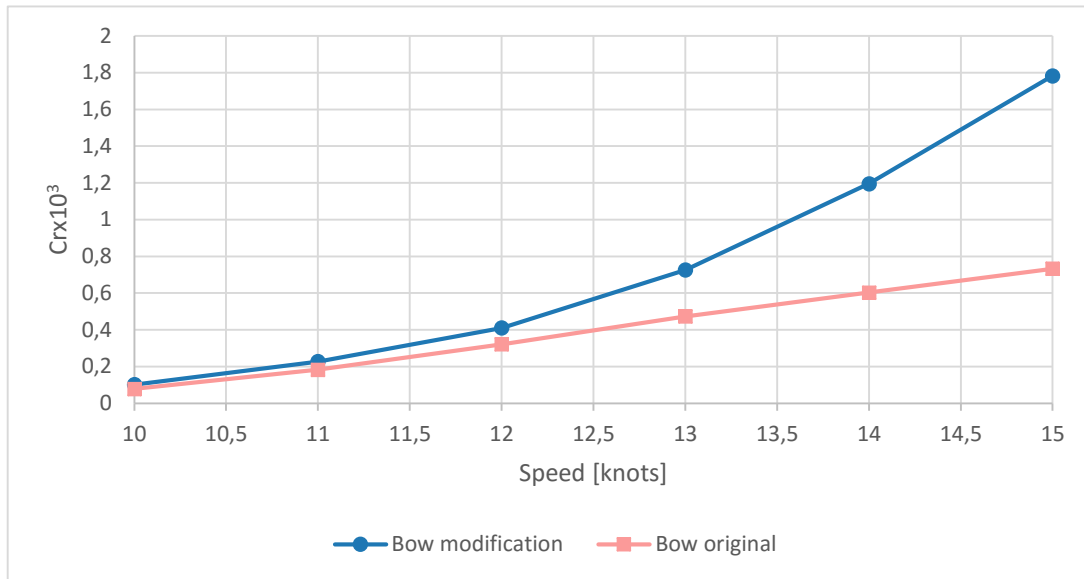


Figure 27 Comparison of wave resistance coefficient of the original and modified bow of the CBC $C_b=0,8$ design

To investigate the effect of the bow design the bow of the MOERI KVLCC2 $C_b=0,8$ design was adapted to fit the CBC $C_b=0,8$ design. As seen in Figure 27 the original CBC bow has a lower residual resistance coefficient with an increasing difference with increasing ship speed. The residual resistance coefficient is mainly composed of the wave resistance coefficient. The hydrostatic values of the two hulls are approximately the same with the largest deviations seen for the position of the LCB. For the modified bow the LCB is moved forwards to 113,485 m in front the aft perpendicular compared to the original bow with the LCB 112,797 m in front of the aft perpendicular. The positions of the LCB for the two bow designs show that the result in Figure 27 is in accordance with the results seen in Figure 26 i.e. moving the LCB forward increases the wave resistance. The sectional area curve of the two bow designs are seen in Figure 28.

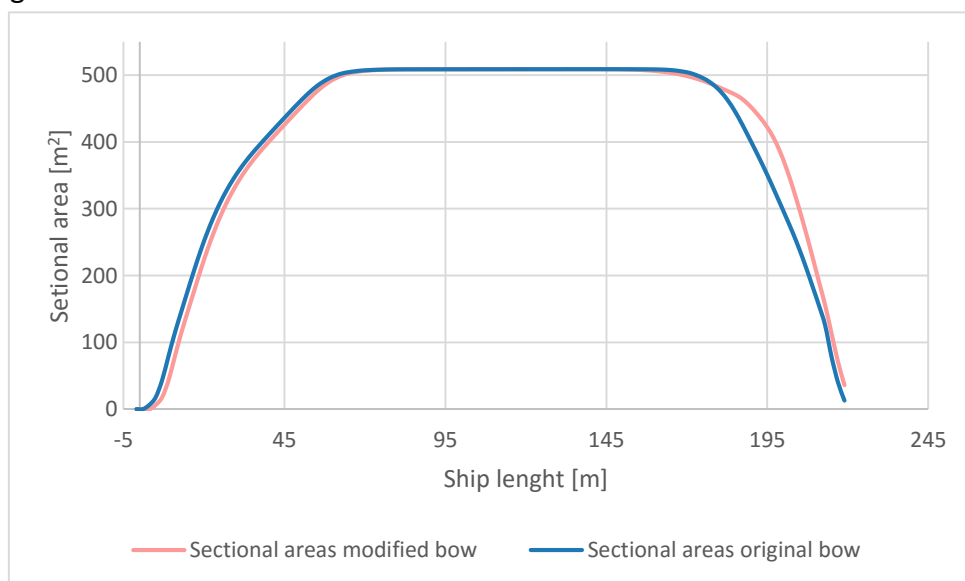


Figure 28 Sectional area curve for the original and modified bow of the CBC $C_b=0,8$ design

As seen in Figure 28 the modified bow has more volume at the bow and a forward shoulder move forward in the lengthwise direction. The more pronounced forward shoulder is likely to cause deeper wave troughs, increasing the wave resistance. This dwarfs the effect of the MOERI KVLCC2 being more distributed in the longitudinal direction initially thought to lower the wave resistance.

4.6 Influence of stern design on calm water resistance

For the CBC $C_b=0,73$ design there were made an alternative stern design. The original design has some unwanted features aft, with waterlines with high angles increasing the chance of separation. The alternative design therefore has a smoother transition between the u-shaped stern and the propeller hub giving waterlines with angles of run below 30° to avoid separation. The calm water resistance for the two designs are seen in Figure 29.

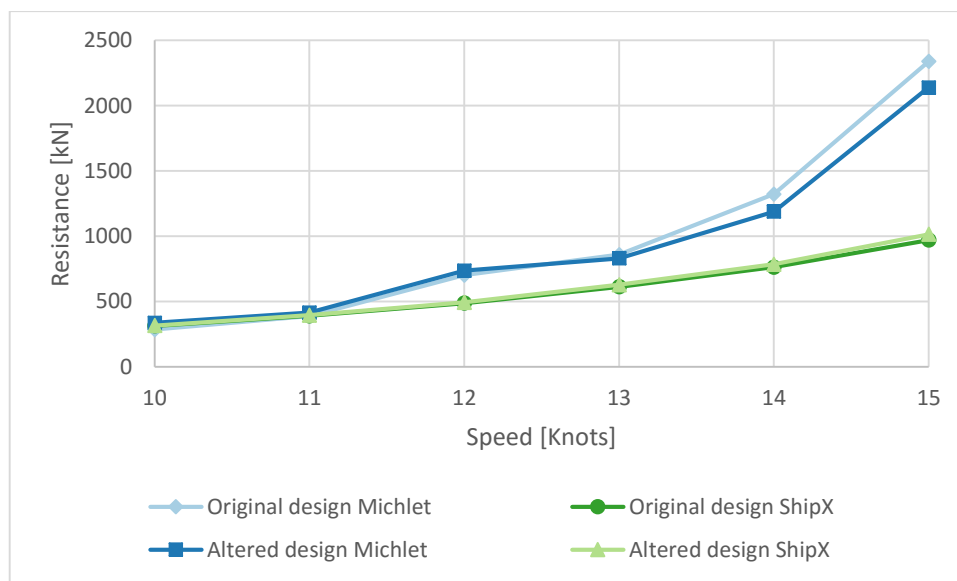


Figure 29 Calm water resistance for two different stern designs of the CBC $C_b=0,78$ design

As seen in Figure 29 the effect of two different stern designs have a little influence on the effective calm water resistance calculated both in ShipX and Michlet. Results from Michlet is included here to give a broader basis for comparison. The methods applied, potential theory and thin ship theory respectively, are however not considering viscous effects. In a more comprehensive resistance calculation the viscous pressure resistance would be included. The viscous pressure resistance is connected to viscous effects originating from flow separation and generation of vortices and circulation. These effects, caused by high angle waterlines, are especially seen at the stern of a ship. By including the viscous pressure resistance, the importance of a well designed aft section is increased. Through the transom stern coefficient seen in equation (22), ShipX account for the transom stern resistance, created by the suction pressure which arise when an external flow carries away the dead water behind the stern.

When paneling a hull, ShipX will insert a hollow, acting as a virtual stern when computing the velocity potential, for waterline angle above 30 degrees. The reason for using this hollow stern is to simulate the effect of viscous flow separation in the stern region. Combined, ShipX do take into account viscous pressure resistance but not in such a degree that it differs between minor variations of the same design.

The motivation of this thesis is to investigate the effect of block coefficient on the resistance of a ship with a special attention on the forward part of the hull. Keeping the influence of the stern design to a minimum can therefore be beneficial for reducing the uncertainty in the final results. ShipX low sensitivity to stern design contributes to minimizing the number of parameters, other than the breadth, being changed when varying the design within one design series.

4.7 Admiralty coefficient for Colombo Express and KVLCC2

Comparing the performance of ships of different dimensions and displacements is challenging and no standard method is provided. A way of comparing ships of different dimensions and displacements is to compare the energy efficiency by dividing the needed power to move the load of the ship with the brake horse power. One formula for this kind of comparison is the admiralty coefficient given in equation (37)

$$AC = \frac{\Delta^{\frac{2}{3}} \cdot V^3}{P_B} \quad (37)$$

In equation (37) Δ is the displacement in tons, V is the ship speed in knots and P_B is the brake horse power.

Colombo Express is a container ship with length over all of 335 m, breadth of 42,8 m and design draft of 13,0 m. At this draft the Colombo Express has a deadweight of 84 500 tons and a total capacity of 8 606 TEU containers. When she was launched in 2005 the owner, Hapag-Lloyd, claimed she was the world's largest container ship. Colombo Express has a service speed of 25,2 knots. The hull has a slender design with a block coefficient of 0,57 and a high L/B ratio of 7,8.

The admiralty coefficient for 3 different variation of the Colombo Express is investigated. The first is the full scale original design of the Colombo Express. The second is the Colombo Express design scaled to a displacement of 96 348 tons equal to the designs in the MOERI KVLCC2, while keeping the dimension ratios of the full scale design. The third is scaled to the length of waterline equal to 322,8, which is approximately equal the length of the full scale MOERI KVLCC2 design. The admiralty coefficient of the three variations of the Colombo Express are compared with the admiralty coefficient of the full scale MOERI KVLCC2 design and the scaled design with a block coefficient of 0,8.

As seen in Figure 30 the admiralty coefficients of the three variations of the Colombo Express hull and the two variations of the MOERI KVLCC2 hull have two distinct trends. The MOERI KVLCC2 hulls have a declining admiralty coefficient across the entire speed range investigated. For the Colombo Express hulls the admiralty coefficient is approximately constant until a speed of 16 knots before declining.

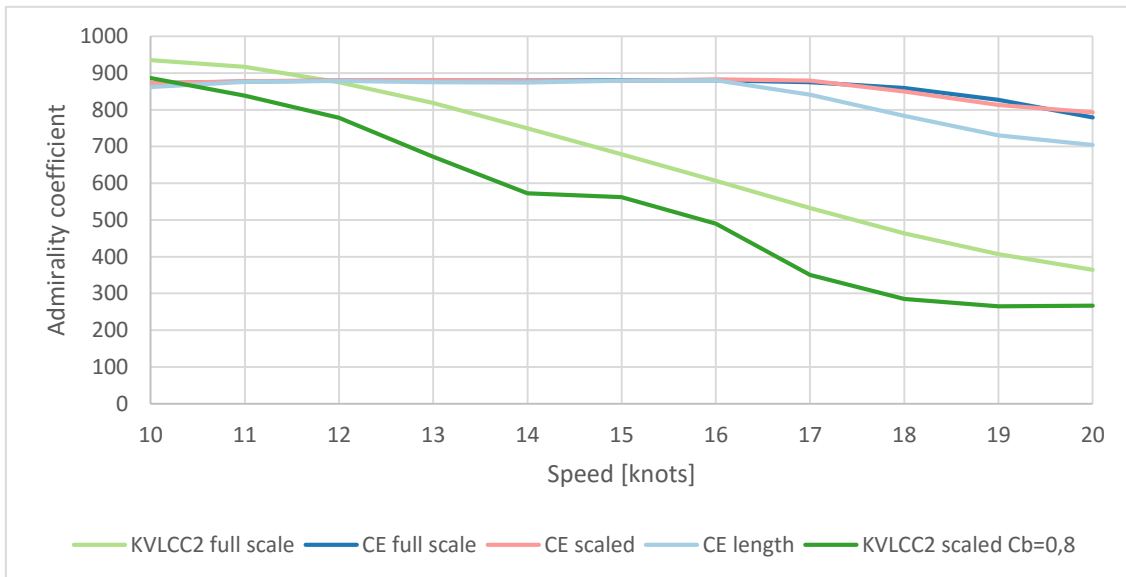


Figure 30 Admiralty coefficient for design variations of Colombo Express and MOERI KVLCC2

An explanation for these two different trends may be attributed to the fact that the Colombo Express is designed for a higher service speed compared to the MOERI KVLCC2. The Colombo Express has a service speed of 25,2 knots (Marine Log, 2005) while the MOERI KVLCC2 has a service speed of 15,5 knots (FORCE Technology, 2014). In general, container ships have a higher design speed because the cargo is more time sensitive, such as refrigerated content or deliveries with a strict deadline, and therefore require a reduced shipping time. For bulk carriers time constraints are not that apparent and there is a greater focus on cost efficiency, resulting in lower service speeds.

The design difference is seen in the difference in block coefficient between the three variations of the Colombo Express hull and the two variations of the MOERI KVLCC2 hull. The Colombo Express hull variations have a block coefficient ranging from 0,583 to 0,579 while the two MOERI KVLCC2 hull variations both have a block coefficient of 0,81. When looking at the variation of Colombo Express and MOERI KVLCC2 with the same displacement of approximately 96 300 tonnes the Colombo Express design has a much lower effective power. At 13 knots the effective calm water power of the Colombo Express design is 3663,6 kW and 4699,2 kW for the MOERI KVLCC2 design. The difference in effective calm water power increases with increasing ship speed.

Looking at the sectional area curve for the two designs with equal displacement there is a distinct difference in how the displacement is distributed longitudinally. The comparison of the sectional areas of the scaled Colombo Express design and the MOERI KVLCC2 $C_b=0,8$ design is seen in Figure 31. The two designs have approximately the same displacement but different length and breadth.

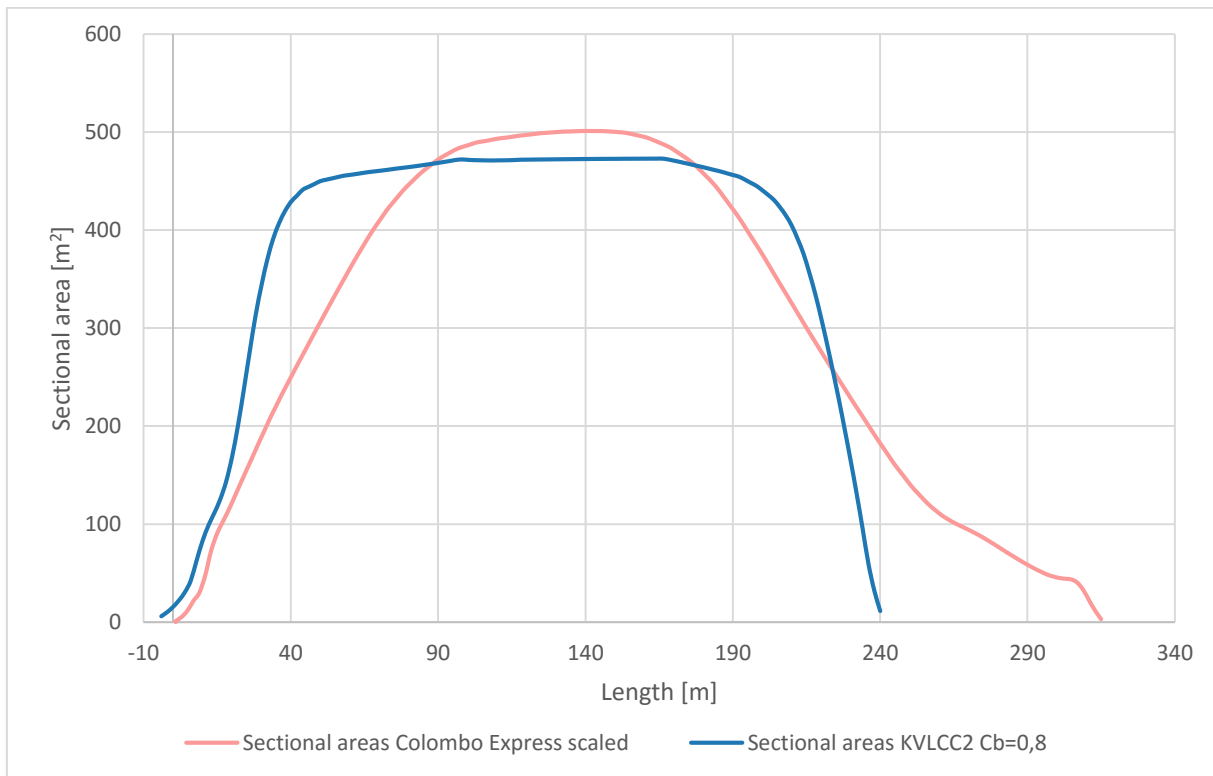


Figure 31 Sectional areas of the Colombo Express scaled design and the MOERI KVLCC2 $C_b=0,8$ design

The increased midship sectional areas of the Colombo Express scaled design is due to a breadth of 41,31 m compared to a breadth of 32,65 m of the MOERI KVLCC2 $C_b=0,8$ design. The longitudinal distribution of displacement seen in the Colombo Express scaled design gives a lower entrance angle at the bow and less pronounced shoulders. In the comparison seen in Figure 31 combined with the effective calm water resistance it is seen that it may be an advantage to reduce the block coefficient by increasing the length of a vessel with constant displacement.

5 Discussion

The motivation for this thesis is to investigate the effect on brake power when reducing the block coefficient with constant length, draft and displacement and a variation in the breadth. The breadth is varied to change the block coefficient. Keeping the displacement constant demonstrates a constant capacity of carrying bulk goods, and is a natural way of comparing ships of different block coefficient. Comparing ships with constant displacement is however not the only way of comparing ship performance. It is from a ship owner's perspective desirable to have the lowest cost of transporting a unit weight of goods per unit length. This means that with assumed constant fuel prices and fuel efficiency regardless of design, ships of different displacements can be compared directly to each other. The goal of lowering the cost of transportations does not necessary lock the dimensions of a ship. To achieve the lowest transportation cost, restrictions on length, draft, breadth and displacement may be lifted in the design process.

Changing the block coefficient of a ship while keeping the displacement constant can be done with other means than varying the breadth. A pure variation in length or a combination with breadth variation would also change the block coefficient, still having the possibility to keep the displacement constant. The sectional area curve of the Colombo Express indicates that distributing displacement longitudinally may be beneficial when comparing resistance of hulls with equal displacement. A change in length will however result in different Froude numbers for each design at a given speed and a possibly reduced wave resistance coefficient. With constant speed the resistance will be beneficial for the longest designs due to a lower Froude number. Thus, the pure effect of varying breadth may be dwarfed by the effects of lengthened hull and reduced Froude number. For this reason, the breadth of the designs in this thesis was varied and not the length or a combination of the two. This isolates and accentuate the effect of varying the breadth of the designs. Only changing the breadth also reduces the number of parameters which may affect the total resistance of each hull design. This reduces the uncertainty and increases the credibility of the results.

The results for the two different design series are giving two different optimal block coefficients, with 0,73 for the CBC series and 0,78 for the MOERI KVLCC2 series. It is not expected that one block coefficient is the optimal for all hull shapes regardless of displacement. It is however expected that within a confined range of displacement the optimal block coefficient will be within the range of 0,73-0,78. The designs in the two design series in this thesis range from approximately 93 000 tons to 96 000 tons with an estimated deadweight of 80 000 tons fully loaded.

Regression analysis of the existing bulk carrier fleet show that the ship length increases as the ship deadweight increases (Kristensen, 2012). Assuming a constant speed, an increased length will reduce the Froude number and increase the Reynolds number of a longer ship. Reducing the Froude number will reduce the wave resistance coefficient. Increasing the Reynolds number will according to equation (19) reduce the frictional resistance coefficient. The overall effect of an increase in length with constant speed is a proportional reduction in wave resistance compared to the frictional resistance.

A proportional increase of frictional resistance implies that a shift toward optimizing the cargo carrying capacity wrt wetted surface of the hull. A such optimization implies that a decreased breadth and increased block coefficient will be beneficial. The Froude number is however not found to decrease in such a degree that decreasing the wave resistance by decreasing the block coefficient not will be beneficial. It is therefore probable to conclude that the optimal block coefficient range found in this thesis will apply to large parts of the ships in the New Panamax segment and lower part of the Capsize segment, with a slight increase of the optimal block coefficient as the displacement increases. The increase in optimal block coefficient is however not thought to approach the current block coefficient average of Capesize vessels of 0,84. Within the New Panamax segment and lower part of the Capsize segment the optimal block coefficient for a specific hull is expected to be in the range of 0,73 to 0,78. The variation is due to differences in waterlines, entrance angle and LCB who may have additional influence to the resistance other than block coefficient.

The designs investigated in this thesis is in the lower part of the current Capesize segment, just above the largest ship in the current Panamax restrictions. All the designs will however be within the New Panamax restriction, which will be a dominating restriction for future newbuilds. The New Panamax will allow ship with a deadweight up to approximately 120 000 tons to pass through the canal and thereby including up to 90% of the world bulk carrier fleet built since 1996 (Stott, 2012). This implies that the findings in this thesis can have a very broad impact for the majority of new built bulk carriers.

As seen in Figure 1 the average block coefficient of bulk carriers in the $60\,000 < dwt < 200\,000$ range lies above 0,84. If the emissions of the world bulk carrier fleet is assumed at the same level as the $C_b = 0,84$ design of the CBC series there is a considerable potential for emission reduction. It is assumed a linear development of the brake power as a function of block coefficient between the data point of $C_b = 0,80$ and $C_b = 0,87$ for the CBC series. In Figure 23 the brake power for $C_b = 0,84$ with the linear assumption then becomes 9 625,84 kW. The percentage reduction in brake power from $C_b = 0,84$ to the optimal $C_b = 0,73$ is a total of 22,81%. Other estimates of potential fuel savings from hull optimization, as accounted for in the Previous work chapter, are in the range of 5-16%. Compared to these estimates the potential fuel savings found in this thesis is seemingly high.

The large percentage improvement seen in Figure 23 may originate from the fact that the high block coefficient ($C_b \geq 0,8$) have an increased brake power compared to a real fleet data. The average installed brake power per knot per deadweight ton for new builds from 2007 to 2010 in the range $70\,000 < dwt < 90\,000$ bulk carriers is 0,00891 (Stott & Wright, 2011). Combining the average brake power per knot per deadweight ton from Stott and Wright (2011) with the statistics from Kristensen (2012), the average block coefficient of these vessels are assumed 0,84. Calculating the brake power per knot per deadweight for the CBC $C_b = 0,84$ design, the value is 0,00925 indicating that the power prediction is only 3,9% higher than the $70\,000 < dwt < 90\,000$ bulk carrier average. This proves to show that CBC $C_b = 0,84$ interpolated value has the approximate same brake power as ships of comparable displacement. The optimal block coefficient for the CBC series of 0,73 has an installed brake power per knot per deadweight ton of 0,00682.

This indicates that the large percentage brake power reduction originate from a lowered brake power for the optimal block coefficient, and not a significantly higher brake power for the CBC $C_b=0,84$ interpolation. The seemingly high percentage savings may be explained by the fact that earlier estimations primarily focus optimization of hull lines and propulsion configuration. This thesis lifts the restrictions on dimensions and thereby enables more unconventional L/B ratios, larger reduction in brake power and higher percentage savings. The percentage saving of 22,15% between today's Capesize and New Panamax block coefficient average and optimal block coefficient found in this thesis may therefore be a reasonable value.

Psaraftis and Kontovas (2009) estimates that there worldwide are 2203 bulk carriers with a total deadweight above 60 000 tons. Combined it is estimated that these ships yearly emit 73,74 million tons of CO₂ and consume 23,26 million tons of bunkers oil. Assuming a linear connection between the reduction in brake power and CO₂ emission, a 22,81% reduction in brake power of the world bulk carrier fleet above 60 000 dwt results in a yearly CO₂ reduction of 17,06 million tons and 5,31 million tons of bunkers oil. In comparison the total CO₂ emission from the entire Norwegian offshore petroleum industry was 11,13 million tons in 2014 (Miljødirektoratet, 2015). Assuming a low price scenario on IFO180 bunker oil of US\$ 250/ton (2011-2012 average of US\$ 600/ton) the annual worldwide fuel savings adds up to US\$ 1 326,4 million per year or in average US\$ 602 088 per ship. Any future carbon tax on international shipping will add to the potential savings. Assuming the low carbon tax scenario of US\$ 30/ton the financial savings from the CO₂ reduction add up to US\$ 511,8 million. A future global carbon tax is however a very uncertain scenario and should not be emphasized in the calculations of the potential savings.

The potential yearly financial savings from fuel reduction of up to US\$ 1 326,4 million implies that investments made to lift restrictions on ship dimensions by e.g. expanding ports can be done at a negative abatement cost. There is however a challenge in the fact that the financial cost of expanding the ports will lay on the port owner while the financial gain will lay on the ship owner. This unbalance must be solved to create the right incentives for port expansion.

In this thesis the forward part of the bow and bulb has been tried remained unchanged for all designs to limit the number for parameters being changed between each design. As stated by Steen and Minsaas (2014), a bulb may reduce the wave resistance with 5-20%. For an individual hull design, a bulb must be individually designed to reduce the wave resistance. Designing individual bulbs to match all the 30 hulls design in this master thesis would be very time consuming and outside the scope. The effect of a bulbous bow will be most prominent for the designs with the highest wave resistance, where the bow wave pattern is largest. Bulbous bows have greatest effect on conventional displacement ships that operates at relative high Froude numbers in the range of 0,25-0,4 (Steen, 2011). The Froude numbers of the CBC series is 0,145 and 0,138 for the MOERI KVLCC2 series. With the low Froude numbers of both the design series indicate that the effect of a well designed bulbous bow will be in the lower range of 5-20%.

Combining the insights of the effect of bulbous bows at low Froude number and high wave resistance it is probable that more well designed bulbous bows may reduce the brake power of the designs with the highest wave resistance. The effect is assumed to be small, but may reduce the percentage savings in brake power slightly.

The bow of the MOERI KVLC2 was initially assumed to give a lower wave resistance than the adaptation of the CBC bow. As seen in the comparison of the wave resistance coefficient in Figure 27, it is however the CBC bow that has the lowest wave resistance coefficient. The difference in wave resistance is attributed the fact that when modified for the CBC hull, the MOERI KVLC2 bow gets a more pronounced forward shoulder. The transition between the bow and the parallel midship of the modified bow is therefore dominated by a sectional area curve with an uneven curvature. The comparison of the wave resistance seen in relation with the sectional area curve in Figure 27 and Figure 28 emphasizes the importance of smooth transitions and well designed forward shoulders. It is evident that a poor transition between the bow and parallel midship can cancel the effect of a well designed bow with a minimal bow wave.

When varying the LCB there are some limiting factors on how far aft the LCB can be moved. Moving the LCB forward may create a pronounced forward shoulder increasing the size of the shoulder wave system, which in turn increases the wave resistance. Moving the LCB aft may however be more complicated and cause several challenges. When moving the LCB aft the fullness of the hull is moved aft and thereby changing the waterlines of the stern. With a aft LCB the fullness requires high angle waterlines to meet the geometry of the propeller hub construction.

The high angle waterlines give an increased chance of flow separation and generation of vortices and circulation. This gives poor inflow conditions to the propeller and increases the viscous pressure resistance. The inflow conditions to the propeller is crucial to create a high propulsive efficiency and reduce the required delivered power of a ship. If the LCB is optimized with regard to pure hull resistance, it may disturb the propeller inflow conditions. If the propeller inflow conditions are to be preserved the position of the LCB must be optimized with regards to the brake power delivered from the ship engine. The flow separation and generation of vortices and circulation appearing in the near vicinity of the propeller is, however, not fully accounted for in ShipX or Michlet. A calculation where this is taken into account would emphasize the importance of a well designed stern, increasingly more difficult to achieve with a backward LCB. In turn this will limit how aft the LCB may be moved.

A limitation in this thesis is that the hull designs only are compared at 13 knots. This to constrict the number of calculations performed. 13 knots is in the lower range of service speeds of bulk carriers and seeing ships with a higher service speeds is not unusual. At low speeds the Froude number will be low. At low Froude numbers the resistance will be dominated by frictional resistance. The frictional resistance is largely determined by the wetted surface of the hull. When the speed increases, the increase in total resistance is dominated by the wave resistance.

The wave resistance is, compared to the frictional resistance, to a larger degree dependent on the hull shape. With an increased speed the difference between hulls with low and high wave resistance will increase rapidly.

However, the results show that 13 knots is sufficient to differentiate the hulls within a series and observe the effect of the wave resistance. With increased speed the findings in this thesis is expected only to be further sustained. With slow steaming, where commercial trade ships operating at a much lower service speed than design speed, the speed of 13 knots is not an unlikely speed for bulk carriers in the Capesize and New Panamax segment. Another way to evaluate the design is to use multiple speeds, drafts, sea states and directions based on the operating profile of expected use. Only a small percentage of a ships operating profile is at the given design speed and draft. Optimizing a ship for this condition may therefore lead to increased brake power at other operating profiles. Evaluating a large number of operating profiles will however quickly lead to a large matrix of operating profile combinations, increasing the numbers of calculations exponentially.

The variations of the designs are implemented by using DELFTship to move stations and modify the breadth of them to achieve the desired hull dimensions. The variation is systematic in the way the dimensions are chosen. The design implementation by varying the hull geometry that enables the variation is, however, not fully controlled. The consequence of this is that parameters that may be effecting the brake power of the hull, is not kept constant and effect the result without being identified. The number of hull designs and the authors previous experience with ship design has also resulted in design which can be developed further. This is particularly apparent for the stern design of the CBC series. An optimized stern design would increase the propeller inflow and reduce the viscous pressure resistance. On the other hand, as discussed earlier and seen in Figure 29, the effect of the stern design with the numerical calculation method applied is negligible. A more high fidelity calculation method considering viscous effects would on the other hand in a larger extent consider the stern design.

A design feature which can be developed further is the transition area between the bow and the parallel midship section. A close study of the waterline of a selection of the designed hulls reveal that they consist of multiple smaller bends where the curvature of the waterline changes. The optimal waterline has of one smooth transition toward the parallel midship. ShipX satisfies the boundary conditions some distance away from the hull surface which may smooth over the changing curvature. However, it is still considered that the inconsistent curvature will cause additional wave resistance giving rise to an unsystematic uncertainty in the obtained calm water wave resistance calculations. An improvement in the designs may reduce the percentage savings of applying the optimal block coefficient.

The initial design of the hulls and the modification breadth to achieve the desired hull dimensions is considered a weakness in how the method in this thesis is applied. Nonetheless, if lines of each hulls were to be fully optimized this would have been a very time consuming task outside the scope of this thesis.

An optimization of each hull either manually or using simulation based design could have been beneficial for the resistance of each hull but it remains uncertain if it would change the final conclusion obtained in this thesis.

The method applied in thesis, despite weaknesses in the implementation by the author due to lack of experince, is considered a time effective and accurate method for evaluating a large range of designs where the dimensions are varied. The method is more precise for hulls outside conventional dimensional ratios compared to empirical methods and more overarching and time effective than numerical hull optimization methods using CFD. The time aspect is especially apparent when calculating the added resistance in waves, where applying CFD very computational demanding and time consuming.

6 Conclusion

For both the design series there is, by using potential theory, found an optimal block coefficient with regards to brake power. For the CBC series, the block coefficient is found at $C_b=0,73$, with a clear increase in brake power for both increasing and decreasing block coefficients. For the MOERI KVLCC2 series, there is an optimal block coefficient found to be $C_b=0,78$.

Compared to the results calculated with the empirical methods by Lindstad et al. (2014) and Holtrop and Mennen (1984) using the identical hull dimension there is a difference in trend. The numerical results show that there is an optimal block coefficient while the empirical results show a decreasing brake power with decreasing block coefficient for both the design series.

Combining the results of the two hull series it is likely to assume that the optimal block coefficient for $60\,000 < dwt < 200\,000$ bulk carriers is in the range of 0,73 to 0,78. The optimal block coefficient is expected to increase slightly with increasing displacement.

Comparing the results from Kristensen (2012) in Figure 1 there is a clear discrepancy between the block coefficient of the current world fleet of Capesize and New Panamax bulk carriers and the optimal block coefficient found for the two hull series in this thesis. Today's fleet has higher block coefficient than the optimal block coefficient found in this thesis. A regression analysis performed by Kristensen (2012) show that not for any displacement of $60\,000 < dwt < 200\,000$, the block coefficient is below 0,84. To build ships with an optimal block coefficient and reduce brake power the design should have an increased breadth to distribute the displacement and create a finer bow entrance.

Reducing the block coefficient from the current average of 0,84 to the optimal range can reduce the brake power, and thus total fuel consumption and emissions to air with 22,81%, saving a total of 17,05 million tons CO_2 and up to US\$ 1 326,4 million in fuel savings on a yearly basis.

For a hull with the same displacement and dimensions moving the LCB aft will reduce the calm water resistance. The reduced resistance is due to displacement moved aft creating a finer bow entrance and smaller bow wave system. The limiting factor when moving the LCB aft will be the propeller inflow conditions, not exhaustively investigated in this master thesis.

The effect of the transition between the bow and the parallel midship on the wave resistance is found to be significant. With a poor transition there will be a pronounced forward shoulder creating wave troughs which increase the wave resistance.

As a simplification for calculating the added resistance in waves for North-Atlantic conditions it is a good approximation to use a significant wave height of 4 m as a proxy for the significant wave height of 2-5,5 m and assume that the accumulated annual effect of the waves resulting from head-waves, side-waves and following-waves will be 50% of 4m significant head waves. This will, however, be dependent on the individual hull design and how well it is designed to reduce added resistance in waves.

7 Recommendation for further work

To limit the numbers of parameters varied, simplify the comparison of results and increase credibility, only breadth has been varied within each hull series. In the comparison with the scaled Colombo Express it is clear that distributing displacement longitudinally may be beneficial when comparing resistance of hulls with equal displacement. A recommendation for further work is to further develop the hull series where a combination of length and breadth is varied. The effect of a variation of the length in combination with breadth can then be investigated. A limitation, when increasing the length of ships, is longitudinal strength, since the longitudinal bending moments increases with length. Lack of longitudinal strength may cause jack knife deformations or breaking of midship hull girders. Therefore, structural calculations should be performed to investigate the structural feasibility of designs with increased length. Optimizing the bulbous bow for each design will also give a more comprehensive picture of the total brake power required.

The numerical methods used in this thesis have limitations. Potential theory is a computational efficient when evaluating multiple designs at once. Not considering viscous effects and not simulating any turbulence around the ship hull potential theory will be a simplification not fully reflecting all resistance components acting on a hull. Using more comprehensive numerical methods (e.g. computational fluid dynamics) to calculate the calm water resistance of each hull may give a more precise answer with a higher credibility. Setting up a proper calculations and ensuring a sufficient hull meshing to perform a CFD calculation is time consuming and therefore not applied in this thesis. A recommendation for further work is to perform CFD calculations on all or some of the hulls in this thesis to validate the results from ShipX obtained with potential theory.

This master thesis has only focused on the resistance of a ship to reduce fuel consumption and emissions to air. For new technology and design principles to be implemented in shipping it also has to be proven economically sustainable. A total assessment of the profit and cost of the recommended changes have to be investigated. The assessment should include building costs, fuel cost and prices, cargo carrying capacity and time charter income.

8 References

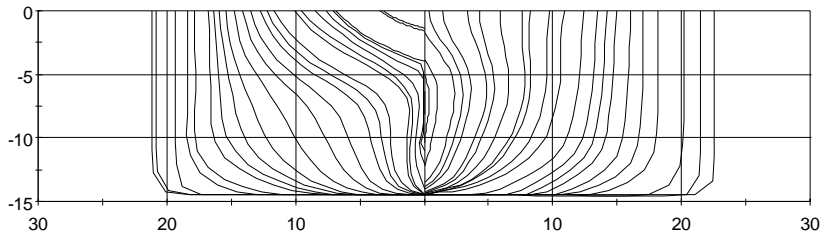
- ABS. (2013). Ship Energy Efficiency Measures: Status and Guidance In ABS (Ed.).
<http://ww2.eagle.org/en/news/press-room/2013/abs-releases-ship-energy-efficiency-measures-advisory.html>.
- Amdahl, J. & Fuglerud, G. (2003). *TMR 4100 - Marin teknikk intro, TMR 4105 - Marin teknikk 1: kompendium* (3. utg. ed.). Trondheim: Marinteknisk senter, NTNU.
- Arribas, F. P. (2007). Some methods to obtain the added resistance of a ship advancing in waves. *Ocean Engineering*, 34(7), 946-955.
- Bales, S. L., Lee, W. T., Voelker, J. M., David, W. T. & Bethesda, M. (1981). Standardized Wave and Wind Environments for NATO Operational Areas: Naval Ship Research Development Center Ship Performance Dtp. .
- BBC. (2015). Egypt launches Suez Canal expansion. Retrieved from
<http://www.bbc.com/news/world-middle-east-33800076>
- Bilgili, L. & Celebi, U. B. (2015). Establishment of an emission estimation approach for bulk carriers related to block coefficient (pp. 813-818).
- Canal de Panamá. (2013). Annual Report 2013. Retrieved from
<http://www.pancanal.com/eng/general/reporte-anual/2013/flash.html>
- Canal de Panamá. (2016). Panama Canal Expansion Retrieved from
<http://micanaldepanama.com/expansion/>
- Cyberiad. (2015). Michlet 9.33 User's manual.
- DNV-GL. (2014). DNV GL reduces the impact of variations in ship construction. Retrieved from
<https://www.dnvgl.com/news/dnv-gl-reduces-the-impact-of-variations-in-ship-construction-7337>
- DNV. (2010). Pathways to low carbon shipping
- Doust, D. J. & O'Brien, T. P. (1959). *Resistance and propulsion of trawlers*. Newcastle: North-East Coast Institution of Engineers and Shipbuilders.
- Equasis. (2014). Equasis statistics - World fleet 2014. from EMSA
<http://www.emsa.europa.eu/implementation-tasks/equasis-a-statistics/item/472.html>
- Faltinsen, O. M. (1990). *Sea loads on ships and offshore structures*. Cambridge: Cambridge University Press.
- Fathi, D. E. & Hoff, J. R. (2015). ShipX Vessel Responses (Veres) Theory Manual: MARINTEK AS.
- FORCE Technology. (2014). MOERI KVLCC2 tanker Geometry and Conditions. *SIMMAN2014*.
- Fujii, H. & Takahashi, T. (1975). Experimental study on the resistance increase of a ship in regular oblique waves. *Proc. 14th ITTC*, 4, 351-360.
- Gerritsma, J. & Beukelman, W. (1971). *Analysis of the resistance increase in waves of a fast cargo ship* (Vol. 334). Delft: Laboratorium voor Scheepsbouwkunde.
- Grigson, C. W. (1993). An accurate smooth friction line for use in performance prediction. *RINA Trans*, 135, 14.
- Guo, B. (2011). *Numerical and experimental investigation of added resistance in waves*. (2011:329), Norwegian University of Science and Technology, Faculty of Engineering Science and Technology, Trondheim.
- Havelock, T. H. (1914). Ship Resistance: The Wave-Making Properties of Certain Travelling Pressure Disturbances. *Proceedings of the Royal Society of London. Series A, Containing Papers of a Mathematical and Physical Character (1905-1934)*, 89(613), 489-499.
doi:10.1098/rspa.1914.0016
- Holden, K. O., Fagerjord, O. & Frostad, R. (1980). *Early design-stage approach to reducing hull surface forces due to propeller cavitation*: SNAME.
- Holtrop, J. & Mennen, F. (1982). *An approximate power prediction method* (Vol. 689).

- Holtrop, J. & Mennen, F. (1984). A statistical re-analysis of resistance and propulsion data. *ISP*, 31(363).
- IMO. (2015). Third IMO GHG study 2014.
- IMO. (2016a). Introduction to IMO. Retrieved from <http://www.imo.org/en/About/Pages/Default.aspx>
- IMO. (2016b). Low carbon shipping and air pollution control. Retrieved from <http://www.imo.org/en/MediaCentre/HotTopics/GHG/Pages/default.aspx>
- International Transport Forum. (2015). The impact of mega-ships. Retrieved from <http://www.itf-oecd.org/impact-mega-ships>
- ITTC. (1999). Performance, Propulsion 1978 ITTC Performance Prediction Method
- ITTC. (2002). *Testing and Extrapolation Methods: Propulsion, Performance Propulsion Test*. Retrieved from <http://itc.info/downloads/Archive%20of%20recommended%20procedures/2006%20Recommended%20Procedures/7.5-02-03-01.1.pdf>
- Jarabo, A. & McMillan, C. (2013). *Ship efficiency : the guide : a comprehensive guide to ship eco-efficiency technologies and measures* (2nd ed. ed.): Fathom Shipping.
- Jensen, G. (1994). Moderne Schiffslinien. *Handbuch der Werften*, 22.
- Kim, H.-J., Choi, J.-E. & Chun, H.-H. (2016). Hull-form optimization using parametric modification functions and particle swarm optimization. *Official Journal of the Japan Society of Naval Architects and Ocean Engineers (JASNAOE)*, 21(1), 129-144. doi:10.1007/s00773-015-0337-y
- Kristensen, H. O. (2012). *Determination of Regression Formulas for Main Dimensions of Tankers and Bulk Carriers based on IHS Fairplay data*. Retrieved from Project no. 2010-56 Emissionsbeslutningsstøttesystem:
- Kristensen, H. O. & Lützen, M. (2012). *Existing Design Trends for Tankers and Bulk Carriers - Design Changes for Improvement of the EEDI in the Future*. Paper presented at the IMDC2012, Glasgow, United Kingdom. http://orbit.dtu.dk/ws/files/33437984/Kristensen_and_L_tzen_IMDC_06_Jan_2012.pdf
- Larsson, L. & Raven, H. C. (2010). *Principles of Naval Architecture Series - Ship Resistance and Flow*: Society of Naval Architects and Marine Engineers SNAME.
- Larsson, L., Stern, F. & Visonneau, M. (2013). *Numerical Ship Hydrodynamics : An assessment of the Gothenburg 2010 Workshop*. Dordrecht: Springer.
- Lewis, E. V. (1988). *Principles of naval architecture : 2 : Resistance, propulsion and vibration* (2nd revision. ed.). Jersey City, N.J.: Society of Naval Architects and Marine Engineers.
- Lindstad, H., Jullumstrø, E. & Sandaas, I. (2013). Reductions in cost and greenhouse gas emissions with new bulk ship designs enabled by the Panama Canal expansion. *Energy Policy*, 59, 341.
- Lindstad, H., Sandaas, I. & Steen, S. (2014). Assessment of profit, cost, and emissions for slender bulk vessel designs. *Transportation Research Part D*, 29, 32-39. doi:10.1016/j.trd.2014.04.001
- Loukakis, T. A. & Sclavounos, P. D. (1977). *Some extensions of the classical approach to strip theory of ship motions including the calculation of mean added forces and moments*: National Technical University of Athens.
- Marine Log. (2005). Colombo Express. *Marine Log*, 110(12), 22.
- Maritime Connector. (2015). Bulk carrier. Retrieved from <http://maritime-connector.com/bulk-carrier/>
- Maritime Professional. (2012). New Container Ship Hull Design to Vastly Save Fuel. Retrieved from <http://www.maritimeprofessional.com/news/container-ship-hull-design-vastly-227400>
- Miljødirektoratet. (2015). Petroleumsvirksomhet til havs : Utslipp av Karbondioksid (CO2). Retrieved from <http://www.norskeutslipp.no/no/Komponenter/Utslipp/Karbondioksyd/?ComponentType=utslipp&ComponentPageID=51&SectorID=700#>
- Newman, J. N. (1976). *Linearized wave resistance theory*. Paper presented at the International seminar on wave resistance, Japan.
- Newman, J. N. (1977). *Marine hydrodynamics*

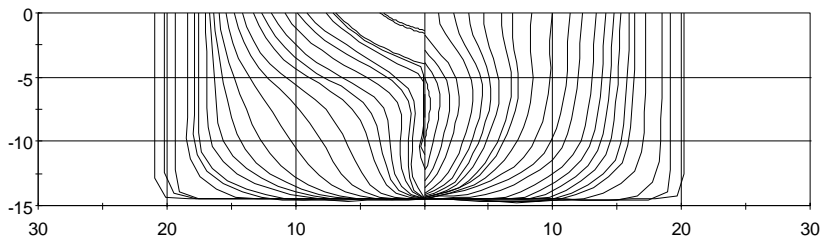
- Nordås, D. E. & Steen, S. (2012). Optimization of Bow Shape for Large, Slow Ships: Institutt for marin teknikk, Norges Teknisk-Naturvitenskapelige Universitet.
- Psaraftis, H. & Kontovas, C. (2009). CO2 emission statistics for the world commercial fleet. *WMU Journal of Maritime Affairs*, 8(1), 1-25. doi:10.1007/BF03195150
- Ringen, E., Alterskjær, A., Berget, K. & Fathi, D. (2012). *ShipX Ship Speed & Powering Plug-In*. Retrieved from
- Steen, S. (2011). *Motstand og propulsjon, propell- og foilteori* (Vol. UK-2011-99). Trondheim: Marinteknisk senter, Institutt for marin teknikk.
- Steen, S. (2014). *Motstand og propulsjon, propell og foilteori : kompendium* (Vol. UK-2014-99). Trondheim: Akademika forlag Kompendieforlaget.
- Steen, S. & Fathi, D. (2000). ShipX Wave Resistance Plug-In (Waveres) 3.0- User's Manual: MARINTEK AS.
- Steen, S. & Minsaas, K. J. (2014). *Ship resistance : TMR4220 naval hydrodynamics : lecture notes* (rev. nov. 2013. ed. Vol. UK-2014-80/IV). Trondheim: Akademika forlag Kompendieforlaget.
- Stott, P. W. (2012). *New panamax and its implications for ship design and efficiency*. Paper presented at the Low Carbon Shipping Conference 2012, Newcastle, UK.
- Stott, P. W. & Wright, P. N. H. (2011). Opportunities for improved efficiency and reduced CO 2 emissions in dry bulk shipping stemming from the relaxation of the panamax beam constraint. *Transactions of the Royal Institution of Naval Architects Part A: International Journal of Maritime Engineering*, 153(4), 215-230. doi:10.3940/rina.ijme.2011.a4.213
- Taggart, R. (1980). *Ship design and construction*. New York: The Society of Naval Architects and Marine Engineers.
- Van der Boom, H. (2010). *Ship Performance Analysis on Full Scale*. Paper presented at the Workshop NMRI-MARIN.
- Watson, D. G. M. (1998). *Practical ship design* (Vol. vol. 1). Amsterdam: Elsevier.

Appendix

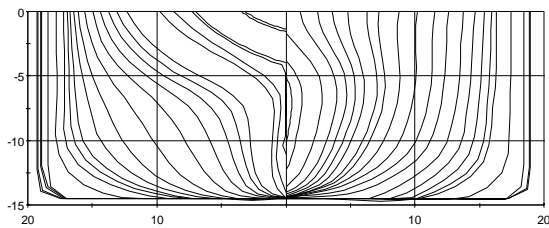
Appendix A Hull grids for the MOERI KVLCC2 series



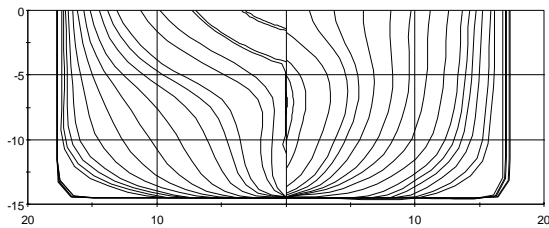
$C_b=0,59$



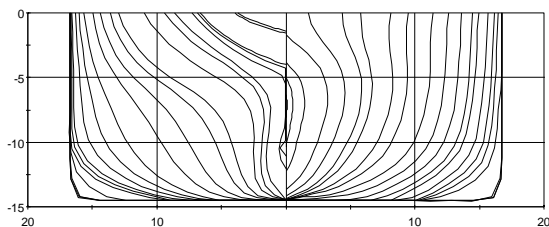
$C_b=0,63$



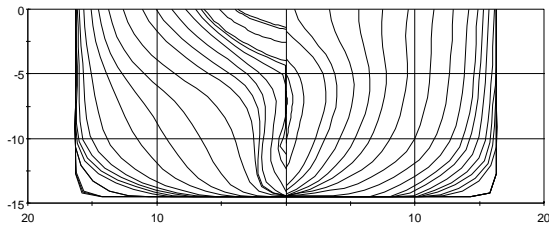
$C_b=0,68$



$C_b=0,74$

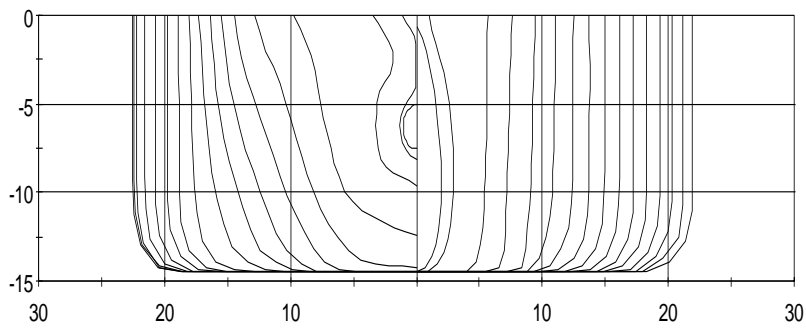


$C_b=0,78$

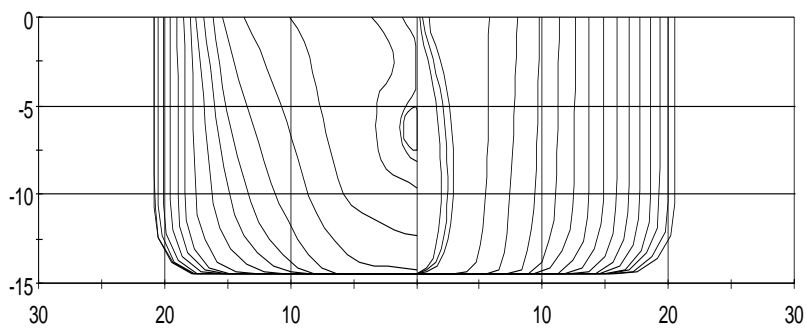


$C_b=0,80$

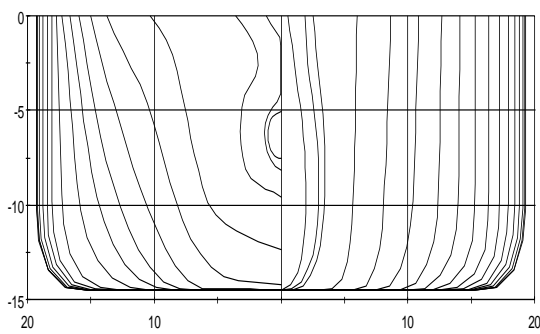
Appendix B Hull grids for the CBC series



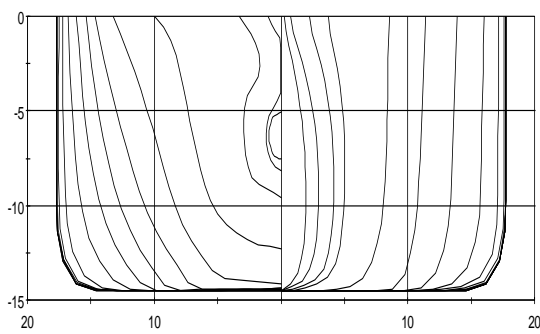
$C_b=0,64$



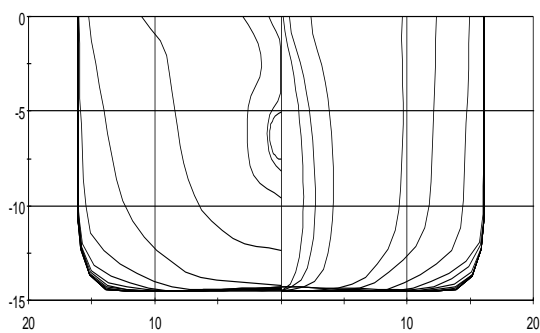
$C_b=0,68$



$C_b=0,73$

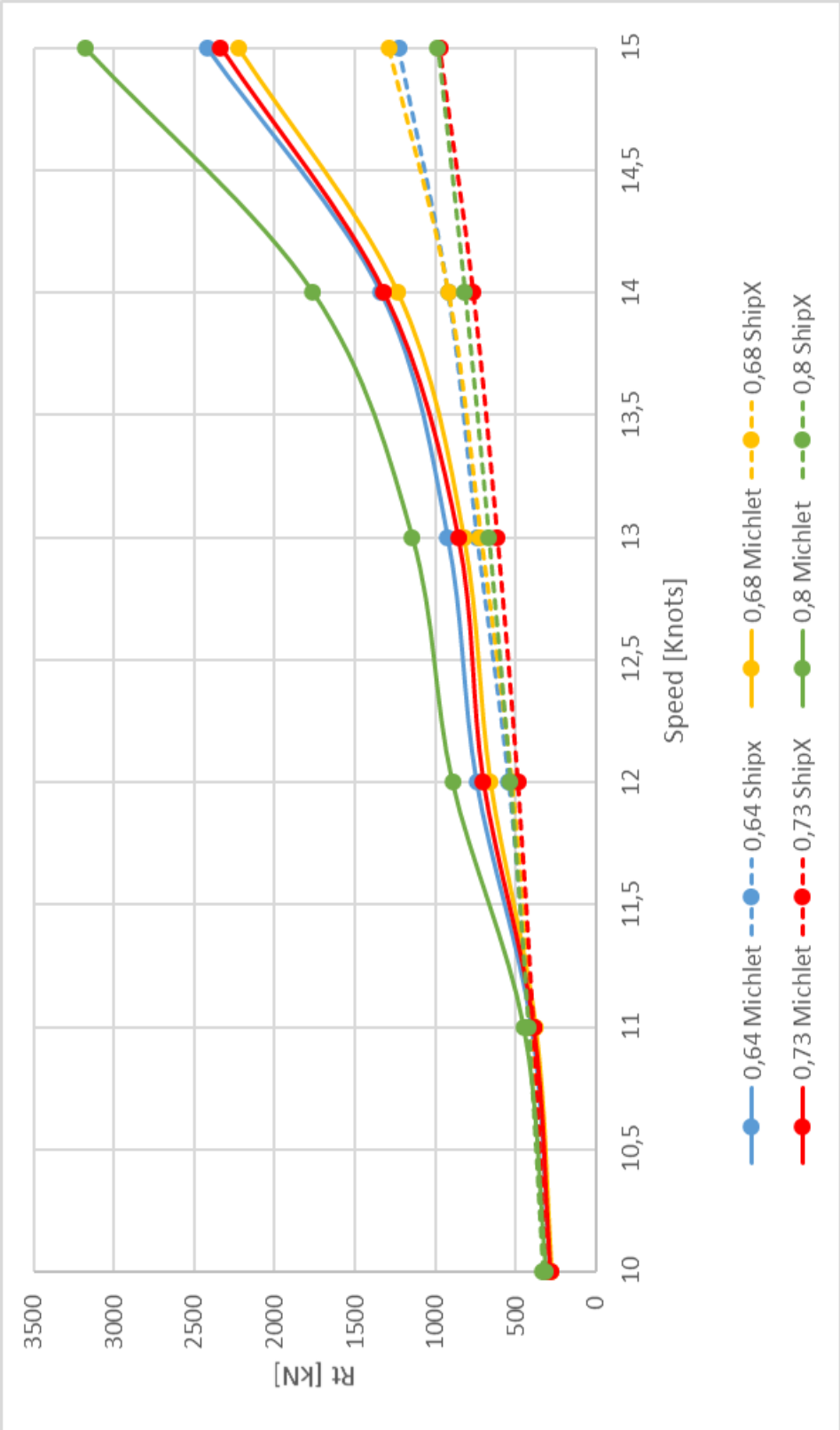


$C_b=0,80$



$C_b=0,87$

Appendix C Calm water resistance prognosis for the CBC series



Appendix D Results from numerical and empirical calculations

Block coefficient	Calm water brake power [kW]	Pcalm+0,5Pwave [kW]	Mongstad - NY [kW]	Lindstad (2013) [kW]	Holtrop +15% [kW]
0,87	8674,9	11093,6	10740	8500	8500
0,8	6605,3	8512,2	8140,3	7900	7500
0,73	5914,7	7469,40	7430	7100	7200
0,68	7141,4	8753,3	8540	6700	6500
0,64	7282,9	8867,8	8850	6500	6400
0,59	11341,8	12776,8	12590	5900	5900
0,63	7647,8	9120,0	8790	6200	6200
0,68	7574	9063,8	8675	6500	6500
0,74	6974,1	8681,2	7950	6900	6900
0,78	6478,7	8181,1	7490	NA	NA
0,8	6861,6	8499,1	8040	NA	NA
0,73 LCB=-0,5%	5910,5	7396,6	7430	7900	7500
0,73 LCB=0%	5897	7401,6	7370	7900	7500
0,73 LCB=0,5%	6006,6	7541,3	7350	7100	7200
0,73 LCB=1%	6114,5	7691,4	7610	7100	7200
0,73 LCB=1,5%	6287,7	7953,6	7740	7100	7200
0,73 LCB=2%	6437	8130,5	8100	7100	7200
0,73 mod. aft	6090,3	7726,6	7560	7100	7200
0,68 LCB=-0,5%	7052	8613,4	8630	7100	7200
0,68 LCB=0%	7243,0	8840,4	8850	6700	6500
0,68 LCB=0,5%	6583,0	8169,6	8170	6700	6500
0,68 LCB=1%	7192,1	8801,9	8730	6700	6500
0,68 LCB=1,5%	7229,0	8863,2	8760	6700	6500
0,68 LCB=2%	7457,0	9123,0	8970	6700	6500

CBC series CBC LCB variation series MOERI KVLC2 series